Copyright Warning & Restrictions

The copyright law of the United States (Title 17, United States Code) governs the making of photocopies or other reproductions of copyrighted material.

Under certain conditions specified in the law, libraries and archives are authorized to furnish a photocopy or other reproduction. One of these specified conditions is that the photocopy or reproduction is not to be "used for any purpose other than private study, scholarship, or research." If a, user makes a request for, or later uses, a photocopy or reproduction for purposes in excess of "fair use" that user may be liable for copyright infringement,

This institution reserves the right to refuse to accept a copying order if, in its judgment, fulfillment of the order would involve violation of copyright law.

Please Note: The author retains the copyright while the New Jersey Institute of Technology reserves the right to distribute this thesis or dissertation

Printing note: If you do not wish to print this page, then select "Pages from: first page # to: last page #" on the print dialog screen

INFORMATION TO USERS

The most advanced technology has been used to photograph and reproduce this manuscript from the microfilm master. UMI films the text directly from the original or copy submitted. Thus, some thesis and dissertation copies are in typewriter face, while others may be from any type of computer printer.

The quality of this reproduction is dependent upon the quality of the copy submitted. Broken or indistinct print, colored or poor quality illustrations and photographs, print bleedthrough, substandard margins, and improper alignment can adversely affect reproduction.

In the unlikely event that the author did not send UMI a complete manuscript and there are missing pages, these will be noted. Also, if unauthorized copyright material had to be removed, a note will indicate the deletion.

Oversize materials (e.g., maps, drawings, charts) are reproduced by sectioning the original, beginning at the upper left-hand corner and continuing from left to right in equal sections with small overlaps. Each original is also photographed in one exposure and is included in reduced form at the back of the book. These are also available as one exposure on a standard 35mm slide or as a 17" x 23" black and white photographic print for an additional charge.

Photographs included in the original manuscript have been reproduced xerographically in this copy. Higher quality 6" x 9" black and white photographic prints are available for any photographs or illustrations appearing in this copy for an additional charge. Contact UMI directly to order.

U·M·I

University Microfilms International
A Bell & Howell Information Company
300 North Zeeb Road, Ann Arbor, MI 48106-1346 USA
313/761-4700 800/521-0600

Order Number 9003135

Close-range, noncontact distance measurement by controlled image irradiance

Kim, Jaeho, D.Eng.Sc.

New Jersey Institute of Technology, 1989

U·M·I
300 N. Zeeb Rd.
Ann Arbor, MI 48106

CLOSE-RANGE, NON-CONTACT DISTANCE MEASUREMENT BY CONTROLLED IMAGE IRRADIANCE

by
Jaeho Kim

Dissertation submitted to the Faculty of the Graduate School
of the New Jersey Institute of Technology in partial fulfillment
of the requirements for the degree of
Doctor of Engineering Science
1989

APPROVAL SHEET

Title of Thesis: **CLOSE-RANGE, NON-CONTACT DISTANCE MEASUREMENT BY CONTROLLED IMAGE IRRADIANCE**

Name of Candidate: Jaeho Kim
Doctor of Engineering Science, 1989

Thesis and Abstract Approved: _____ _____
Dr. Harry Herman — Date
Professor
Mechanical Engineering

Signatures of other members of the thesis committee.

_____ _____
Date

_____ _____
Date

_____ _____
Date

_____ _____
Date

ABSTRACT

Title of Thesis: **CLOSE-RANGE, NON-CONTACT DISTANCE MEASUREMENT BY CONTROLLED IMAGE IRRADIANCE**

Jaeho Kim, Doctor of Engineering Science, 1989

Thesis directed by: Dr. Harry Herman

Dimensional measurement or check is a major part of the inspection and quality control in manufacturing. Most of the measurement applications are based on contact methods. While a number of non-contact methods are available, they are limited in accuracy, in flexibility, or in the range of application areas. An optical, close-range, non-contact distance measurement method has been developed for manufacturing and other applications. Based on a simple imaging principle, the method derives the distance information from the power response of a small axial image area, the irradiance of which is controlled by an active controlled illumination of the corresponding object area. The proposed method uses a low power laser beam for the illumination and can be used on both diffusive and reflective surfaces. The proposed system configuration and development is discussed with the requirements of the application environments. Based on the proposed system, the controlled illumination using a laser beam and the theoretical responses from diffusive and reflective surfaces are analyzed. The results are compared with the empirical data obtained from an experimental system.

VITA

Name: Jaeho Kim.

Degree and date to be conferred: D. Eng. Sc., 1989

Secondary education: Seoul High School, Seoul, Korea, 1974.

Collegiate institutions attended	Dates	Degree	Date of Degree
New Jersey Institute of Technology	'85-'89	D. Eng. Sc.	May '89
New Jersey Institute of Technology	'83-'85	M.S.M.E.	May '85
Hanyang University	'74-'78	B.S.	Feb. '78

Major: Mechanical Engineering

Publications:

"Microcomputer for the Dynamics Laboratory", *Microprocessors and Microsystems*, vol 10 no 5 May 1986, Butterworth, UK, by J. Kim and J. L. Martin.

TABLE OF CONTENTS

Content Page

I. INTRODUCTION 1

II. DISCUSSION OF METHODS FOR DISTANCE MEASUREMENT AND CONTROL 4

2.1. Methods used in inspection and quality control in manufacturing 4

2.1.1. Contact methods 4

2.1.2. Non-contact methods 6

2.2. Methods for middle or long range distance measurement 6

2.3. Displacement measurement 8

2.3.1. Triangulation method 8

2.3.2. Interferometry 8

2.3.3. Doppler method 9

III. OPTICS FUNDAMENTALS 10

3.1. Geometric Optics 10

3.1.1. Optical system definition 10

3.1.2. Gaussian image formation 12

3.1.3. Thin lens concept 14

3.2. Diffraction 14

3.2.1. Fresnel diffraction 14

3.2.2. Fraunhofer diffraction 16

3.3. Radiometry 17

3.3.1. Definition of radiometric quantities and units 17

3.3.2. Lambert's cosine law 19

3.3.3. Axial irradiance produced by a circular diffuse source 19

3.4. Laser 21
3.4.1. Introduction to lasers 21
3.4.2. Mode configuration 22
3.4.3. Coherence 22
3.4.4. Gaussian beam characteristics 23
IV. FOCUSING CONTROL SYSTEM DEVELOPMENT AND CONFIGURATION 26
4.1. Problems of the simple imaging system for distance control application 26
4.2. Controlled surface illumination 28
4.2.1. Requirements of the controlled illumination 28
4.2.2. Illumination source 28
4.3. Optical system arrangement 29
4.3.1. Controlled illumination system 31
4.3.2. Imaging system 31
4.3.3. The relationship between the location of the target surface and the detector response 32
V. CONTROLLED SURFACE ILLUMINATION BY A GAUSSIAN BEAM 34
5.1. Gaussian beam shaping 34
5.2. The location and size of transformed beam waist 39
5.3. The intensity distribution of a transformed beam 40
5.4. Consideration of diffraction effects and aberration 41
5.5. Other considerations 42
5.6. Surface irradiance 43
VI. ANALYSIS OF REFLECTIVE SURFACE RESPONSE 48
6.1. Response from a vertically positioned flat surface 48

6.1.1. Determination of the location of the detection window 50
6.1.2. The formation of the imaged beam 52
6.1.3. Power response of the detection system 54
6.2. Response from an inclined flat surface 55
6.2.1. The formation of the imaged beam 55
6.2.2. Power response of the detection system 64
6.3. Consideration of the effect of the limited aperture 68
VII. ANALYSIS OF DIFFUSE SURFACE RESPONSE 82
7.1. Location of the image plane 82
7.2. Intensity distribution on the image plane 85
7.3. The method for the analysis of the power response of the detector 86
7.4. Radiance of the object surface 90
7.5. Response from a vertical object surface 91
7.5.1. Response from an object surface located at the object plane 92
7.5.2. Response from an object surface located at a random position 95
7.6. Response from an inclined object surface 100
VIII. DISCUSSION OF EXPERIMENT 107
8.1. Experimental system 107
8.1.1. Controlled illumination 107
8.1.2. Imaging system 110
8.1.3. Experiment procedure 115
8.2. Reflective surface response 115
8.3. Diffusive surface response 120
8.4. Responses from other target surfaces 124

IX. ADDITIONAL DISCUSSIONS 133
9.1. Difficulties and problems in the experiment 133
9.2. Suggested corrective methods 134
9.3. Consideration for practical system 135
X. CONCLUSION 137
BIBLIOGRAPHY 139

LIST OF TABLES

Table Page

8.1. System components specification 109

8.2. beam shaping data 111

8.3. List of test surfaces 127

LIST OF FIGURES

Figure Page

3.1. Optical system definition 11
3.2. Image formation by an optical system 13
3.3. Diffraction geometry 15
3.4. Axial irradiance produced by a circular diffuse source 20
3.5. Gaussian beam propagation 24
4.1. Optical system arrangement 30
5.1. Gaussian beam transformation by a lens 36
5.2. Radiation from a diffuse source 46
6.1. Reflection of the illumination beam on the object surface 49
6.2. Formation of the imaged beam - vertical object surface 53
6.3. Formation of the imaged beam - inclined object surface 57
6.4. Beam cross section on the plane of the aperture 59
6.5. Geometry of the detection window 65
6.6. Truncated cross section of the imaged beam 69
6.7. Overlapping cases of the detection window and the projected aperture 72
6.8. Overlapping area - Case 2 74
7.1. Imaging system 84
7.2. Projection of the detection window 88
7.3. Imaging of a vertical surface - object plane 93
7.4. Imaging of a vertical surface - random location 97
7.5. Imaging of an inclined surface 101
7.6. Radiation angle - θ' 104

8.1. Experimental system 108
8.2. Single lens representation of the imaging system 113
8.3(a,b). Reflective surface response - empirical 116
8.3(c). Reflective surface response - empirical 118
8.4(a,b). Reflective surface response - theoretical 119
8.4(c,d). Reflective surface response - theoretical 121
8.4(e). Reflective surface response - theoretical 122
8.5(a,b). Diffusive surface response - theoretical 123
8.5(c,d). Diffusive surface response - theoretical 125
8.5(e,f). Diffusive surface response - theoretical 126
8.6(a,b). Responses from test surfaces 128
8.6(c,d). Responses from test surfaces 129
8.6(e,f). Responses from test surfaces 130
8.6.(e.f). Responses from test surfaces 131
8.6(i). Responses from test surfaces 132

CHAPTER I

INTRODUCTION

The dimensional check or measurement of a workpiece is a major part of inspection and quality control in manufacturing. In the dimensional determination, the distance is measured between two points on the workpiece or between a point on the workpiece and a reference point located outside of the workpiece. Typically, the distance is measured by a device which contacts the surface point(s). The measurement can be read directly or amplified to increase the measuring accuracy. The measurement is based on a distance control method using pressure to ascertain that a contact is made between two surfaces - the surface of the measuring device and the surface of the workpiece. The amount of the contact pressure and the size of the contact area are the important factors which affect the accuracy of the measurement. Depending on the hardnesses of the two contact surfaces, the contact pressure should be controlled so as not to damage one or both of the surfaces. The measuring accuracy can be affected by the size of the contact area as the dimension varies from one surface point to another on the same surface depending on the surface profile and irregularities.

For accurate measurement, a very small contact area and light contact pressure will be required. Sensitive measuring systems employ a spring-loaded solid touch probe with a small round tip to reduce the contact area and to apply light contact pressure.

In a manual measurement process, the time required for aligning the measuring probe and finding the measurement will be increased if more accuracy is demanded or if the workpiece becomes larger. It can be a difficult task to au-

tomate such dimensional measurement in applications which require a single or multiple point measurements on workpieces, the shapes and sizes of which are different and considerably large so that the use of special inspection gages is difficult or impractical. Also, there can be a situation which requires the measurement of the coordinates of the surface points of a large and complicated workpiece which must be controlled by computer vision or by remote manual operation. In such a situation, the alignment of the measuring probe to the desired target point can be a very difficult task, particularly, if three dimensional data is required. Also, there may be a risk of forceful collision between the measuring probe and the workpiece, damaging the measuring system and/or the workpiece. This risk will be increased if there is an abrupt change of the slope of the workpiece surface and if the measuring probe must move to different surface-points consecutively.

For measurement applications such as those discussed above, a non-contact distance measurement method will have considerable advantages over the conventional contact methods if the non-contact method can provide the same information and accuracy. To satisfy this objective, an optical system has been configured to provide the results of the contact methods without the contact requirement. This optical method is based on a simple imaging principle together with controlled surface illumination, and can provide close range, non-contact distance control by means of focusing control. The three basic elements of the contact method - the size of the contact area, the distance between the contact probe and the target surface, and the contact pressure - are simulated in the proposed optical method. The size of the contact area is equivalent to the size of the illumination spot on the surface, and the distance is controlled using the power registered by the detector

output in the optical system.

The discussion of the non-contact optical method is arranged as follows. Before the discussion of the proposed method, conventional distance control or measurement methods will be discussed for comparison in Chapter II. The discussion of the methods will include the contact and noncontact methods. Additionally, non-contact displacement methods will be discussed in context of their relevant application areas. As the discussion of the optical method is mostly based on optics, a review of optics fundamentals is provided in Chapter III. In Chapter IV, the development of the optical system will be discussed from the basic requirements of the optical system as a distance measurement system to the proposed, functional system configuration. Based on the proposed system configuration, the controlled surface illumination will be discussed in various aspects in Chapter V, and the detector response will be analyzed for the reflective and the diffusive surfaces in Chapter VI and VII. In Chapter VIII, the experimental system will be discussed, and the experimental results will be compared with the theoretical responses. Chapter IX will discuss the problems encountered during the experiment and the suggested corrective measures for these problems. The limitations, design notes, and practical considerations about the proposed system will also be discussed. Chapter X summarizes the conclusions.

CHAPTER II

DISCUSSION OF METHODS FOR DISTANCE MEASUREMENT AND CONTROL

In inspection and quality control in manufacturing, the dimensional measurement is mostly based on the methods which require a contact between the measuring system and the workpiece. There are non-contact measurement methods available for limited applications. Typical non-contact methods can be found in the middle or long range distance measurement applications. In this chapter, these measurement methods will be discussed. Additionally, a number of displacement measurement methods will be discussed because of their non-contact nature and relevance.

2.1 Methods used in inspection and quality control in manufacturing

In the dimensional measurement in inspection and quality control, the distance is measured between two surface points of the workpiece or between a surface point of a workpiece and a reference point which is located outside of the workpiece. During measurement, a contact is made between the workpiece and the measuring tool. For non-contact measurement, the measuring system maintains a specific distance to the surface of the workpiece. For the inspection of mass production items, specific gages are used to measure or check the dimensions of the items.

2.1.1. Contact methods

Simple measurement is done with standard measuring tools such as micrometer, vernier calipers, height gages, etc. For the inspection of mass production items, specific gages are used to measure or check the dimension of the items.

The measuring tools and gages can be assembled from gage blocks, dial test indicators, touch probes, etc. For accurate measurement, the displacement of the contact probe is amplified using following methods[1].

Mechanical amplification:

Mechanical amplification is done with levers, gear trains, or reeds. Dial indicators use gears to amplify readings. Amplifications with these indicators can range 40-to 1 to as much as 1500-to-1. In this case a pointer or ball probe is attached to the end of a rack. The linear motion of the rack is transferred to a gear train. A needle is attached to the output gear. The ratio of input-to-output of the gears determines the amplification. The standards of the dial indicators (American Gage Designers - AGD) have been established. They have been standardized to sensitivities of 0.001 to 0.00005 inches per division. Another type of widely used indicator is the dial test indicator. The dial is generally graduated to read 0-15-0 in 0.001 or 0.0005 of an inch increments with a total range of 0-to-0.030 inches.

Electronic amplification:

There are a number of different methods used for electronic amplification. Electrical gaging uses an indicator probe, which is similar to the standard dial gage. The probe contacts the workpiece and actuates one of two on-off switches. The gages can be read from 0.001 to 0.0001 inches. This electrical gage is essentially mechanical.

Electronic gage has continuous output. The probe is moved by contacting the work piece. The movement acts, through the movement of an armature, on the alternating current which is brought to the gaging head.

Electronic amplification uses a movement of the contact probe to move a coil in a electromagnetic field. This sets up an induced current flow in two

oppositely wound coils. This induced current is amplified and fed into a voltmeter.

2.1.2. Non-contact methods

For limited applications, following non-contact methods can be used[1].

Spark method:

Spark method uses a spark gap between the probe and the workpiece. This method permits the continuous comparison of the shape of the workpiece with a master. This method is used for tracing contours.

Pneumatic indicators:

This gaging process operates according to the constant pressure but uses a varying air flow per unit time. The gage head masters the quantity of air permitted to escape from the orifice between the workpiece and the walls of the gage head. Assuming the air pressure is constant, the space between the head and the work is changed for different workpieces. A noncontact gaging head is used where the quantity of air escaping is controlled by the diameter of the orifice and the clearance between the work and the gage.

2.2. Methods for middle or long range distance measurement

Optical range finding method:

Optical range finders mostly use the coincidence focusing method, in which an object is positioned at the dead center of the finder and two images of the same object are merged. Typical example is the coupled-rangefinder-focusing(CRF) method, which is used in the photographic cameras such as Leica M-camera and others.

The autofocusing method used in the photographic cameras is based on the similar principle used in the optical range finder, but, for focusing, electronic

phase detection is used instead of the optical image merging in the optical range finder. The phase-detection range finders compare two parts of a beam of light from the same object using charge-coupled-device(CCD) linear detector array. This is a passive method that the light must come from the object. In some cameras, an infrared light source is employed for active measurement. Other example is the stereo imaging method using two digital cameras. In this method, the distance to an object is derived using the two screen coordinates of the pattern of the object, which is recognized by optical processing.

Time elapse methods:

Using the properties of a propagating wave, the distance is derived from the elapsed time of a wave travel from the wave generator to the receiver which detects the reflected wave from a target. For short to middle range applications, sonic or ultrasonic wave is used. A radar uses electromagnetic waves for middle or long range distance measurement application.

If a laser beam is used for measurement, the accuracy of the measurement depends on the parameters like the accuracy of the speed of light, which is accurate to about 1 part in 100,000, the atmospheric condition, and the speed of electronic instrument to measure elapsed-time, which is typically 1 nanosecond. With an assumed velocity of light of 300,000km/s, light travels a distance of about 30cm for 1 nanosecond, so a range measurement error of about 15cm can result[2].

Amplitude modulation method:

This method involves the amplitude modulation of a light beam at a modulation frequency w in the range of 30 MHz. The phase of the modulation envelope of the returned light is then compared with the phase at the transmitter. The detection circuit is arranged so that when the optical path from

the modulator to the reflector and back is $(0.5M + 1/4)$ wavelengths of the modulation frequency, a null is obtained. The distance is obtained by varying w and measuring the values for which the the detection circuit gives a null. By measuring a number of nulls, the ambiguity in the value of the integer M is resolved. Under good atmospheric conditions, it has been estimated that sensitivities of one part in 10,000,000 over distances of 30 km or more are possible[2].

2.3. Displacement measurement

There are a number of optical methods available for precise measurement of the displacement of a target surface. The information of the absolute distance to the target surface can not be derived from these methods.

2.3.1. Triangulation method

A low power HeNe or diode laser projects a spot of light on a diffusive surface. A portion of the light is scattered from the surface and is imaged by a converging lens on a linear diode array or a linear position detector. If the diffusive surface has a component of displacement parallel to the light incident on it from the laser, the spot of the light on the surface will have a component displacement parallel and perpendicular to the axis of the detector lens. The component of the displacement perpendicular to the axis causes a corresponding displacement of the image on the detector array. The displacement of the image on the detector can be used to determine the displacement of the diffusive surface[3].

2.3.2. Interferometry

In measurement, interferometry method uses a mirror or a reflector instead of the actual target surface.

Michelson interferometry:

This method can be used to make precise relative, linear displacement measurements of one mirror relative to the other or to detect and/or measure surface variations between the two mirrors. Typical linear displacement accuracy is within one-quarter wavelength of the light being used. If HeNe laser light with 632.8nm wavelength is used, an accuracy of 0.000158mm can be achieved.

Two frequency interferometry:

Using a laser which operates at two slightly different frequencies, f_1 and f_2, with opposite circular polarizations, linear movement can be detected by optical beating phenomena and counting the amplitude variation of $(f_1 - f_2)/2$. Using Doppler shift, velocity detection is also possible.

Other interferometry methods:

There are other interferometry methods: Fizeau interferometry, holographic interferometry, etc.

2.2.3. Doppler method

Using the Doppler shift of a wave propagation, the displacement, velocity, and acceleration of the target can be obtained.

CHAPTER III

OPTICS FUNDAMENTALS

This chapter provides a brief review of the areas of optics, which are relevant to the optical system to be discussed.

3.1. Gaussian Optics

Gaussian or first-order optics is often referred to as the optics of the perfect optical system. The first-order equations are based on the simplified expressions of the exact trigonometric ray path equations by using the first order approximations of the trigonometric functions. These approximate equations are valid for an paraxial region, which is an infinitesimal thread-like region about the optical axis. A well-corrected optical system will follow the first-order expressions almost exactly; also, the first-order image positions and sizes provide a convenient reference from which to measure departure from perfection[4].

3.1.1. Optical system definition

An optical system, which may consist of a single element or a multiple-element group, can be treated as a "black box" whose characteristics are defined by its cardinal points and its entrance and exit pupils, as illustrated in Figure 3.1.

The cardinal points are the first and second focal points, the first and second principal points, and the first and second nodal points. The focal points are defined as those points at which light rays parallel to the optical axis are brought to common focus on the axis. If the rays entering the system and those emerging from the system are extended until they intersect, the points

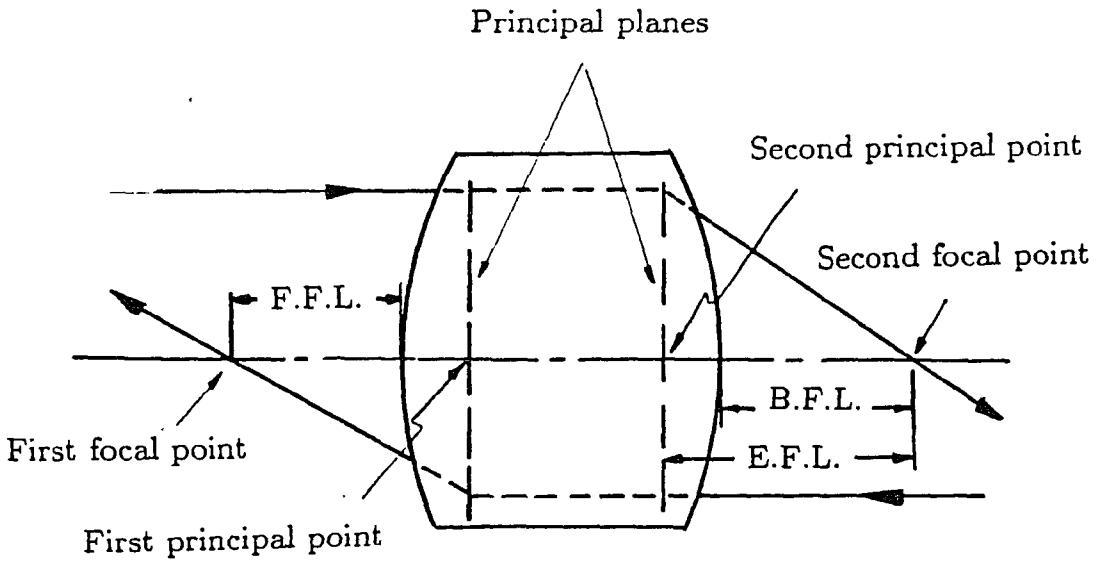

Figure 3.1. Optical system definition

of the intersection will define a surface, usually referred to as the principal plane. The principal point is the intersection of the principal plane and the axis. The effective focal length(efl) is the distance from the principal point to the focal point. The distances from the focal points to the nearest surfaces of the system are defined as the front focal length and back focal length, respectively. The entrance pupil and the exit pupil represent the finite apertures through which light must pass through to enter and to exit the system. The finite extent of the two pupils is found by geometrically projecting the smallest aperture of the system through the imaging elements onto the entrance and exit planes[5].

3.1.2. Gaussian Image formation

The relationship of the locations of the object plane s_1 and the image plane s_2 is defined by

$$\frac{1}{s_2} = \frac{1}{f} - \frac{1}{s_1} \tag{3.1a}$$

or

$$s_2 = \frac{s_1 f}{s_1 - f} \tag{3.1b}$$

where f denotes the effective focal length of the system and positive signs are used for s_1 and s_2 as in Figure 3.2.

The lateral magnification of an optical system is the ratio of the image size to the object size and is given as

$$m = -\frac{s_2}{s_1} \tag{3.2}$$

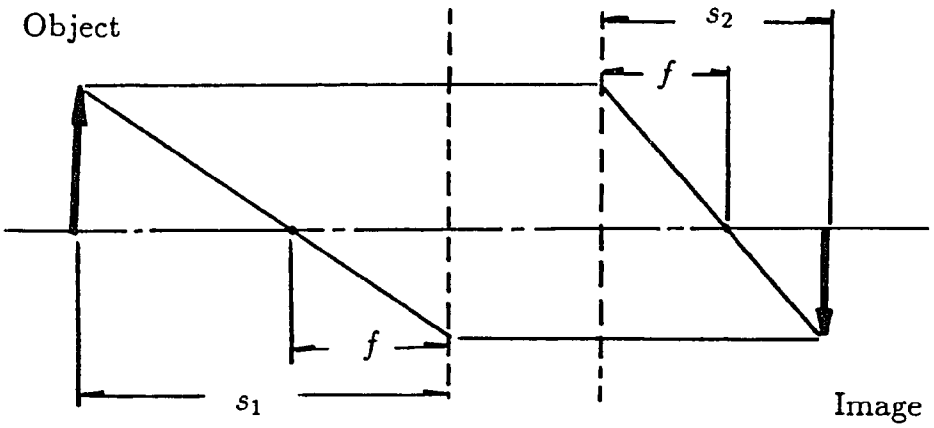

Figure 3.2. Image formation by an optical system

3.1.3. Thin-lens concept

If the thickness of a lens element is small enough so that its effect on the accuracy of the calculation may be neglected, the element is called a thin lens. Since the thickness is assumed to be zero, the principal points of a thin lens are coincident with the location of the lens[4]. As this thin-lens concept is very useful one for preliminary analysis and calculation, this concept will be used throughout this thesis together with the principal plane-concept unless specified otherwise.

3.2. Diffraction

When light rays pass through an aperture, their paths deviate from the paths predicted by geometric optics due to the diffraction effects of the aperture.

3.2.1. Fresnel diffraction

Fresnel diffraction formula provides the ground for an analysis of aperture diffraction effects[5].

$$U(x_o, y_o) = \frac{\exp(jkz)}{jkz} \int\int_A U(x_1, y_1) \cdot \exp\left\{ j\frac{k}{2z}[(x_o - x_1)^2 + (y_o - y_1)^2] \right\} dx_1 dy_1 \quad (3.3)$$

In this formula, the complex amplitude of the field $U(x_o, y_o)$ of an observation point Po is related to the complex amplitude of a given aperture field $U(x_1, y_1)$, as illustrated in Figure 3.3. Area A denotes the region of integration in the whole aperture, and

$$k = \frac{2\pi}{\lambda} \quad (3.4)$$

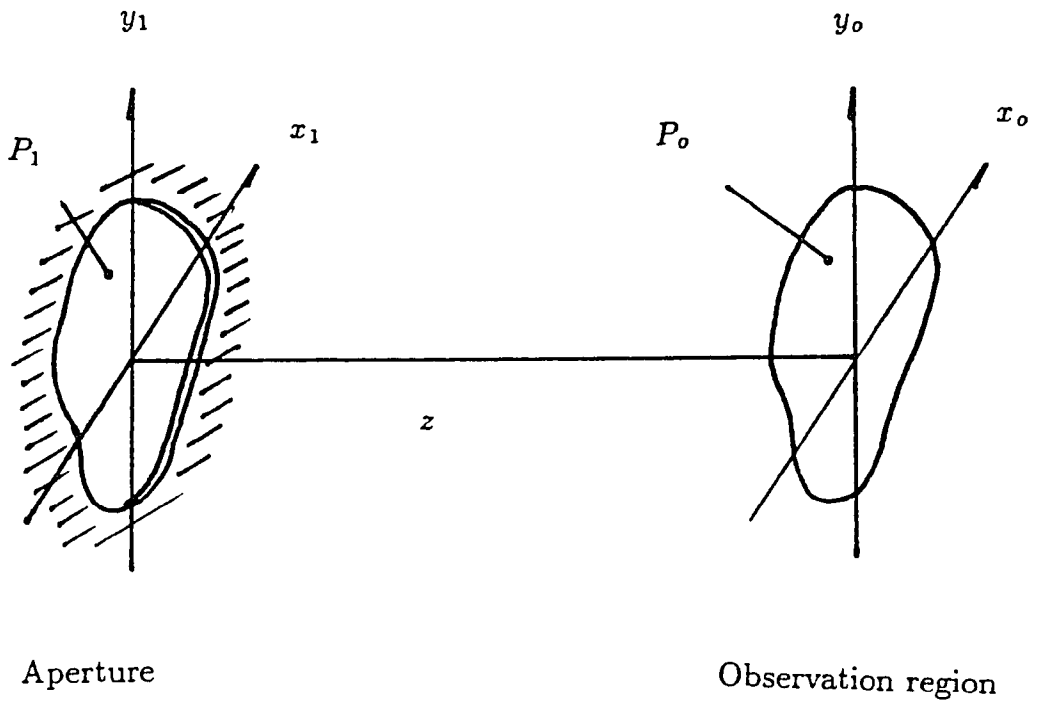

Figure 3.3. Diffraction geometry

is the propagation constant of free space. For circular aperture, Fresnel diffraction formula is given by [6]

$$U(r_o) = \frac{jk\exp(-jkz)}{z}\int_0^a U(r_1)J_0(kr_1r_o) \cdot \exp\left[-j\frac{k}{2z}(r_1^2+r_o^2)\right] r_1 dr_1 \qquad (3.5)$$

where r_1 and r_0 are the radius coordinates in the planes of the aperture and the observation, a is the radius of aperture, and J_0 is a zero order Bessel function.

3.2.2. Fraunhofer diffraction

If the restriction,

$$z_0 >> \frac{k(x^2+y^2)_{max}}{2} \qquad (3.6)$$

is imposed in the Fresnel diffraction formula, the far-field diffraction pattern can be found from a Fourier transformation of the aperture distribution. This pattern is called Fraunhofer diffraction[5], for which we may write

$$U(x_0,y_0) = \frac{\exp(jkz)}{j\lambda z}\exp\left[j\frac{k}{2z}(x_0^2+y_0^2)\right] \cdot \int\int_A U(x_1,y_1)\exp\left[-j\frac{2\pi}{\lambda z}(x_0x_1+y_0y_1)\right] dx_1dy_1 \qquad (3.7)$$

For a circular aperture with radius a, the Fraunhofer diffraction can be expressed as[6]

$$U(r_o) = \frac{jk}{z}\exp\left[-jkz\left(1+\frac{r_o^2}{2z^2}\right)\right]\int_0^a U(r_1)J_0\left(\frac{kr_1r_o}{z}\right) r_1 dr_1 \qquad (3.8)$$

For a circular aperture with uniform amplitude field $U(r_1) = 1$, the diffraction pattern becomes

$$U(r_o) = j \exp\left[-jkz\left(1 + \frac{r_o^2}{2z^2}\right)\right]\left(\frac{ka^2}{2z}\right)\left[\frac{2J_1(kar_o/z)}{kar_o/z}\right] \tag{3.9}$$

where J_1 is a Bessel function of first kind of order 1. The intensity distribution can be written as

$$I(r_o) = \left(\frac{ka^2}{2z}\right)^2\left[\frac{2J_1(kar_o/z)}{kar_o/z}\right]^2 \tag{3.10}$$

This pattern is usually referred to as the Airy pattern, which defines the diffraction limit of an ideal lens[8]. The Airy pattern has successive maxima and minima. The first minimum occurs at

$$r_o = 1.22\frac{\lambda z}{a} \tag{3.11}$$

The amount of energy contained within the first ring with a radius defined by Eq.(3.11) is 86% of the total energy.

3.3. Radiometry

Radiometry deals with the measurement and specification of radiation[4,8,9].

3.3.1. Definition of radiometric quantities and units

Radiant energy:

The fundamental quantity for optical radiation is radiant energy. It is characterized by the symbol Q and is in units of joules(J).

Radiant power:

This is defined as the partial derivative with respect to time of radiant energy. This is in units of watts(W).

$$P = \frac{\delta Q}{\delta t} \qquad \text{watts} \tag{3.12}$$

Radiant intensity:

Radiant intensity is defined as the radiant power per unit solid angle radiated in a given direction from a point source. It is given the symbol I and is measured in units of watts per steradian(W/sr).

Steradian:

A steradian is the solid angle subtended by $1/4\pi$ of the surface area of the sphere. Thus, a sphere subtends 4π steradians from its center.

Solid angle:

A solid angle in steradians is defined by determining the area of that portion of the surface of a sphere which is included within the solid angle and dividing this area by the square of the radius of the sphere.

Radiance:

The radiation characteristics of an extended source are expressed in terms of power per unit solid angle per unit area(W/sr-cm^2) and the symbol is N.

Irradiance:

Irradiance, H, is the incident power per unit area and is obtained by multiplying the intensity of the source by the solid angle subtended by the unit area.

$$H = I\frac{1}{S^2} = \frac{P}{4\pi S^2} \tag{3.12}$$

3.3.2. Lambert's Cosine Law

For radiant energy emitted by a planar source, the radiant intensity I in W/sr varies as the cosine of the angle between the viewing direction and the surface normal. Surfaces for which this relationship is valid are called Lambertian or diffuse surfaces.

$$I_\theta = I_o \cos\theta \tag{3.13}$$

where I_θ is the radiant intensity at angle θ and I_o is the radiant intensity normal to the surface. The radiance from a Lambertian source is independent of the viewing angle. For a perfect diffuse source, the radiance is also independent of the angle of the incident light.

3.3.3. Axial irradiance produced by a circular diffuse source

As illustrated in Figure 3.4, a point P is located at a distance S from a Lambertian source of radius R and is on the normal axis of the source.
The irradiance dH produced at the point by an infinitesimal area dA located at the coordinates (r, ϕ) on the source is

$$\begin{aligned} dH &= I_\theta \cos\theta \frac{\cos^3\theta}{S^2} \\ &= \frac{N dA \cos^4\theta}{S^2} \\ &= \frac{N \cos^4\theta r dr d\phi}{S^2} \\ &= \frac{N \cos^4\theta S \tan\theta d(S\tan\theta) d\phi}{S^2} \\ &= N \cos\theta \sin\theta d\theta d\phi \end{aligned} \tag{3.14}$$

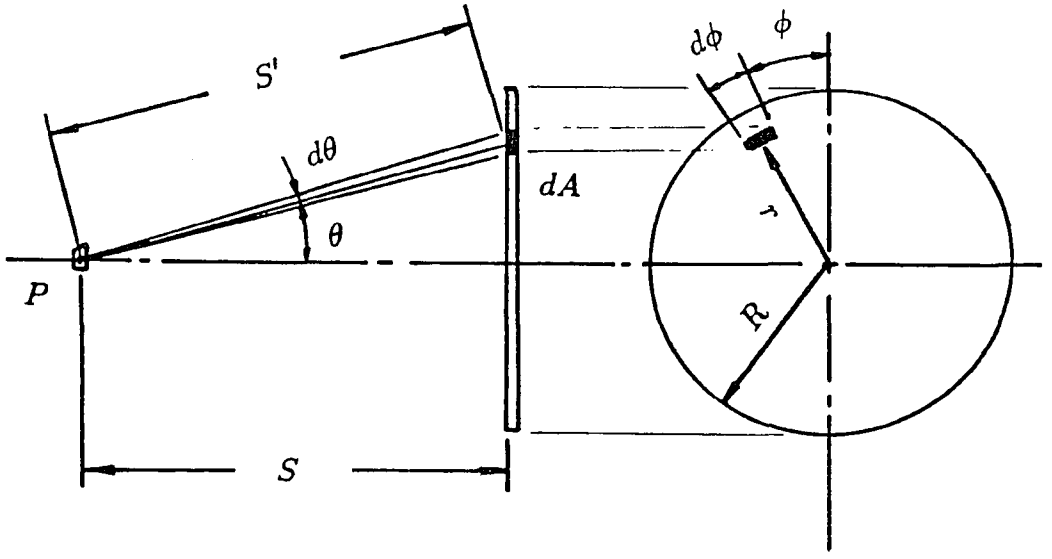

Circular diffuse source

Figure 3.4. Axial irradiance produced by a circular diffuse source

where θ is the inclination angle from the surface normal, N is the radiance of the source, and I_θ is the radiant intensity of dA at angle θ from the surface normal. The total irradiance H produced at the point by the whole circular source can be obtained by integrating dH over the source,

$$\begin{aligned} H &= \int_0^{2\pi} \int_0^{\theta} dH d\theta d\phi \\ &= \int_0^{2\pi} N \frac{\sin^2 \theta}{2} d\phi \\ &= \pi N \sin^2 \theta \qquad \text{watt/cm}^2. \end{aligned} \tag{3.15}$$

3.4. Laser

3.4.1. Introduction to lasers

Lasers are radiation sources capable of delivering intense coherent electromagnetic fields ranging from infrared to ultraviolet or even higher frequency regions.

A laser system consists of: a laser medium consisting of an appropriate collection of atoms, molecules, ions, or semiconducting material; a pumping process to excite this medium into high quantum energy levels; optical feedback elements that allow a beam of radiation to either pass once through the laser medium or bounce back and forth repeatedly through the laser medium. When the laser medium interacts with an electromagnetic field, transitions between various quantum energy levels of this medium will occur through absorption, spontaneous emission, and stimulated emission processes at frequencies characteristic to the medium.

Laser pumping provides a condition of population inversion, in which more atoms are excited in some higher quantum energy level than are in some

lower energy level in the laser medium. Stimulated emission during down level transition provides laser amplification.

Oscillation in a resonant laser cavity which is formed by small mirrors placed at each end will occur whenever the amplification through stimulated emission is sufficiently high to exactly balance the attenuation caused by various losses in the system. One of the losses is the useful laser output extracted through a partially transmitting mirror. This output, which can be in continuous or pulsed operation, is a highly coherent beam with propagation characteristics determined by the modes of the laser resonant cavity.

3.4.2. Mode configuration

The shape and arrangement of mirrors in the cavity tends to maintain particular transverse electromagnetic field configurations with sufficiently low loss. Oscillation and further amplification by the laser material will take place only in these modes. These different modes are designated by TEM_{mn}, where m and n designate the orders of the mode. The beam operating in the fundamental mode, TEM_{oo}, possesses a Gaussian intensity distribution. The size of the beam waist in this mode is determined by the configuration and the arrangement of the mirrors[2].

3.4.3. Coherence

Laser beam has a high degree of coherence, both temporally and spatially. The temporal coherence of the laser beam can be explained by that the amplitude and phase of the laser output at any one time is strongly correlated with the amplitudes and phases at earlier or later times. The spatial coherence can be described by that there is a very high degree of correlation between the instantaneous amplitudes, and especially between the instantaneous phase

angles, of the wave front at any points across the laser beam[10].

3.4.4. Gaussian beam characteristics

A detail description of the Gaussian beam has been developed[2,6,7]. The propagation characteristics - w and R, the beam radius and the radius of curvature of the wave front at the distance z from the beam waist - are described by

$$w^2(z) = w_o^2 \left[1 + \left(\frac{\lambda z}{\pi w_o^2}\right)^2\right], \tag{3.16}$$

$$R(z) = z \left[1 + \left(\frac{\pi w_o^2}{\lambda z}\right)^2\right]. \tag{3.17}$$

The propagation of the beam is depicted in Figure 3.5.

The beam radius w describes the effective size of the beam cross section and is the distance at which the amplitude is reduced to $1/e$ times that on the axis.

For large z, the beam expands linearly with a far-field diffraction angle given by

$$\theta = \frac{\lambda}{\pi w_o^2}. \tag{3.18}$$

From Eqs. 3.16 and 3.17, the beam waist w_o and the distance z can be derived from the known w and R as

$$w_o^2 = \frac{w^2}{\left[1 + \left(\frac{\pi w^2}{\lambda R}\right)^2\right]}, \tag{3.19}$$

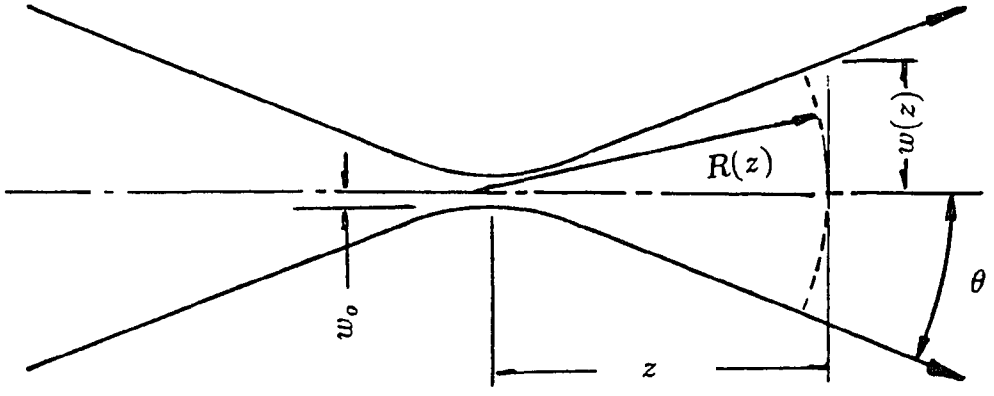

Figure 3.5. Gaussian beam propagation

$$z = \frac{R}{\left[1 + \left(\frac{\lambda R}{\pi w^2}\right)^2\right]}. \tag{3.20}$$

The field u of the Gaussian beam is given by

$$u(r,z) = \frac{w_o}{w} \exp\left\{-j(kz - \Phi) - r^2\left(\frac{1}{w^2} + \frac{jk}{2R}\right)\right\} \tag{3.21a}$$

where

$$\Phi = \tan^{-1}(\lambda z / w_o^2) \tag{3.21b}$$

and r is the radial distance from the beam axis, $k = 2\pi/\lambda$ is the propagation constant in the medium.
The intensity distribution I is

$$I(r,z) = I_o \left[\frac{w_o}{w(z)}\right]^2 \exp\{-2[r/w(z)]^2\}. \tag{3.22}$$

The peak intensity I_o, obtained at the center of the beam waist, can be found from the total power P_o as follows.

$$\begin{aligned} P_o &= \int_0^{2\pi} \int_0^{\infty} I_o \exp\left[-2(r/w_o)^2\right] r dr d\phi \\ &= I_o \frac{\pi w_o^2}{2}. \end{aligned} \tag{3.23}$$

Hence

$$I_o = \frac{2P_o}{\pi w_o^2}. \tag{3.24}$$

CHAPTER IV

FOCUSING CONTROL SYSTEM DEVELOPMENT AND CONFIGURATION

In an imaging system, the intensity distribution of the image depends on the radiation characteristics of the object. If the radiation of the object surface is provided by external incoherent illumination, the intensity distribution of the image will be directly related to the radiance of the object surface. If the distance between the object surface and the imaging system is changed, the image will become blurred and the intensity distribution of it will be changed. The relationship between the object distance and the image intensity variation of a simple imaging system has a potential for distance control but does not provide the necessary information or precision to be used as a control variable for close-range focusing control or distance control. The relationship can be controlled to yield an information which can be used to find a certain distance to the object by a specific configuration of an imaging system by controlling the variables involved in the relationship.

4.1. Problems of the simple imaging system for distance control application

As the surface profile depends on the surface shape and roughness, very accurate measurement on a specific target point on the surface depends on the ability of the measuring system to measure as small an area as possible. Furthermore, as the target area becomes small, it becomes more critical that the measuring system align on the target point precisely.

In a conventional imaging system such as a microscope, the distance between the object and the microscope is controlled by the image analysis of

an observer, which involves optical processing to determine the best imaging situation. Alternatively, an optical range finding technique can be used to determine the distance to the object, which is based on image alignment. The stereo imaging method and the autofocusing method used in photographic cameras can be categorized as such a method. To monitor a certain area of the target surface, a specific area of the image plane, which is the corresponding image area of the reference target surface formed by the imaging system, should be used. The total irradiance of the corresponding image area will be affected by a number of different external conditions. If the target surface has an even intensity distribution, the intensity variation or the total power of the image plane may not necessarily change. Even if they do, the variation will not be great enough for precise distance variation interpretation.

If the radiance of the target surface is provided by external illumination sources, the total irradiance of the image area varies depending on the amount and power of the incident light on the target surface. This can be caused by the instability of the illumination sources, any stationary or moving obstacles between the illumination sources and the target surface, the existence of any stray light from the environment, etc.

If the target has a polished surface, this surface may act like an an optical mirror, and the image detected by the system may be only an image reflected by the mirror instead of the polished surface itself.

The radiation of the target surface, which is provided by uncotrolled external illuminations, make it very difficult to distinguish the desired target point from its environment, to guide, or to align the imaging system to the target point.

4.2. Controlled surface illumination

To reduce or eliminate the obstacles discussed in the previous section, the surface radiance should be controlled to induce a suitable variation of the irradiance on the image area.

4.2.1. Requirements of the controlled illumination

The intensity of the illumination should be high enough to remove the influence of environmental lights and should be stable enough to maintain the radiance of the target surface within acceptable level. The illumination should be controlled to provide high radiance only on the small spot on the surface so that the spot can be easily distinguished from the surrounding surface and so that the imaging system can be aligned to the desired spot. The direction of the active illumination should be controlled to align the illuminated target point on the optical axis of the imaging system to be used on a reflective surface.

The illumination should be controlled to provide the variation of the size and intensity of the target surface to cause the specific irradiance variation on the image area to be used as the distance control information.

4.2.2. Illumination source

There are two types of illumination sources:incoherent and coherent. Typical thermal radiation sources are incoherent sources. Monochromatic laser beams possess a high coherency with a beam profile of specific intensity distribution. Conventional thermal light sources not only emit many wavelengths but also emit randomly with the result that total energy is, on the average, radiated in all directions. The amount of energy in particular direction is proportional to the solid angle subtended by the observing device. Any attempt to

increase the brightness of an image over the brightness of the source of the lens cannot succeed, because even under ideal conditions the reduced area of the the image just makes up for the reduced collection angle that the lens intercepts from the source. In contrast, the coherent light produced by a laser is generated over a sizable volume with the proper phase, so that when it is focused with a lens, all the individual contributions by the atoms in lasing medium are in correct phase to add up. Accordingly,with a suitable lens, essentially all the energy of the laser can be concentrated into a very small spot, resulting in much greater energy density than the energy density of the source[2,10,11].

Accordingly, the laser radiation has superior characteristics to the incoherent radiation for an active illumination medium. The coherent property makes it possible to focus the laser beam into a spot only a few wavelengths in diameter. The single-wavelength characteristic helps to effectively identify and select a target point from the environment and reduces the correction requirement for the chromatic aberration of the imaging lens.

4.3. Optical system arrangement

Based on the requirements of application environment, the limitations of an imaging system, and the requirements of the controlled illumination discussed in the previous sections, an optical system can be configured as in Figure 4.1 to be used as a focusing control system. The optical system is represented as a single lens system.

Two different systems - an imaging system and an illumination control system - are combined to establish a specific relationship between the distance to the target surface and the irradiance on the image plane.

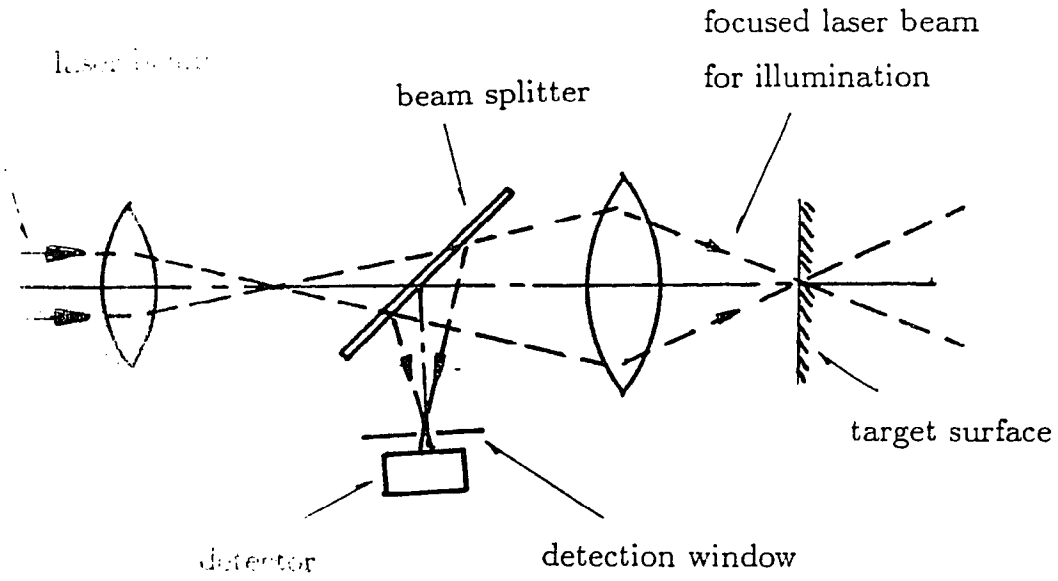

Figure 4.1. Optical system arrangement

4.3.1. Controlled illumination system

The controlled illumination is provided by a laser beam which has the Gaussian beam characteristics. The laser is focused by the lens to form the beam waist at a specific distance from the lens. The distance between the beam waist and the lens is specifically determined by the beam sizes at the beam waist and the lens plane. Alternatively, the size of the beam waist can be determined by the distance between the beam waist and the lens and the size of the beam profile at the lens plane from Eqs. 3.19 - 3.20.

The Gaussian beam provides a varying illumination condition on the target surface depending on the location of the target surface. The size and the intensity of the illuminated spot on the target surface become minimum and maximum, respectively, when the target surface is located at the beam waist. With the increase of the distance between the target surface and the beam waist, the illuminated spot on the taget surface will become larger in size and lower in intensity as expressed in Eq. 3.16- 3.22.

If the target surface is diffusive, the illuminated area will scatter the incident beam in all directions and can be distinguished from its surrounding area by its higher radiant intensity. The size and the radiant intensity of this spot are determined by those of the profile of the gaussian beam incident on the area.

If the surface is highly reflective, the Gaussian beam will be reflected on the surface and will propagate with the beam charateristics changed by the surface curvature and the texture of the surface.

4.3.2. Imaging system

The imaging system consists of the imaging lens and detection unit and has the identical axis as the laser focusing system.

The imaging system uses the same lens used in the laser beam focusing as an imaging lens. The imaging lens collects the scattered and/or reflected beam, which is provided by the controlled illumination system, and forms the image on the detection plane which is defined by the location of the detector window. The detection window is a pinhole mask and controls the amount of light energy reaching the detector. As the detection window has a fixed size and is located on the axis, the response of the detector is the total irradiance of the image formed on the detection window.

4.3.3. The relationship between the location of the target surface and the detector response

For a reflective target surface, the reflected beam on the surface will enter the imaging system and form a new waist. This location of the new beam waist is defined as the location of the detector. As the size and the location of the new beam waist formed changes depending on the location of the target surface, the detector has a window which has a fixed opening area with a circular shape to monitor the power of the beam passing through the window.

The location and the size of the detection window and the detector is the position of the new beam waist formed by the imaging lens when the target surface is located at the waist of the illumination beam. For the target surface not positioned at the location of the waist of the illumination beam, the imaging system will form the beam waist at other than the location of the detection window and the beam cross section on the detection window will become larger. The power detected through the detection window will vary specifically depending on the location of the target surface.

For a diffusive target surface, the surface scatters the incident Gaussian beam and the illuminated surface can be distinguished from its surroundings by its

high radiance. The size and the intensity of this area is defined by those of the incident Gaussian beam. The imaging system will form the image of the illuminated area on the detection window. Similarly to the case of the reflective surface, the size and the intensity of the image formed on the detection window will become smallest and highest when the target surface is located at the waist of the illumination beam. The power response of the detector varies in a specific pattern with relation to the distance between the target surface and the waist of the illumination beam.

This pattern is a bell-shaped curve in both the reflective and the diffusive cases of the target surface characteristics with the peak response occuring when the target surface is located at the waist of the illumination beam.

By monitoring the response curve of the detector as the distance between the optical system and the target surface varies, the situation that the target surface is located at the waist of the illumination beam can be found.

CHAPTER V

CONTROLLED SURFACE ILLUMINATION BY A GAUSSIAN BEAM

In an imaging system, the energy distribution of the image is directly related to the those of the object. The object can be defined as the area on a target surface, which is selectively illuminated by an Gaussian beam. Therefore, the size and the radiation intensity of the object are determined by those of the incident Gaussian beam on the surface and by the reflection characteristics of the surface. The proposed focusing control method depends on the diverging rate of the illumination beam. Because that the propagation characteristics of the Gaussian beam is determined solely by the size of the beam waist as described by Eqs.3.16 - 3.18, smaller size of the beam waist is desirable to increase the efficiency of the focusing control. It is generally necessary to shape the Gaussian beam to a desired specification from a practical laser output, which normally has a small diverging rate and a substantial beam size. Using one or more lenses, the propagation characteristics of the Gaussian beam can be changed to a desired specification. In addition, there are other factors to be considered in beam shaping by a lens; the distance to the new beam waist from the lens and the effect of the lens aperture which limits the transmitting beam radius.

5.1. Gaussian beam shaping

An ideal lens leaves the transverse field distribution of an incoming Gaussian beam mode unchanged. However, it changes the radius of the curvature of the beam wave front $R(z)$ and forms a new beam waist. An ideal thin lens of focal length f transforms an incoming spherical wave with a radius

R_1 immediately to the left of the lens into a spherical wave with a radius R_2 immediately to the right of it. The diameter of the beam is the same immediately to the left and to the right of the thin lens[6]. From the known parameters of the input beam - the radius w_o and the location d_1 of the beam waist -, the parameters of the beam transformed by an ideal thin lens of focal length f can be derived using Eqs. 3.16-3.20 as follows. Referring to Figure 5.1, the radius R_2 of curvature of the transformed wave right after the lens can be found from the geometric imaging form Eq.3.1.

$$
\begin{aligned}
R_2 &= \frac{fR_1}{R_1 - f} \\
&= \frac{\left[1 + \left(\frac{\pi w_o^2}{\lambda d_1}\right)^2\right] f d_1}{\left[1 + \left(\frac{\pi w_o^2}{\lambda d_1}\right)^2\right] d_1 - f} \\
&= \frac{\left[1 + \left(\frac{\pi w_o^2}{\lambda d_1}\right)^2\right] f d_1}{\left[1 + \left(\frac{\pi w_o^2}{\lambda d_1}\right)^2\right] d_1 - f} \frac{d_1}{d_1} \\
&= \frac{f\left[d_1^2 + \left(\frac{\pi w_o^2}{\lambda}\right)^2\right]}{d_1^2 + \left(\frac{\pi w_o^2}{\lambda}\right)^2 - d_1 f}.
\end{aligned}
\tag{5.1}
$$

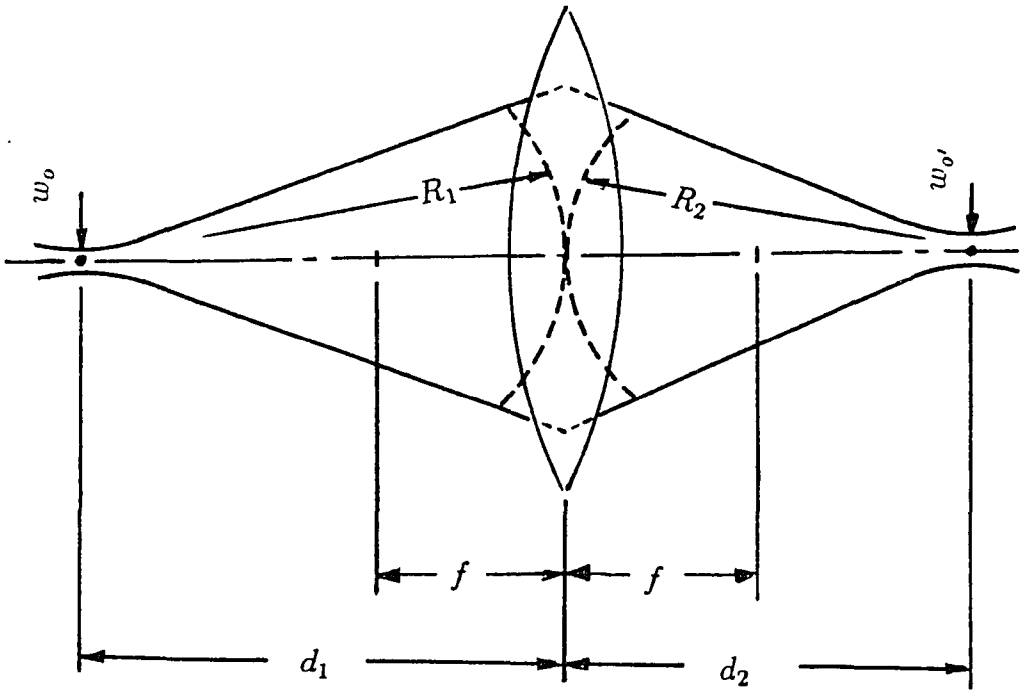

Figure 5.1. Transformation of Gaussian beam by a lens

The beam radius w_l at the plane of the thin lens can be given as

$$\begin{aligned} w_l^2 &= w^2(d_1) \\ &= \left[1 + \left(\frac{\lambda d_1}{\pi w_o^2}\right)^2\right] w_o^2. \end{aligned} \tag{5.2}$$

The location of the new beam waist can be derived as

$$d_2 = \frac{R_2}{1 + \left(\frac{R_2 \lambda}{\pi w_l^2}\right)^2}, \tag{5.3}$$

$$= \frac{\left\{\frac{f\left[d_1^2 + \left(\frac{\pi w_o^2}{\lambda}\right)^2\right]}{d_1^2 + \left(\frac{\pi w_o^2}{\lambda}\right)^2 - d_1 f}\right\}}{1 + \left(\frac{\left\{\lambda \frac{f\left[d_1^2 + \left(\frac{\pi w_o^2}{\lambda}\right)^2\right]}{d_1^2 + \left(\frac{\pi w_o^2}{\lambda}\right)^2 - d_1 f}\right\}}{\pi w_o^2 \left[1 + \left(\frac{\lambda d_1}{\pi w_o^2}\right)^2\right]}\right)^2},$$

$$= \frac{f\left[\pi w_o^2 + \frac{(\lambda d_1)^2}{\pi w_o^2}\right]^2 \left[d_1^2 + \left(\frac{\pi w_o^2}{\lambda}\right)^2\right] \left[d_1^2 + \left(\frac{\pi w_o^2}{\lambda}\right)^2 - d_1 f\right]}{\left\{\lambda f\left[d_1^2 + \left(\frac{\pi w_o^2}{\lambda}\right)^2\right]\right\}^2 + \left[\pi w_o^2 + \frac{(\lambda d_1)^2}{\pi w_o^2}\right]^2 \left[d_1^2 + \left(\frac{\pi w_o^2}{\lambda}\right)^2 - d_1 f\right]^2}. \tag{5.4}$$

Finally, the radius of the new beam waist can be given as

$$w_{o'}^2 = \frac{w_l^2}{1+\left(\frac{\pi w_l^2}{\lambda R_2}\right)^2}, \tag{5.5}$$

$$= \frac{w_o^2\left[1+\left(\frac{\lambda d_1}{\pi w_o^2}\right)^2\right]}{1+\left(\frac{\pi w_o^2\left[1+\left(\frac{\lambda d_1}{\pi w_o^2}\right)^2\right]}{\left\{\lambda\frac{f\left[d_1^2+\left(\frac{\pi w_o^2}{\lambda}\right)^2\right]}{d_1^2+\left(\frac{\pi w_o^2}{\lambda}\right)^2-d_1 f}\right\}}\right)^2},$$

$$= \frac{\left\{\lambda f\left[d_1^2+\left(\frac{\pi w_o^2}{\lambda}\right)^2\right]\right\}^2 w_o^2\left[1+\pi+\left(\frac{\lambda d_1}{\pi w_o^2}\right)^2\right]}{\left\{\lambda f\left[d_1^2+\left(\frac{\pi w_o^2}{\lambda}\right)^2\right]\right\}^2+\left[\pi w_o^2+\frac{(\lambda d_1)^2}{\pi w_o^2}\right]^2\left[d_1^2+\left(\frac{\pi w_o^2}{\lambda}\right)^2-d_1 f\right]^2}. \tag{5.6}$$

Although the above relationships are based on the transformation by an ideal thin lens, they are equally applicable to more complex systems, provided that the distances from the principal planes and the combined focal length are used. The specifications of the desired shape of the final beam can be given by the radius w_f of the beam waist and the distance z_f of the beam waist from the transforming lens. It may be necessary to shape the beam in a cascade system with multiple lens elements for successive transformation. The sizes of the lenses can be determined from the beam sizes on the each lens surfaces. In addition, the effects of the limited apertures of the lenses - the effective power transmission rate and the diffraction effect - should be considered.

5.2. The location and size of a transformed beam waist

There is a region around the beam waist, where the diverging rate of the beam is considerably small. This region is called Rayleigh or confocal region and defined by

$$\pm z_R = \frac{\pi w_o}{\lambda}, \tag{5.6}$$

using w_o as the general notation for the radius of the beam waist. The distance z_R defines the location at which the beam radius becomes $\sqrt{2}w_o$. The location of the transformed beam waist, d_2 in Eq.5.4, is slightly differ from that of the geometric image point which can be defined by R_2 in Eq.5.5. The distance between these two locations is given by

$$\begin{aligned} z_e &= R_2 - d_2 \\ &= d_2 \left[1 + \left(\frac{\pi w_f^2}{\lambda d_2} \right)^2 \right] - d_2 \\ &= \frac{1}{d_2} \frac{\pi w_f^2}{\lambda} \\ &= \frac{z_R}{d_2}. \end{aligned} \tag{5.7}$$

where w_f is the radius of the transformed beam waist. In the beam transformation for strong down-sizing of w_f,

$$d_2 >> z_R,$$

and the distance z_e in Eq.5.7 approaches an infinitesimal value. In this case, an Airy disk pattern is formed at the geometric image point, if an ideal lens is used in the beam transformation. The first ring of the Airy disk contains

86% of the beam energy transmitted through the effective aperture of the transforming lens. The first ring is defined by a radius w_A, which can be given, from Eq.3.11, as

$$w_A = \frac{0.61\ R_2\lambda}{r_p}, \tag{5.8}$$

where r_p is the effective lens aperture. If the predicted size of the transformed beam waist is smaller than the Airy disk, the Airy disk will dictate the minimum spot size[12].

5.3. The intensity distribution of a transformed beam

The intensity distribution of the Gaussian beam is Gaussian in every beam cross section while the beam radius increases as it expands through space, as expressed in Eq.3.22. A Gaussian beam after transformed by an optical system has a peak intensity, which occurs at the center of the beam waist,

$$I_f = T_i \cdot \left(\frac{w_o}{w_f}\right)^2 I_o, \tag{5.9}$$

where T_i is the optical system transmission, w_o and I_o are the radius and the peak intensity of the beam before transformation, and w_f is the radius of the transformed beam waist. The power of the transformed beam P_f is less than the original power P_o of the untransformed beam due to the limited apertures of the lenses.

$$\begin{aligned} P_f &= \int_0^{2\pi}\int_0^{r_p(0)} I_f \exp[-2(r/w_f)^2] r dr d\phi \\ &= \frac{\pi}{2} I_f w_f^2 \cdot \left(1 - \exp\left\{-2[r_p(0)/w_f]^2\right\}\right), \end{aligned} \tag{5.10}$$

where $r_p(0)$ is the radius of the nominal aperture of the beam shaping optic system projected onto the normal plane at the transformed beam waist and represents the cut-off radius which defines the zone with valid beam intensity. The nominal aperture of the beam shaping optic system is determined by one of the elements in the system, which has the smallest ratio of the aperture size to the beam diameter on the element surface. For other cross section of the transformed beam, the cut-off radius can be defined by

$$r_p(z) = r_p(0)\frac{w(z)}{w_f}. \tag{5.11}$$

An aperture with radius $r_p = w$ transmits about 86% of the total power in the Gaussian beam. w is the radius of beam waist where the intensity falls $1/e^2$ of the value at the axis. With radius $r_p = \frac{\pi}{2}w$, 99% of the total power can be transmitted through the aperture. Based on Eq. 3.21 and under the condition that the aperture of the optical system is large enough to neglect the diffraction effects, the intensity distribution of the transformed beam can be given by

$$I(z,r) = I_f \frac{1}{1+\left(\frac{\lambda z}{\pi w_f^2}\right)^2} \exp\left\{\frac{-2r^2}{w_f^2\left[1+\left(\frac{\lambda z}{\pi w_f^2}\right)^2\right]}\right\}, \tag{5.12}$$

for $r \leq r_p(z)$, otherwise, the intensity becomes zero.

5.4. Consideration of diffraction effects and aberration

The limited aperture in the beam transforming optic system truncates the Gaussian beam and causes diffraction effects. Along the transformed beam path, the field amplitude distribution in the near- and far-field can be given

by the diffraction formulas Eqs. 3.7 and 3.8, with the far-field pattern appearing in the focused beam spot. For an aperture with radius $r_p > 2w$, the diffraction effects along the beam axis and on the cross section of the propagating Gaussian beam in the near-field and the far-field are negligible. If the aperture radius is smaller than $2w$, then the rings become more prominent and the intensity distribution in the focal plane becomes more similar to that of the Airy disk. When the aperture radius is equal to w, the focused spot is qualitatively indistinguishable from an Airy disk. To make effective use of most of the optical properties of a Gaussian beam, the beam should not be apertured to less than $3w$. At an aperture with radius w or less, the Gaussian beam theory should be discarded and the apertured wave treated essentially as a wave of uniformed intensity[13-15].

Among the lens aberrations, the spherical aberration is a major importance in the beam transformation. The primary effect of the spherical aberration is to shift the effective focal point to a value between the paraxial and marginal foci, somewhat closer to the paraxial foci than to the marginal foci. The aberration also tends to introduce rings in the plane of the best focus, but these rings are in very low intensity. Since a Gaussian beam tends to concentrate its energy more along the axis of the beam , the effect of spherical aberration on a Gaussian beam is, in general, less than it would be for the same optical system with a uniformly illuminated wave[13,14].

5.5. Other considerations

Besides the diffraction and spherical aberration, there are other factors which can cause some deviation from the ideal characteristics of the transformed beam.

Any misalignment of the lens axes in the beam transforming optic system may deviate the axial beam intensity distribution as the axes of the beam and the optic system does not coincide. The imperfections and dusts on the surfaces of the optical elements produce beam scattering and cause interference in the beam path.

Most lasers exhibit both a primary spot and a secondary spot of light when the beam is viewed from a short distance. When the laser beam emerges from the exit mirror of the laser cavity, it passes through two glass surfaces . Internal reflections between these surfaces produce secondary rays which, unlike the primary beam , are highly divergent[16]. To remove this undesired rays, spatial filtering using a small pinhole may be employed.

The instability of the laser output caused by internal and external factors exhibits time-varying fluctuations of the beam intensity. The external instability can be caused by the floating particles in the beam path, which can scatter the beam. The internal instability is caused by the inherent lasing process in the laser cavity, especially, by the fluctuation of the power supply system[12].

5.6. Surface radiance

When the focused laser beam is incident upon the surface of a object body, some of it is, in general, directly reflected, some is diffusely reflected, while the other passes on into the substance of the body. Of this matter, some is absorbed, some os reflected back into the body of the surface of emergence, while the remainder emerges, some of it directly, according to the law of refraction, and the rest diffusely.

The energy relationship of these different reactions can be expressed as

$$Q_{incident} = Q_{absorbed} + Q_{transmitted} + Q_{reflected} \tag{5.13}$$

where Q denotes the energy.

The rate of the reflected energy to the total energy of the incident beam is given by reflectance ρ as

$$\rho = \frac{Q_{reflected}}{Q_{incident}} \tag{5.14}$$

Based on the specular response characteristics of an object body, the reflectance ρ varies depending on the frequency of the incident light[9].

If a surface is smooth and reflective, it reflects the incident light directly following the law of reflection. A flat surface can be defined as a mirror-like surface or a highly polished surface, if the reflected beam maintains the propagation characteristics of the incident Gaussian beam except the propagation direction, which is defined by the law of reflection.

If a surface is diffusive, it scatters the incident light in all directions. There are two general types of scattering; coherent scattering and incoherent scattering. In coherent scattering, a definite phase relationship exists between incoming and scattered waves, and interference can occur by two or more scattering centers. In incoherent scattering, no direct relationship exists between different parts of the scattered waves[2].

For a perfectly diffuse surface with a Gaussian beam illumination, the surface becomes a diffusive radiating source with a radiation intensity distribution identical to that of the incident Gaussian beam, if the scattering on the surface is considered as incoherent scattering by ignoring the interference

effect. The radiance N of an infinitesimal area dA on the diffusive surface can be given as follows.

Refering to Figure 5.2, the total power of the diffuse radiation from the area dA can be given as

$$\begin{aligned} P &= \int_0^{2\pi} \int_0^{\pi/2} N dA \cos\theta \cdot \frac{(rd\theta)(r\sin\theta d\phi)}{r^2} \\ &= \int_0^{2\pi} \int_0^{\pi/2} N dA \cos\theta \sin\theta d\theta d\phi \\ &= 2\pi N dA \left[\frac{\sin^2\theta}{2}\right]_0^{\pi/2} \\ &= \pi N dA \end{aligned} \tag{5.15}$$

The power P of the radiation from the area dA is identical to the power of the reflected beam on that area, and this can be expressed as

$$\begin{aligned} P &= \rho I_A dA \\ &= \pi N dA \end{aligned} \tag{5.16}$$

where $I_d A$ is the intensity of the incident beam.

Hence

$$N = \rho \frac{I_A}{\pi} \tag{5.17}$$

Even for highly polished surfaces, surface scattering can occur. This surface scattering may arise from irregularities such as scratches, digs, particulates which are larger than, comparable to, or smaller than the wavelength of incident beam. Dust particles on the surface, which have average diameters

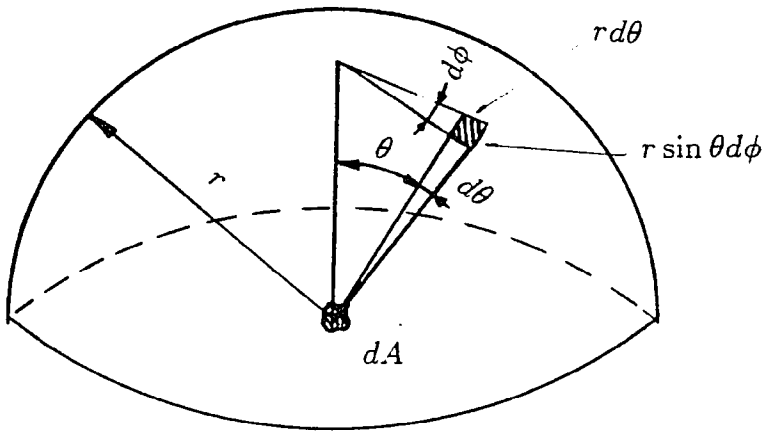

Figure 5.2. Radiation from a diffuse source

of about 1μm, also causes scattering. A number of different theoretical and emperical treatments can be used to evaluate the scattering from the microirregularities on the polished surface[17-20].

CHAPTER VI

ANALYSIS OF REFLECTIVE SURFACE RESPONSE

If an object with highly reflective surface is positioned in the propagating path of the Gaussian beam which is coming out from the system aperture, the beam will be reflected by the surface. The propagation characteristics and the direction of the propagation of the beam may be changed upon reflection on the surface, but the Gaussian intensity profile and coherency of the beam will be reasonably maintained, if the reflective surface has a smooth contour with specific radius of curvature. The degree of the maintaining the Gaussian intensity profile and coherency of the beam after reflection depends on the surface finish.

For a flat surface with mirror-like finish, which has a curvature with infinite radius, the reflected beam will maintain the Gaussian intensity profile, and some of it may reenter the system aperture, be transformed by the objective lens, and reach the detector. The total power of the beam reaching the detector varies depending on the location and inclination of the surface.

In this chapter, the detection response of the optical system will be discussed with relation to the positional variation of the object with a flat and reflective surface, and the location and size of the detection window will be determined.

6.1. Response from a vertically positioned flat surface

A flat surface, positioned normally to the axis of the illumination beam, will reflect the beam without changing its propagation characteristics except for the reversed direction of propagation, as illustrated in Figure 6.1.

The reflected beam will reenter the system aperture, be retransformed by the imaging system to form an imaged beam, and arrive at the plane of the

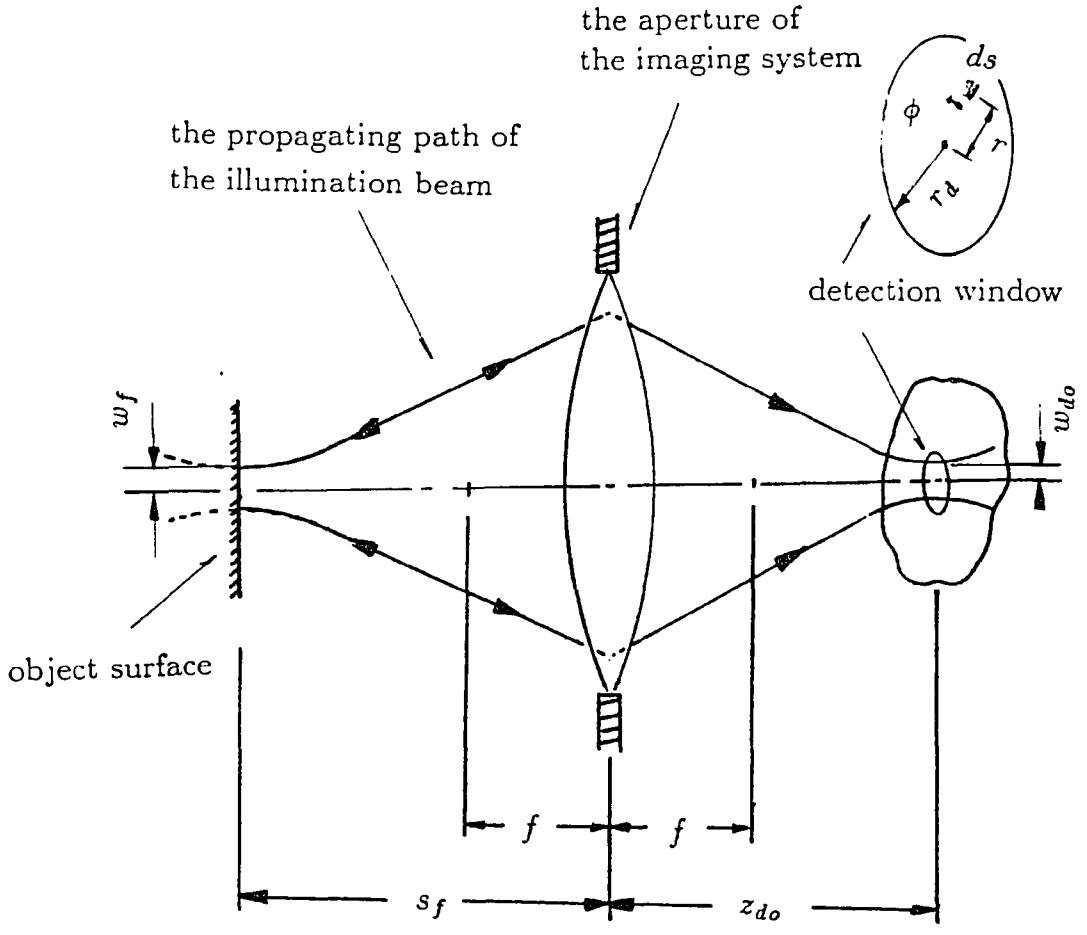

Figure 6.1. Reflection of the illumination beam on the object surface

detection window.

As the reflected beam has the Gaussian intensity profile, the imaged beam will have a new waist, the location and the size of which are determined by the location of the object surface and the focal length of the imaging system. At the plane of the detection window, the cross section of the imaged beam will have a different size and peak intensity, depending on the location of the object surface.

6.1.1. Determination of the location of the detection window

The system focus is defined by the location s_f of the waist of the illumination beam. For an object surface located at the system focus, the waist of the imaged beam will be formed at a location z_{do} and have a radius w_{do}. If the position of the object surface changes, the location and the radius of the imaged beam will change accordingly. However, the radius of the cross section of the imaged beam at a normal plane located at z_{do} can not be smaller than w_{do}.

If the detection window is located at z_{do}, the cross section of the imaged beam at the plane of the detection window will have minimum size and maximum peak intensity only when the object surface is located at a distance s_f from the imaging system.

From Eq.5.3, z_{do} is given by

$$z_{do} = \frac{\left[\pi w_f^2 + \frac{(\lambda s_f)^2}{\pi w_f^2}\right]^2 \left[s_f^2 + \left(\frac{\pi w_f^2}{\lambda}\right)^2\right] \left[s_f^2 + \left(\frac{\pi w_f^2}{\lambda}\right)^2 - s_f f\right] f}{\left\{\left[s_f^2 + \left(\frac{\pi w_f^2}{\lambda}\right)^2\right] \lambda f\right\}^2 + \left[\pi w_f^2 + \frac{(\lambda s_f)^2}{\pi w_f^2}\right]^2 \left[s_f^2 + \left(\frac{\pi w_f^2}{\lambda}\right)^2 - s_f f\right]^2} \quad (6.1)$$

where f is the focal length of the imaging system, and w_f is the radius of

the illumination beam waist, which is located at the system focus.

The location z_{d_o} differs slightly from the image position predicted by geometric optics. The difference will be discussed in more detail in Chapter VII.

The radius w_{d_o} of the waist of the imaged beam at the location z_{d_o} is given as, from Eq.5.6,

$$w_{do}^2 = \frac{\left\{\left[s_f^2 + \left(\frac{\pi w_f^2}{\lambda}\right)^2\right]\lambda f\right\}^2 w_f^2 \cdot \left[1 + \left(\frac{\lambda s_f}{\pi w_f^2}\right)^2\right]}{\left\{\left[s_f^2 + \left(\frac{\pi w_f^2}{\lambda}\right)^2\right]\lambda f\right\}^2 + \left[\pi w_f^2 + \frac{(\lambda s_f)^2}{\pi w_f^2}\right]^2 \left[s_f^2 + \left(\frac{\pi w_f^2}{\lambda}\right)^2 - s_f f\right]^2}. \quad (6.2)$$

The response of the detector which measures the power of the imaged beam that passes through the detection window is given by the total irradiance on the circular region of the detection window.

$$\begin{aligned} P_{d_o} &= \int_0^{2\pi}\int_0^{r_d} I_{d_o} \exp\left[-2(r/w_{d_o})^2\right] r dr d\phi \\ &= \frac{\pi}{2} I_{d_o} w_{d_o}^2 \cdot \left\{1 - \exp[-2(r_d/w_{d_o})^2]\right\} \end{aligned} \quad (6.3)$$

with

$$I_{d_o} = \rho T_i I_f \quad (6.4)$$

where I_{d_o} is the peak intensity at the waist of the imaged beam ;T_i is the transmission rate of the imaging system;ρ is the reflectance of the object surface;I_f is the peak intensity at the waist of the illumination beam;r and ϕ are the polar coordinates at the surface of the detection window.

If w_{do} is used as the radius of the detection window, 86% of the total power of the imaged beam can be detected.

6.1.2. The formation of the imaged beam

A change in position of the object surface causes a change of the location and size of the imaged beam waist and, accordingly, affects the size and intensity distribution of the cross section of the imaged beam at the plane of the detection window. This situation is illustrated in Figure 6.2.

For an object surface located at a distance z from the system focus which is located at a distance s_f from the principal plane of the imaging system, the location z_d and the radius w_d of the imaged beam waist are given, from Eqs.5.3 and 5.6, as

$$z_d(z) = \frac{\left\{ \left\{ \pi w_f^2 + \frac{[\lambda(s_f+z)]^2}{\pi w_f^2} \right\}^2 \left[(s_f+z)^2 + \left(\frac{\pi w_f^2}{\lambda} \right)^2 \right] \right.}{\left. \times \left[(s_f+z)^2 + \left(\frac{\pi w_f^2}{\lambda} \right)^2 - (s_f+z)f \right] f \right\}}$$
$$\left\{ \left\{ \pi w_f^2 + \frac{[\lambda(s_f+z)]^2}{\pi w_f^2} \right\}^2 \left[(s_f+z)^2 + \left(\frac{\pi w_f^2}{\lambda} \right)^2 - (s_f+z)f \right]^2 \right.$$
$$\left. + \left\{ \left[(s_f+z)^2 + \left(\frac{\pi w_f^2}{\lambda} \right)^2 \right] \lambda f \right\}^2 \right\}, \tag{6.5}$$

and

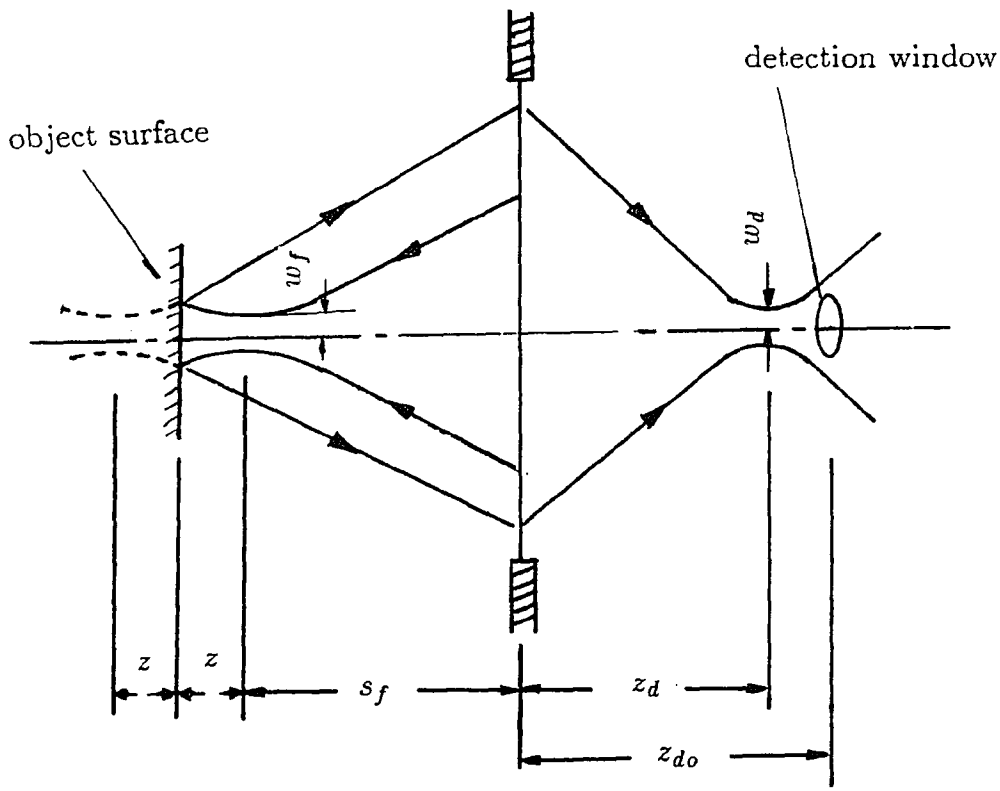

Figure 6.2. Formation of the imaged beam - vertical object surface

$$w_d(z)^2 = \frac{\left\{\left[(s_f+z)^2+\left(\frac{\pi w_f^2}{\lambda}\right)^2\right]\lambda f\right\}^2 w_f^2 \cdot \left[1+\left(\frac{\lambda(s_f+z)}{\pi w_f^2}\right)^2\right]}{\left\{\left\{\pi w_f^2+\frac{[\lambda(s_f+z)]^2}{\pi w_f^2}\right\}^2\left[(s_f+z)^2+\left(\frac{\pi w_f^2}{\lambda}\right)^2-(s_f+z)f\right]^2\right\}} \cdot$$
$$\left\{+\left\{\left[(s_f+z)^2+\left(\frac{\pi w_f^2}{\lambda}\right)^2\right]\lambda f\right\}^2\right\} \tag{6.6}$$

With these parameters of the imaged beam waist, the radius w_{dd} of the cross section of the imaged beam at the plane of the detection window can be expressed as

$$w_{dd}^2(z) = w_d(z)^2\left(1+\left\{\frac{[z_{d_o}-z_d(z)]\lambda}{\pi w_d^2(z)}\right\}^2\right) \tag{6.7}$$

6.1.3. Power response of the detection system

If the aperture size of the imaging system is assumed to be infinite, the detection response can be given by the total radiance on the detection window as

$$\begin{aligned} P_d(z) &= \int_0^{2\pi}\int_0^{r_d}\left[\frac{w_{d_o}}{w_d(z)}\right]^2 I_{d_o}\exp\{-2[r/w_d(z)]^2\}rdrd\phi \\ &= \frac{\pi}{2}I_{d_o}w_{d_o}^2\cdot(1-\exp\{-2[r_d/w_d(z)]^2\}). \end{aligned} \tag{6.8}$$

The effect of the limited aperture will be considered later.

The power response $P_d(z)$ can be compared with P_{do} as

$$\frac{P_d(z)}{P_{d_o}} = \frac{1 - \exp\left\{-2[r_d/w_d(z)]^2\right\}}{1 - \exp[-2(r_d/w_{d_o})^2]}. \tag{6.9}$$

where P_{do} is the power response of the vertical object surface when $z = 0$. This is the normalized rate of the power response for the vertical object surface located at a random position in the path of the illumination beam.

6.2. Response from an inclined flat surface

If the object surface is inclined from the axis normal, the amount of the reflected beam entering the imaging system will be limited because of the limited aperture size of the system. The propagating axis of the imaged beam will be inclined, and the shape, size, and intensity distribution of the cross section of the imaged beam at the plane of the detection window differ from the previous case of the vertical surface.

6.2.1. The formation of the imaged beam

If the axis of the reflected beam does not coincide with that of the imaging system, the imaged beam will have an inclined axis. The location of the imaged beam waist will not lie on the axis of the imaging system except when $\gamma = 0$. The shape of the cross section of the imaged beam on the plane of the detection window will not be circular, and the intensity distribution on the cross section is not Gaussian, in general. The shape and the intensity distribution of the cross section will depend on the parameters of the imaged beam, namely the location and the size of the imaged beam waist and the inclination angle of the imaged beam axis. These parameters of the imaged beam can be determined under an assumption that the aperture size of the imaging system is infinite. This assumption is valid, because the aperture

only limits the amount of energy passing through it and does not affect the path of the imaged beam, if the diffraction effect by the aperture edge is ignored.

For an inclined object surface located at a distance z from the system focus, the distance s_2 from the principal plane to the intersection of the axes of the imaged beam and the system is given, from geometric optics, as

$$s_2(z) = \frac{(s_f + z)f}{s_f + z - f}. \tag{6.10}$$

as illustrated in Figure 6.3.

The inclination angle γ_1 of the reflected beam is

$$\gamma_1 = 2\gamma \tag{6.11}$$

The inclination angle γ_2 of the imaged beam axis is given by geometry as

$$\gamma_2(z) = \tan^{-1}\left[\frac{s_f + z}{s_2(z)}\tan\gamma_1\right] \tag{6.12}$$

where γ is the inclination angle of the object surface.

The distance z_1 between the waist of the reflected beam and the the principal plane is

$$z_1(z) = \frac{s_f + z}{\cos\gamma_1} + z \tag{6.13}$$

From Eq. 3.17, the radius R_1 of the spherical wave of the reflected beam arriving at the principal plane can be expressed as

$$R_1(z) = z_1(z)\left\{1 + \left[\frac{\pi w_f^2}{\lambda z_1(z)}\right]^2\right\}. \tag{6.14}$$

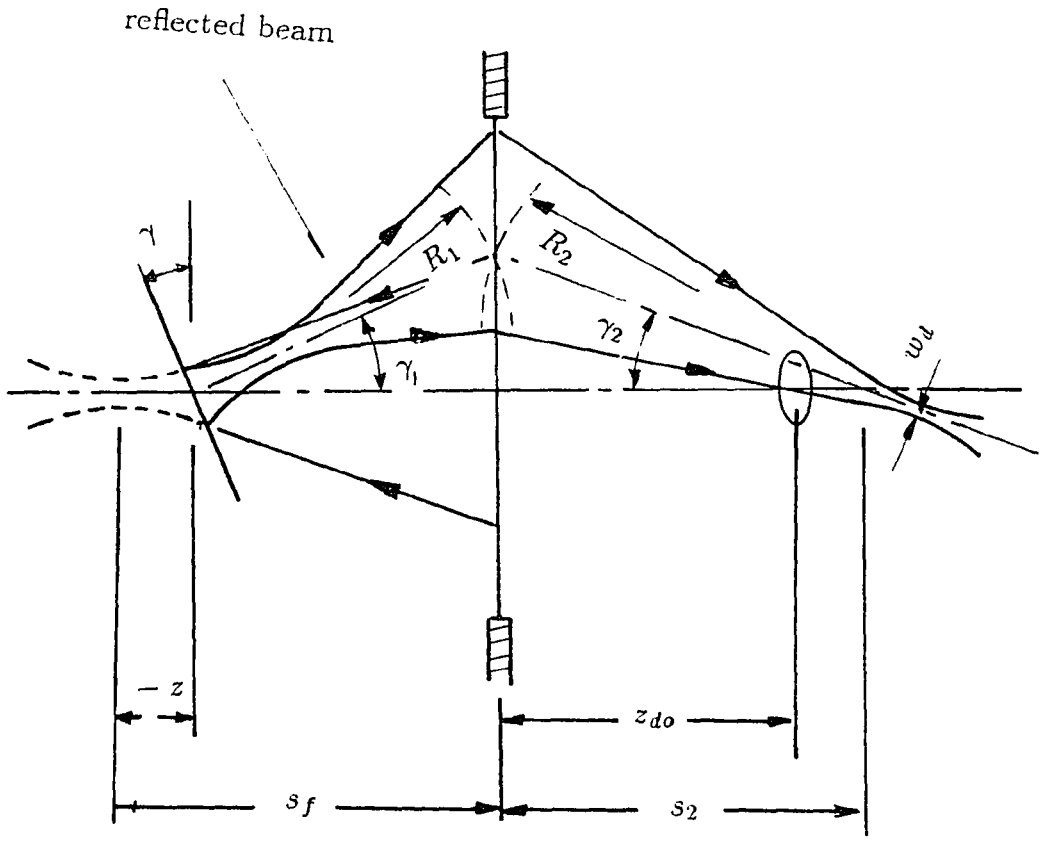

Figure 6.3. Formation of the imaged beam - inclined object surface

From geometric optics, the new radius R_2 of the spherical wave right after the principal plane is

$$R_2(z) = \frac{fR_1(z)\cos\gamma_1}{R_1(z)\cos\gamma_1 - f} \cdot \frac{1}{\cos\gamma_2(z)}. \tag{6.15}$$

The size and shape of the beam cross section does not change across the principal plane. Because of the inclination of the beam axis, the shape of the cross section on the principal plane is not circular unless the inclination angle is zero.

As illustrated in Figure 6.4, the height w_l of the bottom half of the cross section can be used as a reference dimension on the principal plane, and it can be written as

$$[w_l\cos\gamma_1]^2 = w_f^2 \cdot \left(1 + \left\{\frac{\lambda\,[z_1(z) - w_l\sin\gamma_1]}{\pi w_f^2}\right\}^2\right). \tag{6.16}$$

After arranging the terms in Eq.6.16, a quadratic equation in w_l can be derived.

$$\left(1 - \frac{\lambda^2\sin^2\gamma_1}{\pi^2 w_f^2\cos^2\gamma_1}\right) w_l^2 + \left[\frac{2\lambda^2 z_1(z)\sin\gamma_1}{\pi^2 w_f^2\cos^2\gamma_1}\right] w_l - \left[\frac{w_f^2}{\cos^2\gamma_1} + \frac{\lambda^2 z_1^2(z)}{\pi^2 w_f^2\cos^2\gamma_1}\right] = 0 \tag{6.17}$$

The two solutions for w_l in Eq. 6.17 are given by

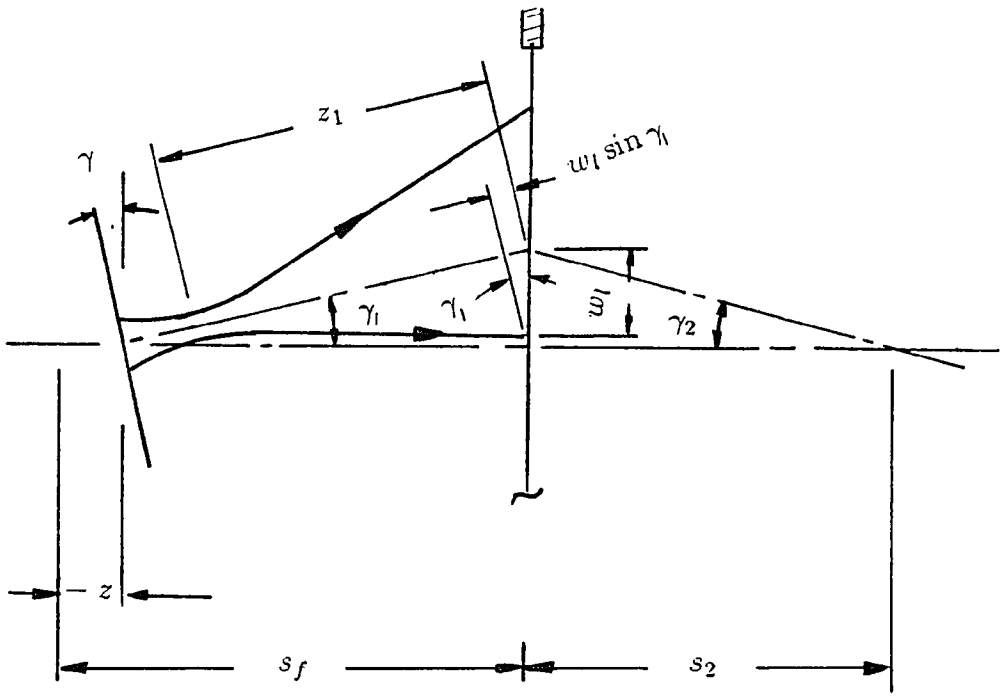

Figure 6.4. Beam cross section on the plane of the aperture

$$w_{l_{1,2}}(z) = -\frac{z_1(z)\lambda^2 \sin\gamma_1}{\pi^2 w_f^2 \cos^2\gamma_1} \Bigg/ \left(1 - \frac{\lambda^2 \tan^2\gamma_1}{\pi^2 w_f^2}\right)$$

$$\pm \frac{\sqrt{\left[-\frac{z_1(z)\lambda^2 \sin\gamma_1}{\pi^2 w_f^2 \cos^2\gamma_1}\right]^2 + \left(1 - \frac{\lambda^2 \sin^2\gamma_1}{\pi^2 w_f^2 \cos^2\gamma_1}\right)\left[\frac{w_f^2}{\cos^2\gamma_1} + \frac{\lambda^2 z_1^2(z)}{\pi^2 w_f^2 \cos^2\gamma_1}\right]}}{1 - \frac{\lambda^2 \sin^2\gamma_1}{\pi^2 w_f^2 \cos^2\gamma_1}}$$

$$= \frac{-\frac{z_1(z)\lambda^2 \sin\gamma_1}{\pi^2 w_f^2 \cos^2\gamma_1} \pm \frac{1}{\cos\gamma_1}\sqrt{w_f^2 \cdot \left\{1 + \left[\frac{\lambda z_1(z)}{\pi w_f^2}\right]^2\right\} - \frac{\lambda^2 \tan^2\gamma_1}{\pi^2}}}{1 - \frac{\lambda^2 \tan^2\gamma_1}{\pi^2 w_f^2}} \tag{6.18}$$

To be a valid solution, w_l must satisfy the following conditions

$$0 \leq \gamma_1 < \frac{\pi}{2}, \tag{6.19a}$$

$$w_l(z) > 0. \tag{6.19b}$$

The valid solution for w_l is given as

$$w_l(z) = \frac{-\frac{z_1(z)\lambda^2 \sin\gamma_1}{\pi^2 w_f^2 \cos^2\gamma_1} + \frac{1}{\cos\gamma_1}\sqrt{w_f^2 \cdot \left\{1 + \left[\frac{\lambda z_1(z)}{\pi w_f^2}\right]^2\right\} - \frac{\lambda^2 \tan^2\gamma_1}{\pi^2}}}{1 - \frac{\lambda^2 \tan^2\gamma_1}{\pi^2 w_f^2}} \tag{6.20}$$

The expression for w_{l_1} of Eq.6.20 is valid whether z_1 is larger or smaller than zero, i.e., whether the waist of the reflected beam is formed in front of the principal plane or in the rear of the principal plane.

The location z_2 and the radius w_d of the imaged beam waist can be derived from w_l, as the dimension of the beam cross section does not change across the principal plane.

By squaring both sides of Eq.6.20, we have

$$w_l^2(z) = \frac{1}{\cos^2\gamma_2(z)} w_d^2 \cdot \left(1 + \left\{\frac{\lambda[z_2 - w_l(z)\sin\gamma_2(z)]}{\pi w_d^2(z)}\right\}^2\right). \qquad (6.21))$$

Rearranging Eq.6.21 for w_d^2,

$$w_d^4 - \left[w_l^2(z)\cos^2\gamma_2(z)\right] w_d^2 + \left\{\frac{\lambda[z_2 - w_l(z)\sin\gamma_2(z)]}{\pi}\right\}^2 = 0 \qquad (6.22)$$

Using Eq. 3.20, w_d can also be written as

$$w_d^4 = \frac{\lambda^2}{\pi^2}[R_2(z)z_2 - z_2^2] \qquad (6.23)$$

After substituting w_d from Eq.6.23 to Eq.6.22, we have

$$\frac{\lambda^2}{\pi^2}[R_2(z)z_2 - z_2^2] - [w_l(z)\cos\gamma_2(z)]^2\frac{\lambda}{\pi}\sqrt{R_2(z)z_2 - z_2^2} + \left\{\frac{\lambda[z_2 - w_l(z)\sin\gamma_2(z)]}{\pi}\right\}^2 = 0 \qquad (6.24)$$

Eq. 6.24 can be rearranged as

$$\sqrt{R_2(z)z_2 - z_2^2} = -\frac{\lambda}{\pi[w_l(z)\cos\gamma_2(z)]^2}\{z_2[R_2(z) - 2w_l(z)\sin\gamma_2(z)] + [w_l(z)\sin\gamma_2(z)]^2\} \qquad (6.25)$$

After squaring both sides of Eq. 6.25, we have

$$R_2(z)z_2 - z_2^2 = \left\{ \frac{\lambda}{\pi[w_l(z)\cos\gamma_2(z)]^2} \right\}^2 \{z_2^2[R_2(z) - 2w_l(z)\sin\gamma_2(z)]^2$$
$$+ 2z_2[R_2(z) - 2w_l(z)\sin\gamma_2(z)][w_l(z)\sin\gamma_2(z)]^2$$
$$+ [w_l(z)\sin\gamma_2(z)]^2\}^2 \qquad (6.26)$$

A quadratic equation in z_2 can be derived from Eq. 6.26 as

$$z_2^2 \left([R_2(z) - 2w_l(z)\sin\gamma_2(z)]^2 + \left\{ \pi \frac{[w_l(z)\cos\gamma_2(z)]^2}{\lambda} \right\}^2 \right)$$
$$+ z_2 \left(2[R_2(z) - 2w_l(z)\sin\gamma_2(z)][w_l(z)\sin\gamma_2(z)]^2 \right.$$
$$\left. - \left\{ \pi \frac{[w_l(z)\cos\gamma_2(z)]^2}{\lambda} \right\}^2 R_2(z) \right)$$
$$+ [w_l(z)\sin\gamma_2(z)]^4 = 0 \qquad (6.27)$$

Of the two possible solutions of z_2 from Eq. 6.27, only one is valid based on the analysis of the case with $\gamma_2 = 0$. This is given as

$$z_2(z) = \frac{-\mathbf{B}_{z_2}(z) + \sqrt{\mathbf{B}_{z_2}^2(z) - 4\mathbf{A}_{z_2}(z)\mathbf{C}_{z_2}(z)}}{2\mathbf{A}_{z_2}(z)} \qquad (6.28a)$$

where

$$\mathbf{A}_{z_2}(z) = [R_2(z) - 2w_l(z)\sin\gamma_2(z)]^2 + \left\{\pi\frac{[w_l(z)\cos\gamma_2(z)]^2}{\lambda}\right\}^2 \quad (6.28b)$$

$$\mathbf{B}_{z_2}(z) = 2[R_2(z) - 2w_l(z)\sin\gamma_2(z)][w_l(z)\sin\gamma_2(z)]^2 - \left\{\pi\frac{[w_l(z)\cos\gamma_2(z)]^2}{\lambda}\right\}^2 R_2(z) \quad (6.28c)$$

$$\mathbf{C}_{z_2}(z) = [w_l(z)\sin\gamma_2(z)]^4 \quad (6.28d)$$

The radius w_d of the imaged beam waist can be obtained from Eq. 6.22 as

$$w_{d_1}^2(z) = \frac{1}{2}w_l(z)^2\cos^2\gamma_2(z) - \frac{1}{2}\sqrt{w_l(z)^4\cos^4\gamma_2(z) - 4\left\{\frac{\lambda\,[z_2(z) - w_l(z)\sin\gamma_2(z)]}{\pi}\right\}^2} \quad (6.29a)$$

$$w_{d_2}^2(z) = \frac{1}{2}w_l(z)^2\cos^2\gamma_2(z) + \frac{1}{2}\sqrt{w_l(z)^4\cos^4\gamma_2(z) - 4\left\{\frac{\lambda\,[z_2(z) - w_l(z)\sin\gamma_2(z)]}{\pi}\right\}^2} \quad (6.29b)$$

If z_2 is smaller than the confocal region z_R of the imaged beam, the radius of the waist of the imaged beam can not be smaller than the confocal radius $w_l(z)\cos\gamma_2(z)/\sqrt{2}$. Considering this condition, w_d^2 can be defined as

$$w_d^2(z) = \begin{cases} w_{d_1}^2(z), & \text{if } |z_2(z)| \le \frac{\pi w_l^2(z)\cos^2\gamma_2(z)}{2\lambda} + w_l(z)\sin\gamma_2(z) \\ w_{d_2}^2(z), & \text{otherwise} \end{cases} \quad (6.30)$$

6.2.2. Power response of the detection system

The power of the imaged beam reaching the detector is the total irradiance on the circular region of the detection window. Because of the inclination of the imaged beam axis, the pattern of the irradiance distribution on the detection window is not Gaussian, as the individual infinitesimal areas in the detection window lie on different normal cross sections of the imaged beam. If the aperture size of the imaging system is assumed to be infinite, the irradiance of an infinitesimal area in the detection window can be derived from the relative position of this area to the center of the imaged beam waist. As illustrated in Figure 6.5, the position of an infinitesimal area ds in the detection window, defined by the polar coordinates (r,ϕ), can be expressed as a function of z_{ds} and a ; theses are the cylindrical coordinate with its origin located at the center of the imaged beam waist. The cylindrical coordinates can be derived as follows.

The distance z_3, measured on the imaged beam axis, from the imaged beam waist to the plane of the detection window is

$$z_3(z) = z_2(z) - \frac{z_{do}}{\cos\gamma_2(z)}. \tag{6.31}$$

The distance y_d, measured on the plane of the detection window, from the center of the detection window to the imaged beam axis is given by

$$y_d(z) = [s_2(z) - z_d]\tan\gamma_2(z). \tag{6.32}$$

The axial distance z_{ds} from the imaged beam waist to the normal cross section where ds lies on can be defined by

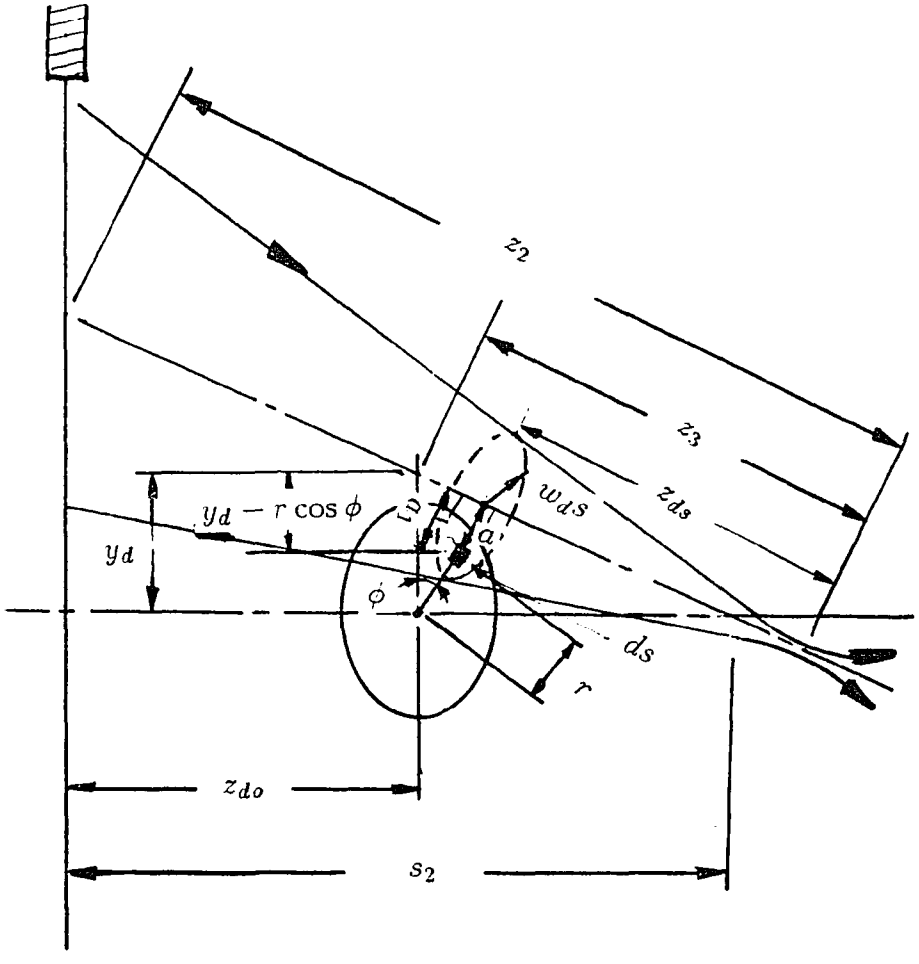

Figure 6.5. Geometry of the detection window

$$z_{ds}(z,r,\phi) = z_3(z) - [y_d(z) - r\cos\phi]\sin\gamma_2(z)$$

$$= z_2(z) - \frac{s_d(z)}{\cos\gamma_2(z)} - [y_d(z) - r\cos\phi]\sin\gamma_2(z) \qquad (6.33)$$

The radial distance a to ds from the axis center of the normal cross section can be expressed by

$$a(z,r,\phi) = \sqrt{a_1^2 + (r\sin\phi)^2}$$

$$= \sqrt{\{[y_d(z) - r\cos\phi]\cos\gamma_2(z)\}^2 + (r\sin\phi)^2} \qquad (6.34)$$

where

$$a_1 = [y_d(z) - r\cos\phi]\cos\gamma_2(z) \qquad (6.35)$$

The mean radius w_{ds} of the normal cross section is given

$$w_{ds}^2(z,r,\phi) = w_d^2(z)\left\{1 + \left[\frac{\lambda z_{ds}(z,r,\phi)}{\pi w_d^2(z)}\right]^2\right\} \qquad (6.36)$$

The irradiance at ds can be given by

$$H_{ds}(z,r,\phi) = I_{do}\cdot\left[\frac{w_{do}}{w_{ds}(z,r,\phi)}\right]^2 \exp\left\{-2\left[\frac{a(z,r,\phi)}{w_{ds}(z,r,\phi)}\right]^2\right\} \qquad (6.37)$$

where I_{do} and w_{do} are the radius and the peak intensity of the imaged beam waist when $z = 0$ and $\gamma = 0$, as defined by Eqs.6.2 and 6.4.

The power dP_{ds} at ds can be expressed by

$$dP_{ds}(z,r,\phi) = H_{ds}(z,r,\phi) r dr d\phi \cos\gamma_2(z) \tag{6.38}$$

In the above equation, the projected area $ds\cos\gamma_2$ is used instead of ds to include the effect of the area reduction due to the inclination of the imaged beam axis.

The total power P_d on the detection window can be given as

$$\begin{aligned} P_d(z) &= \int_0^{2\pi}\int_0^{r_d} dP_{ds}(z,r,\phi) \\ &= \int_0^{2\pi}\int_0^{r_d} H_{ds}(z,r,\phi)\cos\gamma_2(z) r dr d\phi \qquad (6.39) \\ &= \int_0^{2\pi}\int_0^{r_d} I_{do}\cdot\left[\frac{w_{do}}{w_{ds}(z,r,\phi)}\right]^2 \\ &\qquad \times \cos\gamma_2(z)\exp\left\{-2\left[\frac{a(z,r,\phi)}{w_{ds}(z,r,\phi)}\right]^2\right\} r dr d\phi \\ &= I_{do}w_{do}^2\cos\gamma_2(z)\int_0^{2\pi}\int_0^{r_d}\frac{\exp\left\{-2\left[\frac{a(z,r,\phi)}{w_{ds}(z,r,\phi)}\right]^2\right\}}{w_{ds}^2(z,r,\phi)} r dr d\phi \qquad (6.40) \end{aligned}$$

The normalized power response can be expressed as

$$\frac{P_d(z)}{P_d(0)} = \frac{\int_0^{2\pi}\int_0^{r_d}\frac{\exp\left\{-2\left[\frac{a(z,r,\phi)}{w_{ds}(z,r,\phi)}\right]^2\right\}}{w_{ds}^2(z,r,\phi)} r dr d\phi}{\int_0^{2\pi}\int_0^{r_d}\frac{\exp\left\{-2\left[\frac{a(0,r,\phi)}{w_{ds}(0,r,\phi)}\right]^2\right\}}{w_{ds}^2(0,r,\phi)} r dr d\phi} \tag{6.41}$$

where $P_d(0)$ is the power response when $z = 0$.

6.3. Consideration of the effect of the limited aperture

In the previous discussions, the aperture size of the imaging system was assumed to be infinite. In a practical imaging system, the finite sized aperture limits the energy input into the system by allowing only a portion of the beam to enter the clear aperture area.

If the object surface is inclined or located too far away from the aperture, the beam will be truncated by the aperture. The imaged beam will have the truncated cross section and propagate maintaining valid Gaussian intensity profile only in the truncated cross section, if the effect of the diffraction of the limited aperture is not considered.

The shape of the truncated beam cross section can be defined as the overlapping area of the two closed contours ;one is the circle representing the aperture, the other is the shape representing the beam cross section on the aperture plane. The sizes of the circle and the shape of the beam cross section can be defined by the radius r_a of the aperture and the height w_l of the bottom half of the cross section, respectively. The distance between the contours is determined by the location and inclination angle of the object surface.

As the imaged beam contracts or expands during propagation, the truncated cross section will be maintained, and the shape and size of the truncated section will be defined by the overlapping area of the two transformed contours, as illustrated in Figure 6.6.

At the plane of the detection window, the truncated beam cross section with valid intensity can be defined as follows.

The transformed height w_{lt} of the bottom half of the cross section of the untruncated beam at the plane of the detection window can be given, from

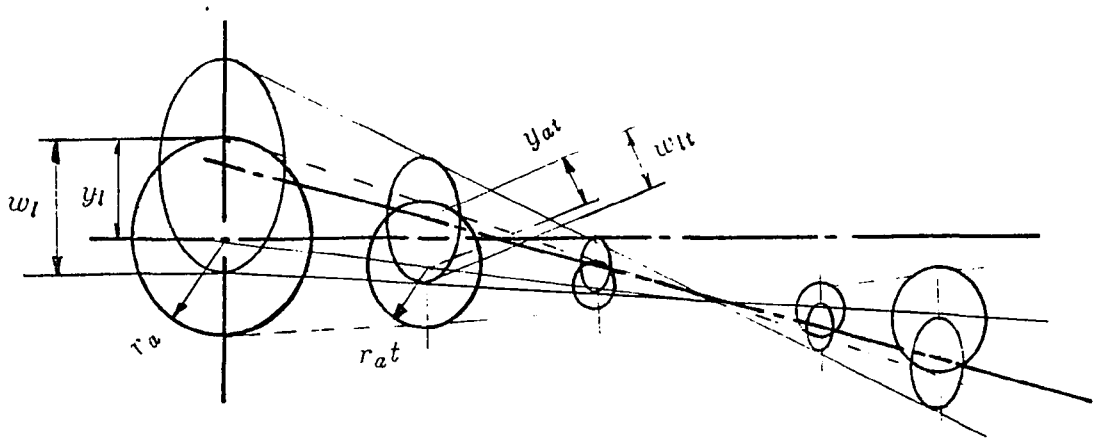

Figure 6.6. Truncated cross section of the imaged beam

Eqs. 6.20 and 6.31, as

$$w_{lt}(z) = -\left\{ \frac{\left[z_2(z) - \frac{z_{do}}{\cos\gamma_2(z)}\right]\lambda^2 \tan^2\gamma_2(z)}{\pi^2 w_d(z)^2} \right\} \Big/ \left[1 - \frac{\lambda^2\tan^2\gamma_2(z)}{\pi^2 w_d(z)^2}\right]$$
$$+ \frac{\frac{1}{\cos\gamma_2(z)}\sqrt{w_d(z)^2\left(1+\left\{\frac{\lambda\left[z_2(z)-\frac{z_{do}}{\cos\gamma_2(z)}\right]}{\pi w_d(z)^2}\right\}^2\right) - \frac{\lambda^2\tan^2\gamma_2(z)}{\pi^2}}}{1-\frac{\lambda^2\tan^2\gamma_2(z)}{\pi^2 w_d(z)^2}} \quad (6.42)$$

The radius r_{at} and distance y_{at} of the projected aperture at the plane of the detection plane can be given as

$$r_{at}(z) = r_a \frac{w_{lt}(z)}{w_l(z)}, \quad (6.43)$$

and

$$y_{at}(z) = y_l(z)\frac{w_{lt}(z)}{w_l(z)},$$
$$= (s_f + z)\tan\gamma_1 \frac{w_{lt}(z)}{w_l(z)}. \quad (6.44)$$

where y_l is the distance between the beam axis and the center of the aperture on the plane of the aperture, and w_l is the height of the bottom half of the beam cross section on the plane of the aperture.

The distance $y(z)$ between the center of the projected aperture and the center of the detection window on the detection plane is

$$y(z) = |y_d(z) - y_{at}(z)| \quad (6.45)$$

To reach the detector, the beam must pass through the detection window which has a circular shape with radius r_d.

The cross section of the beam which can reach the detector is defined by the overlapping area of the detection window and of the projected aperture on the plane of the detection window, under assumption that the reflected beam is not truncated before entering the imaging system. Because the detection window and the projected aperture have circular shapes with radii r_d and r_{at} respectively, six different overlapping cases can occur as illustrated in Figure 6.7.

The power response of the detector in the individual cases can be derived as follows.

Case 1: The two circles intersect at two points and the projected aperture encloses the center of the detection window.

The power response of the detector can be given, by means of Eqs. 6.37 - 6.39, as

$$\begin{aligned} P_d(z) =& 2\int_0^{\phi_1(z)}\int_0^{r_1(z,\phi)} I_{ds}(z,r,\phi)\cos\gamma_2(z) r\,dr\,d\phi \\ &+ 2\int_{\phi_1(z)}^{\pi}\int_0^{r_d} I_{ds}(z,r,\phi)\cos\gamma_2(z) r\,dr\,d\phi \end{aligned} \tag{6.46}$$

where $\phi_1(z)$ defines the angle of the intersection, and $r_1(z,\phi)$ is the distance from the center of the detection window to the boundary of the transformed aperture.

The angle $\phi_1(z)$ can be defined from the law of cosines as

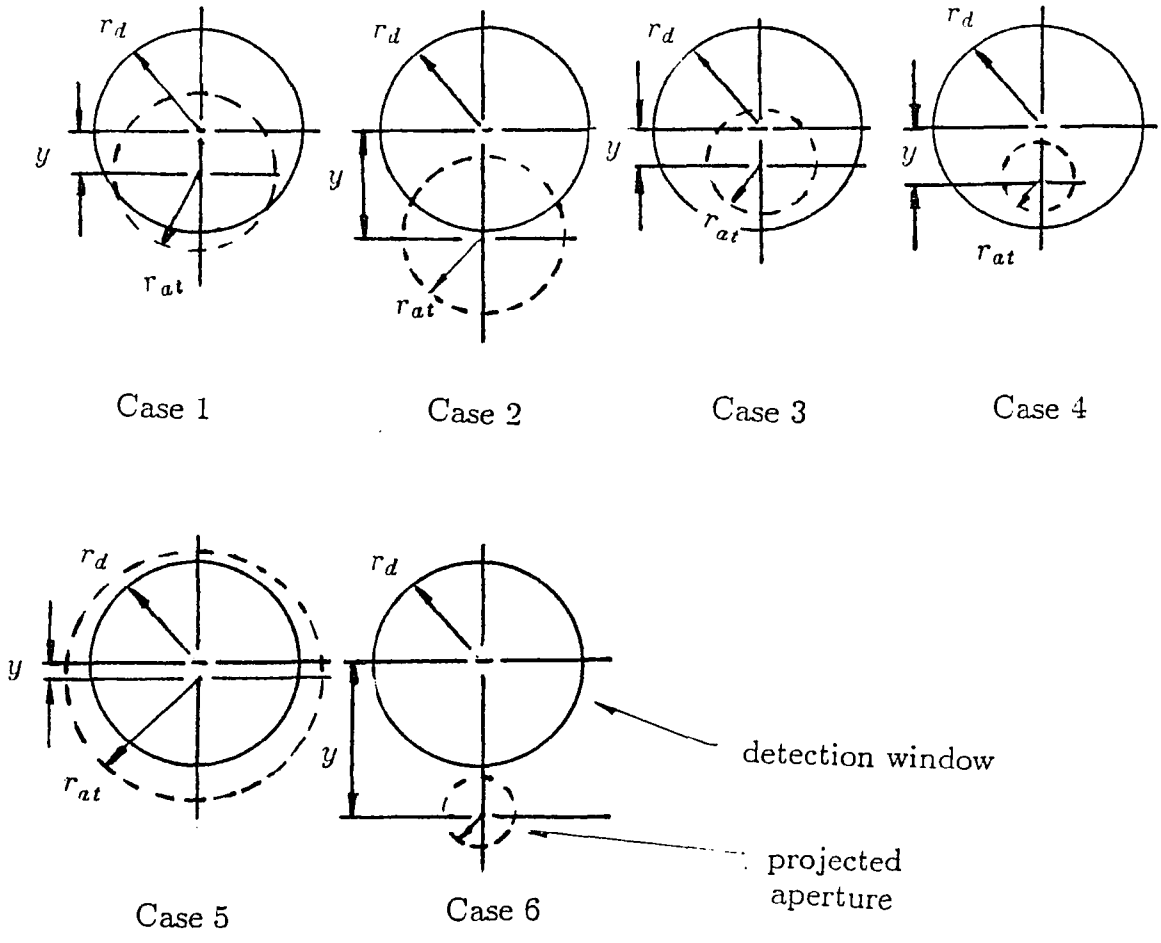

Figure 6.7. Overlapping cases of the detection window and the projected aperture

$$\begin{aligned}\cos[\pi - \phi_1(z)] &= -\cos\phi_1(z) \\ &= \frac{r_d^2 + y^2(z) - r_{at}^2(z)}{2y(z)r_d} \\ &= \Psi(z) \end{aligned} \tag{6.47}$$

with condition,

$$0 \leq \phi_1(z) = \cos^{-1}[-\Psi(z)] \leq \pi$$

From Figure 6.8, $r_1(z, \phi)$ can be given by

$$r_1^2(z, \phi) = r_{at}^2(z)\sin^2\phi + [r_{at}(z)\cos\phi - y]^2 \tag{6.48a}$$

or

$$r_1(z, \phi) = \sqrt{r_{at}^2(z) + y^2(z) - 2y(z)r_d\cos\phi} \tag{6.48b}$$

The necessary conditions for this overlapping case can be expressed by,

$$|\Psi(z)| < 1 \qquad \text{and} \qquad y(z) < r_{at}(z)$$

Case 2: The two circles intersect at two points and the projected aperture does not enclose the center of the detection window.
The necessary condition for this case can be given by

$$|\Psi(z)| < 1 \qquad \text{and} \qquad y(z) > r_{at}(z)$$

The power response of the detector can be expressed as

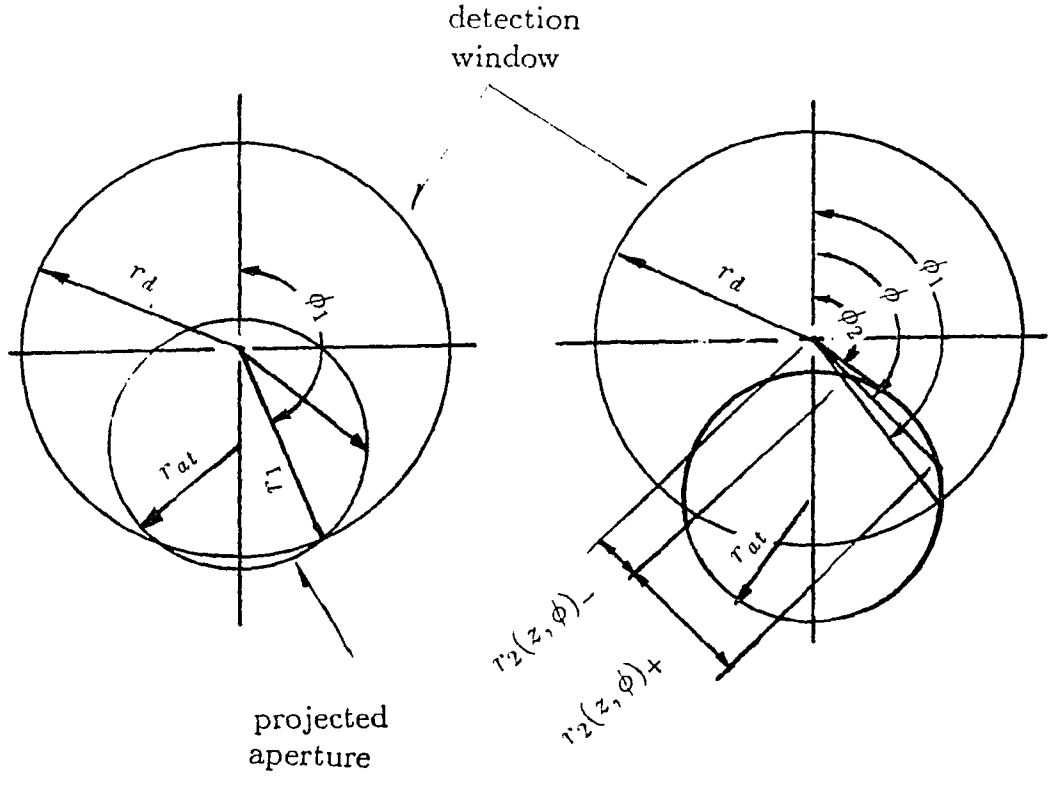

Figure 6.8. Overlapping area - Case 2

$$P_d(z) = 2\int_{\phi_2(z)}^{\phi_1(z)} \int_{r_{2-}(z,\phi)}^{r_{2+}(z,\phi)} I_{ds}(z,r,\phi)\cos\gamma_2(z) r\,dr\,d\phi$$

$$+ 2\int_{\phi_1(z)}^{\pi} \int_{r_{2-}(z,\phi)}^{r_d} I_{ds}(z,r,\phi)\cos\gamma_2(z) r\,dr\,d\phi \qquad (6.49)$$

where $\phi_2(z)$ defines the angle of the tangent to the projected aperture, and $r_{2+}(z,\phi)$ and $r_{2-}(z,\phi)$ are the distances from the center of the detection window to the boundary of the projected aperture. The angle $\phi_2(z)$ can be given as

$$\sin[\pi - \phi_2(z)] = \sin\phi_2(z)$$

$$= \frac{r_{at}(z)}{y(z)} \qquad (6.50)$$

or

$$\phi_2(z) = \sin^{-1}\left[\frac{r_{at}(z)}{y(z)}\right] \qquad (6.51)$$

with condition,

$$\pi/2 \leq \phi_2(z) \leq \pi$$

From Figure 6.8, r_{2-} and r_{2+} can be derived as follows.

$$r\sin\phi = r_{at}(z)\sin\theta \qquad (6.52)$$

$$-r\cos\phi + r_{at}(z)\cos\theta = y(z) \qquad (6.53)$$

Eq. 6.52 can be expressed as

$$r = r_{at}(z)\frac{\sin\theta}{\sin\phi} \tag{6.54}$$

After substituting r with the expression of Eq.6.53 and rearranging the terms, Eq. 6. 53 can be expressed as

$$\begin{aligned}\cos\theta &= \sqrt{1-\sin^2\theta} \\ &= \frac{y(z)}{r_{at}(z)} + \frac{1}{\tan\phi\sin\theta}\end{aligned} \tag{6.55}$$

After squaring both sides of Eq.6.55, we have

$$1-\sin^2\theta = \left[\frac{y(z)}{r_{at}(z)}\right]^2 + \left(\frac{1}{\tan\phi}\right)^2\sin^2\theta + 2\left[\frac{y(z)}{r_{at}(z)}\right]\left(\frac{1}{\tan\phi}\right)\sin\theta \tag{6.56}$$

From this quadratic equation in $\sin\theta$, the solutions for $\sin\theta$ can be derived as

$$\begin{aligned}\sin\theta &= \frac{-\frac{y(z)}{r_{at}(z)\tan\phi} \pm \sqrt{\left[\frac{y(z)}{r_{at}(z)\tan\phi}\right]^2 - \left(1+\frac{1}{\tan^2\phi}\right)\left\{\left[\frac{y(z)}{r_{at}(z)}\right]^2 - 1\right\}}}{1+\frac{1}{\tan^2\phi}} \\ &= \frac{\tan\phi\left\{-\frac{y(z)}{r_{at}(z)} \pm \sqrt{\left[\frac{y(z)}{r_{at}(z)}\right]^2 - \left(\tan^2\phi+1\right)\left\{\left[\frac{y(z)}{r_{at}(z)}\right]^2 - 1\right\}}\right\}}{\tan^2\phi+1} \\ &= \frac{\tan\phi\left[-\frac{y(z)}{r_{at}(z)} \pm \sqrt{\sec^2\phi - \left[\frac{y(z)}{r_{at}(z)}\right]^2\tan^2\phi}\right]}{\sec^2\phi} \\ &= \sin\phi\left[-\frac{y(z)}{r_{at}(z)}\cos\phi \pm \sqrt{1-\left[\frac{y(z)}{r_{at}(z)}\right]^2\sin^2\phi}\right]\end{aligned} \tag{6.57}$$

From Eq.6.54 and 6.57, we have

$$r = r_{at}(z)\frac{\sin\theta}{\sin\phi}$$

$$= -y(z)\cos\phi \pm r_{at}(z)\sqrt{1-\left[\frac{y(z)}{r_{at}(z)}\right]^2\sin^2\phi} \qquad (6.58a)$$

The values of $r_2(z,\phi)_-$ and $r_2(z,\phi)_+$ can be given from Eq.6.58a as

$$r_2(z,\phi)_- = -y(z)\cos\phi - r_{at}(z)\sqrt{1-\left[\frac{y(z)}{r_{at}(z)}\right]^2\sin^2\phi} \qquad (6.58b)$$

$$r_2(z,\phi)_+ = -y(z)\cos\phi + r_{at}(z)\sqrt{1-\left[\frac{y(z)}{r_{at}(z)}\right]^2\sin^2\phi} \qquad (6.58c)$$

Case 3: The detection window is enclosed by the projected aperture.

In this case, there may be no or one intersection point.

The necessary condition can be given by

$$y(z) \le r_{at}(z) - r_d \qquad \text{and} \qquad r_{at}(z) \ge r_d$$

$$\Psi(z) \le -1$$

The power response of the detector becomes,

$$P_d(z) = 2\int_0^{\pi}\int_0^{r_d} I_{ds}(z,r,\phi)\cos\gamma_2(z) r\,dr\,d\phi \qquad (6.59)$$

Case 4: The projected aperture is enclosed by the detection window, and the projected aperture encloses the center of the detection window.

The necessary condition can be given as

$$y(z) \leq r_d - r_{at}(z) \qquad \text{and} \qquad y(z) < r_{at}(z) \leq r_d$$

$$\Psi(z) \geq 1$$

The power response of the detector becomes,

$$P_d(z) = 2 \int_0^{\pi} \int_0^{r_1(z,\phi)} I_{ds}(z, r, \phi) \cos \gamma_2(z) r dr d\phi \tag{6.60}$$

Case 5: The projected aperture is enclosed by the detection window, and the projected aperture does not enclose the center of the detection window. The necessary condition can be given as

$$r_{at} \leq y(z) \leq r_d - r_{at}(z) \qquad \text{and} \qquad r_{at}(z) \leq r_d$$

$$\Psi(z) \geq 1$$

The power response of the detector becomes,

$$P_d(z) = 2 \int_{\phi_1}^{\pi} \int_{r_2(z,\phi)_-}^{r_2(z,\phi)_+} I_{ds}(z, r, \phi) \cos \gamma_2(z) r dr d\phi \tag{6.61}$$

Case 6: No overlapping of the two circles. The following condition must be satisfied for no overlapping.

$$y(z) \geq r_d + r_{at}(z) \qquad \text{and} \qquad \Psi(z) \geq 1$$

There is no beam passing through the detection window, and there is no detection response.

$$P_d(z) = 0 \tag{6.62}$$

The power responses in the different cases above can be summarized in one expression, under an assumption that the beam is not truncated before entering the imaging system.

$$P_d(z) = 2\int_{\tilde{\phi}_1(z)}^{\tilde{\phi}_2(z)}\int_{\tilde{r}_1(z,\phi)}^{\tilde{r}_2(z,\phi)} I(z,r,\phi)\cos\gamma_2(z) r dr d\phi + 2\int_{\tilde{\phi}_3}^{\pi}\int_{\tilde{r}_1(z,\phi)}^{r_d} I(z,r,\phi)\cos\gamma_2(z) r dr d\phi \tag{6.63}$$

where

$$0 \le \tilde{\phi}_1(z), \tilde{\phi}_2(z), \tilde{\phi}_3(z) \le \pi \tag{6.64}$$

and

$$\tilde{\phi}_1(z) = \begin{cases} \sin^{-1}\left[\frac{r_{at}(z)}{y(z)}\right], & \text{if } |\Psi(z)| \ge 1 \text{ and } r_{at}(z) < y(z) < r_d - r_{at}(z) \\ & \quad \text{or if } |\Psi(z)| < 1 \text{ and } y(z) > r_{at}(z); \\ 0, & \text{otherwise.} \end{cases} \tag{6.65}$$

$$\tilde{\phi}_2(z) = \begin{cases} \cos^{-1}[-\Psi(z)], & \text{if } |\Psi(z)| < 1; \\ \pi, & \text{if } \Psi(z) \ge 1 \text{ and } y(z) < r_{at}(z); \\ 0, & \text{otherwise.} \end{cases} \tag{6.66}$$

$$\tilde{\phi}_3(z) = \begin{cases} \cos^{-1}[-\Psi(z)], & \text{if } |\Psi(z)| < 1; \\ \pi, & \text{if } \Psi(z) \ge 1\ ; \\ 0, & \text{otherwise.} \end{cases} \tag{6.67}$$

$$\tilde{r}_1(z,\phi) = \begin{cases} r_{11}(z,\phi), & \text{if } |\Psi(z)| \ge 1 \text{ and } r_{at}(z) < y(z) < r_d - r_{at}(z) \\ & \quad \text{or if } |\Psi(z)| < 1 \text{ and } y(z) > r_{at}(z); \\ r_d, & \text{if } \Psi(z) \ge 1 \text{ and } y(z) \ge r_d + r_{at}(z); \\ 0, & \text{otherwise.} \end{cases} \tag{6.68}$$

$$\tilde{r}_2(z,\phi) = \begin{cases} r_{21}(z,\phi), & \text{if } (\Psi(z) \geq 1 \text{ and } y(z) \geq r_{at}(z)) \\ & \quad \text{or if } (|\Psi(z)| < 1 \text{ and } y(z) < r_{at}(z)); \\ r_{22}(z,\phi), & \text{if } |\Psi(z)| \geq 1 \text{ and } r_{at}(z) < y(z) < r_d - r_{at}(z) \\ & \quad \text{or if } |\Psi(z)| < 1 \text{ and } y(z) > r_{at}(z); \\ r_d, & \text{if } \Psi(z) \geq 1 \text{ and } y(z) \geq r_d + r_{at}(z); \\ 0, & \text{otherwise.} \end{cases} \tag{6.69}$$

where

$$r_{11}(z,\phi) = -y(z)\cos\phi - r_{at}(z)\sqrt{1 - \left[\frac{y(z)}{r_{at}(z)}\right]^2} \tag{6.70}$$

$$r_{21}(z,\phi) = \sqrt{r_{at}^2(z) + y^2(z) - 2r_{at}(z)y(z)\cos\phi} \tag{6.71}$$

$$r_{22}(z,\phi) = -y(z)\cos\phi + r_{at}(z)\sqrt{1 - \left[\frac{y(z)}{r_{at}(z)}\right]^2} \tag{6.72}$$

If the illumination beam has a truncated intensity profile due to the limited aperture of the beam shaping system, the area of the integration should be modified to exclude the area which does not lie within the truncated beam profile. If a numerical integration is used to evaluate Eq. 6.63-6.72, $\tilde{r}_1(z,\phi)$, $\tilde{r}_2(z,\phi)$, and r_d should be compared with the radius r_p of the truncated beam, which is given in Eq. 5.11.

If the object surface is located within a short distance from the system focus and if the inclination angle of the object surface is small, the diffraction effect caused by the limited aperture of the imaging system is not significant. The diffraction effect will be increased significantly, if the distance between the object surface and the aperture increases. If the inclination of the object

surface increases, the truncation of the beam by the aperture becomes considerable, and the diffraction effect will be severe enough so that the Gaussian intensity profile will be no longer valid.

For small z variation with small inclination angle, the diffraction effect is not significant. Even for large z and γ, the normalized power response expressed in Eq. 6.63-6.72 is expected to be reasonable because the power response is the measurement of the total irradiance on the detection window. To include the diffraction effect, the irradiance expression in Eq. 6.37 should be modified.

CHAPTER VII

ANALYSIS OF DIFFUSIVE SURFACE RESPONSE

If a highly diffusive surface is positioned across the propagating path of a laser beam, the surface scatters the incident laser beam in all directions and can be treated as a collection of independent point radiators, the strength of which varies from point to point according to the radiation characteristics of the surface. The distribution of the field amplitude and intensity on the object surface depends on that of the incident Gaussian beam and on the scattering characteristics of the surface.

For this diffusive object surface, the imaging system will form an image of the illuminated area of the object surface at a location predicted by geometric optics. If the plane of the detection window, the location of which was determined in Chapter VI, is used as the fixed image plane, the detector response will depend on the irradiance of the image formed on the detection window. In this chapter, the detector response will be analyzed with relation to the location and the inclination of an object surface, under an assumption that the object surface is flat and perfectly diffusive, i.e., the secondary radiation characteristic of the surface follows Lambert's law[see Chapter III].

7.1. Location of the image plane

If a diffusive surface is positioned at the waist of the illumination beam, which is located at a distance s_f from the principal plane of the imaging system, the imaging system will form an image of the illuminated area of the object surface at a distance s_d from the principal plane of the imaging system. The distance s_d is, from geometric optics, given as

$$s_d = \frac{s_f f}{s_f - f}, \tag{7.1}$$

where f is the focal length of the imaging system.

The magnification of the imaging system is, from Eq. 3.2, given by

$$m = -\frac{s_d}{s_f}. \tag{7.2}$$

This situation is illustrated in Figure 7.1.

The location of the image plane slightly differs from that of the detection window, which was defined in Chapter VI using the Gaussian beam transformation principle. The difference δ_1 of the two locations is given as

$$\delta_1 = s_d - z_{do}, \tag{7.3}$$

where z_{do} is the distance to the detection window from the principal plane of the imaging system and is given by Eq. 6.1.

If w_f is very small and s_f is considerably larger than f, the distance between the image plane and the detection window becomes infinitesimal, i.e., $\delta_1 \approx 0$. If the plane of the detection window is defined as the image plane, the location of the corresponding object plane is determined by

$$s_o = \frac{z_{do} f}{z_{do} - f}, \tag{7.4}$$

where s_o is the distance to the object plane from the principal plane of the imaging system.

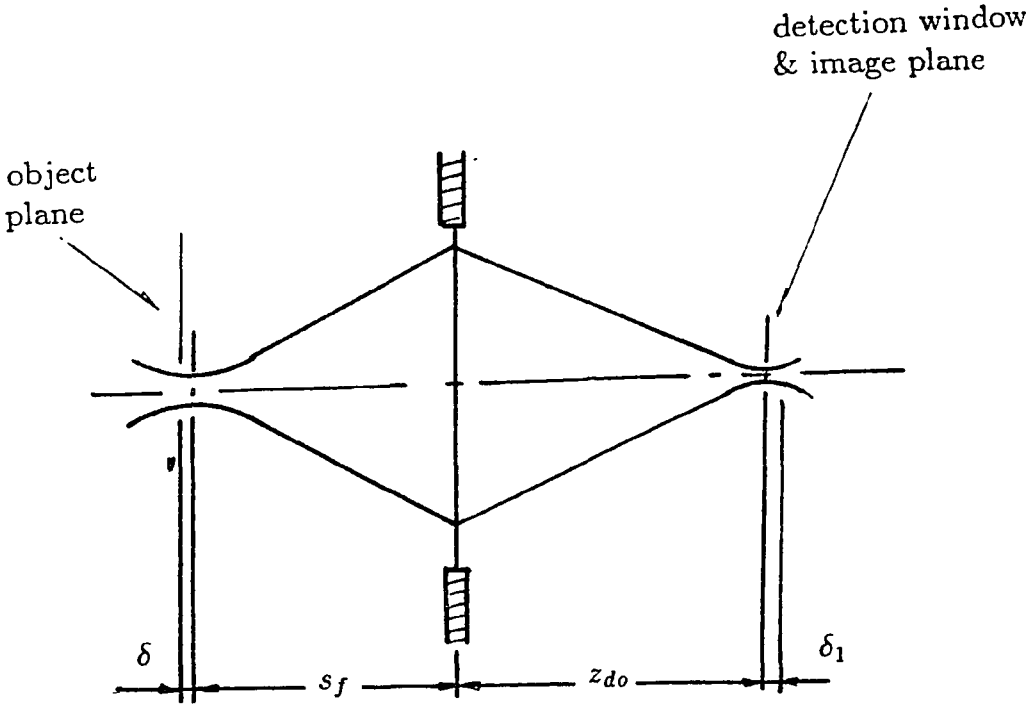

Figure 7.1. Imaging system

The location of the object plane differs slightly from the location of the waist of the illumination beam, and the difference δ of the two locations is expressed as

$$\delta = s_o - s_f. \tag{7.5}$$

Similarly to the case of δ_1, δ becomes infinitesimal if w_f is very small and s_f is considerably larger than f.

7.2. Intensity distribution on the image plane

The intensity distribution $I_i(x_i, y_i)$ on the image plane predicted by geometric optics is an exact replica of the object, magnified and reversed as

$$I_i(x_i, y_i) = \frac{1}{m^2} I_o(-\frac{x_o}{m}, -\frac{y_o}{m}), \tag{7.6}$$

where $I_o(-\frac{x_o}{m}, -\frac{y_o}{m})$ is the intensy distribution on the object plane, x_i and y_i are the point coordinates on the image plane, x_o and y_o are the point coordinates on the object plane, and m is the magnification factor of the system and is given by Eq. 7.2.

In an ideal imaging system, the intensity distribution of the image is a smoothed pattern of the image predicted by geometric optics because of the diffraction effect of the lens aperture, and this is given by[5,21]

$$I_i(x_i, y_i) = \frac{k}{m^2} \int_{-\infty}^{\infty} \int_{-\infty}^{\infty} [h(x_i - mx_o, y_i - my_o)]^2 \times I_g(mx_o, my_o) dx_o dy_o, \tag{7.7}$$

where k is a real constant and $I_g(mx_o, my_o)$ is the geometric intensity distribution pattern given by Eq.7.6. The impulse response $h(x_i - mx_o, y_i - y_o)$ is the Fraunhofer diffraction pattern and is given by

$$h(x_i - mx_o, y_i - my_o) =$$

$$K \int_{-\infty}^{\infty} \int_{-\infty}^{\infty} P(x,y) \exp\left[-j\frac{2\pi}{\lambda s_d}[(x_i - mx_o)z + (y_i - my_o)y]\right] dxdy, \quad (7.8)$$

where K is a complex constant and the value of the pupil function P is unity inside the pupil and zero outside the pupil.

If the object is illuminated by an incoherent source, the image will have the intensity distribution pattern given by Eq.7.8.

If the object surface is illuminated by a coherent monochromatic source, the intensity distribution on the image plane differs from the previous expressions because of the interference effect, and this can be given by

$$I_i(x_i, y_i) = \frac{1}{m^2}\left[\int_{-\infty}^{\infty} \int_{-\infty}^{\infty} h(x_i - mx_o, y_i - my_o) U_g(mx_o, my_o) dx_o dy_o\right]^2, \quad (7.9)$$

where $U_g(mx_o, my_o)$ is the amplitude distribution pattern on the image plane and is given, from geometric optics, as

$$U_g(x_i, y_i) = \frac{1}{m^2} U_o(-\frac{x_o}{m}, -\frac{y_o}{m}), \quad (7.10)$$

where $U_o(-\frac{x_o}{m}, -\frac{y_o}{m})$ is the amplitude distribution pattern on the object plane.

7.3. The method for the analysis of the power response of the detector

If the plane of the detection window is defined as the image plane, the corresponding object plane will be located at a distance s_o from the principal

plane. If a diffusive surface is positioned at the location of the object plane, the imaging system will form an image of the object, the size of which is defined by the illuminated area on the surface by the incident Gaussian beam, on the detection window. Because of the coherent illumination, the intensity distribution on the image plane will have the pattern given in Eq. 7.9.

If the surface is positioned at other than the location of the object plane, the size of the object will increase as the profile of the incident Gaussian beam increases, and the image will be formed in front of or in the rear of the plane of the detection window. With the increase of the distance between the surface and the object plane, the image will be formed further away from the plane of the detection window, and the intensity distribution pattern on the plane of the detection window will be a blurred image of the object. Additionally, vignetting will occur, as the object size grows and the distance between the object and the object plane increases.

Regardless of the position of the object surface, the area of the object surface, which produces the irradiance on the detection window, can be traced by projecting the detection window through the imaging system and onto the object surface. Of the scattering rays emanating from this area of the object surface, only the rays which follow specific ray paths can enter the aperture of the imaging system and reach the detection window. From geometric optics, the path can be determined using the projected detection window on the object plane, as illustrated in Figure 7.2.

Only and all the rays which pass through this projected detection window on the object plane and enter the aperture of the imaging system can reach the detection window, if the diffraction effect of the aperture edge is ignored. The radius r_f of the projected detection window at the object plane is determined

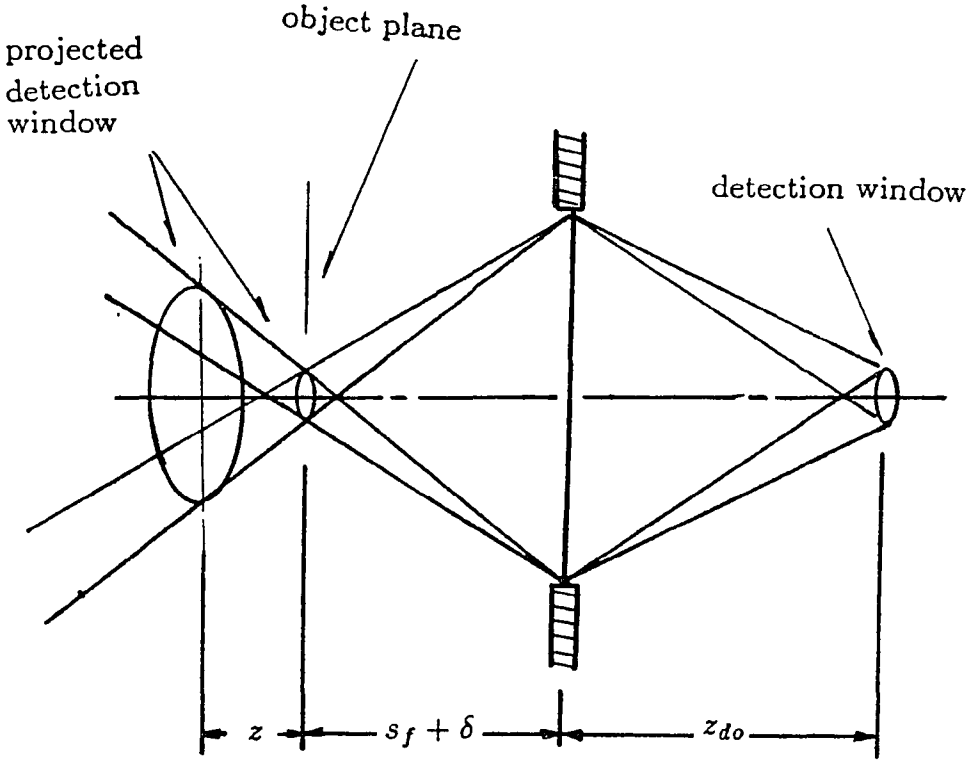

Figure 7.2. Projection of the detection window

as

$$r_f = r_d \frac{s_o}{z_{do}} \tag{7.11}$$

where r_d is the radius of the detection window, and z_{do} is the distance to the detection window from the principal plane of the imaging system.

The rays, which are originated from the object surface and arriving at the detection window, interfere each other adding or cancelling their field amplitudes depending on their phase relationships, as the coherent illumination is used. The resulting intensity distribution pattern differs from that of the incoherent case, in which interference does not occur as no phase relationship exists among the rays. Despite of the difference in the intensity distribution pattern, the total irradiance over a finite area should be equal in both cases because of the same amount and energy of the rays arriving on the area.

The response of the detector which measures the total irradiance on the detection window can be derived based on radiometry by treating the coherent imaging as an incoherent imaging. If the object surface is positioned at the location of the object plane and the value of δ is infinitesimal, the size and the intensity distribution of the waist of the illumination beam can be used as those of object. If the imaging system is assumed to be an ideal diffraction limited system, the corresponding image which is formed on the detection window will be a smoothed pattern of the geometric image which is the replica of the object, magnified and reversed.

If the size of the detection window is larger than the size of the image, most of the energy of the image will be confined within the detection window. Little energy of the outer Fraunhofer rings of the image , which are formed outside of the edge of the detection will be lost. Furthermore, as the object

has a Gaussian intensity profile, the energy of the image will be concentrated at the center region of the image, and the energy loss across the edge of the detection window will be further reduced. As the distance between the object surface and the object plane increases, the intensity across the edge of the detection window will become more even, and the loss and the gain of the energy across the boundary will approach more similar level.

Based on the considerations described above, the total irradiance on the detection window can be derived from geometric imaging and radiometry instead of coherent imaging. In following sections, the detection response will be analyzed using the principles of incoherent illumination, geometric imaging , and radiometry, and the effects of the coherent illumination will be ignored.

7.4. Radiance of the object surface

The radiance of the diffusive object surface which is positioned across the propagating path of the illumination beam depends on the beam intensity of the incident illumination beam surface and on the surface reflectance.

The maximum radiance N_f occurs when the surface located at the waist of the illumination beam and is given, from Eq. 5. 16, by

$$N_f = \frac{1}{\rho}\pi I_f \tag{7.12}$$

where ρ is the reflectance of the object surface, I_f is the peak intensity at the waist of the illumination beam.

For an surface area, the position of which is given by (z, r) using the cylindrical coordinate with the origin at the center of the beam waist, the radiance $N(z, r)$ is expressed as

$$N(z,r) = N_f \left[\frac{w_f}{w(z)}\right]^2 \exp\left\{-2\left[\frac{r}{w(z)}\right]^2\right\} \qquad (7.13a)$$

where w_f is the radius of the beam waist, $w(z)$ is the mean radius of the beam at a distance z from the waist.

If the illumination beam has a truncated profile due to the limited aperture during the beam transformation, the radiance expression in Eq.7.13 is valid only within the truncated beam profile. This condition can be expressed as

$$r < r_p(z) \qquad (7.13b)$$

The truncated beam radius $r_p(z)$ is discussed in Section 5.3 and is expressed in Eq.5.11.

7.5. Response from a vertical object surface

For a diffusive surface positioned vertically to the axis of the illumination beam, the irradiance of the image will be contributed by the radiation rays which are originated from the object surface and follow the specific path, which is determined by the projected window on the object plane and the aperture of the imaging system.

The total irradiance on the detection window depends on the amount and strength of the radiating rays which enter the imaging system through this path. The power response P_d of the detector can be expressed as

$$P_d = T_i P_a \qquad (7.14)$$

where T_i is the transmission of the imaging system, and P_a is the power of the rays entering the system through the path and does not include the

contribution of the rays entering the aperture without passing through the path.

7.5.1. Response from an object surface located at the object plane

If the vertical surface is located at the object plane as illustrated in Figure 7.3, the power P_a intercepted by the aperture can be derived as follows.

For an infinitesimal area ds located at the center of the object plane, the power intercepted by the aperture of the imaging system can be derived using the method used in Eq. 3.14 as follows.

The power $dP_{dm|ds}$ produced at an area dm on the aperture by an infinitesimal radiation area ds, which is located at the center region of the object surface, is given by

$$\begin{aligned} dP_{dm|ds} &= N(\delta,0)ds\cos\theta\cos\theta\frac{dm}{s_o'^2} \\ &= N(\delta,0)ds\cos^2\theta\frac{s_o\tan\theta d(s_o\tan\theta)d\beta}{(s_o/\cos\theta)^2} \\ &= N(\delta,0)ds\cos^2\theta\frac{s_o^2\tan\theta\sec^2\theta d\theta d\beta}{(s_o/\cos\theta)^2} \\ &= N(\delta,0)ds\cos^2\theta\tan\theta d\theta d\beta \end{aligned} \tag{7.15}$$

where $N(\delta,0)$ is the radiance at ds.

Of the radiation from ds, the power $P_{|ds}$ intercepted by the whole aperture

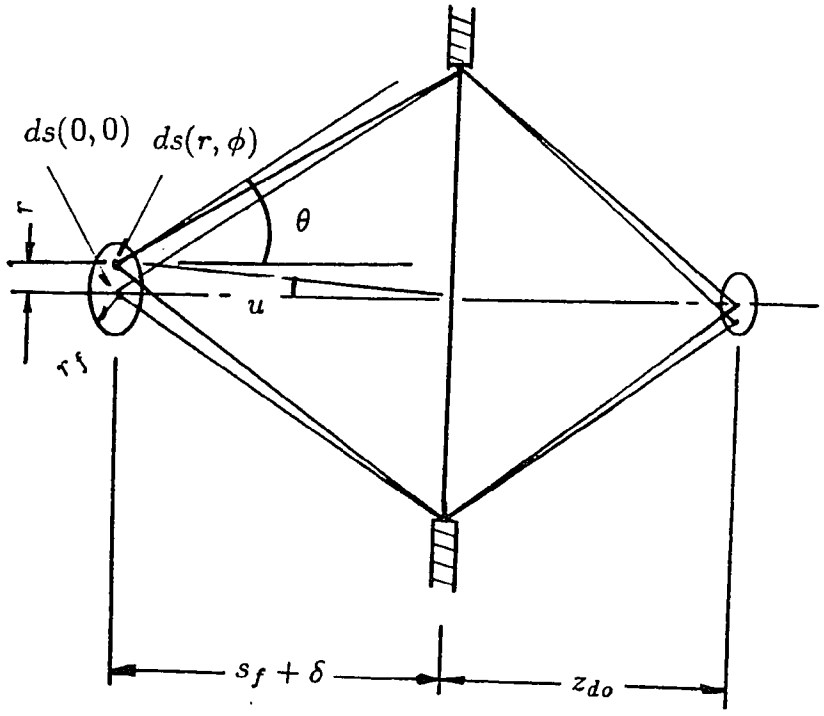

Figure 7.3. Imaging of a vertical surface - object plane

area can be given by

$$\begin{aligned} dP_{|ds} &= \int_0^{2\pi} \int_0^{\theta_a} dP_{dm|ds} \\ &= \int_0^{2\pi} \int_0^{\theta} N(\delta,0) ds \cos^2\theta \tan\theta d\theta d\beta \\ &= 2\pi N(\delta,0) \left[\frac{\sin^2\theta}{2}\right]_0^{\theta_a} ds \\ &= \pi N(\delta,0) \sin^2\theta_a ds \end{aligned} \tag{7.16}$$

If the radiation area ds is not located at the center region of the object, the power intercepted by the aperture can be shown to be[22,23]

$$dP_{|ds} = \frac{\pi N(\delta,r)}{2} \left[1 - \frac{1 + \tan^2 u - \tan_a^\theta}{\sqrt{\tan^4 u + 2\tan^2 u \cdot (1 - \tan^2\theta_a) + \sec^4\theta_a}}\right] ds \tag{7.17}$$

where r is the distance to ds from the axis, $N(\delta,r)$ is the radiance of ds, and θ_a and u are given as

$$\theta = \tan^{-1}\frac{r_a}{s_o} \tag{7.18}$$

$$u = \tan^{-1}\frac{r}{s_o} \tag{7.19}$$

where r_a is the radius of the aperture.

If $r_f << s_o$

$$\tan u = \frac{r_f}{s_o} \approx 0 \tag{7.20}$$

By making $r_f << s_o$, the effect of the off axis distance r can be ignored, and Eq. 7.17 degenerates to Eq.7.16 as

$$dP_{|ds} \approx \pi N(\delta, r) \sin^2 \theta_a ds \tag{7.21}$$

The total power P_{ao} intercepted by the aperture is given, by integrating $dP_{|ds}$ over the radiation area within the projected detection window on the object plane, as

$$\begin{aligned}
P_a &= \int_0^{2\pi} \int_0^{r_f} dP_{|ds} \\
&= \int_0^{2\pi} \int_0^{r_f} \pi N(\delta, r) \sin^2 \theta_a r dr d\phi \\
&= 2\pi^2 N_f \sin^2 \theta_a \int_0^{r_f} \left[\frac{w_f}{w(\delta)}\right]^2 \exp\left\{-2\left[\frac{r}{w(\delta)}\right]^2\right\} r dr \\
&= 2\pi^2 N_f \sin^2 \theta_a \left[\frac{w_f}{w(\delta)}\right]^2 \left[-\frac{w^2(\delta)}{4} \exp\left\{-2\left[\frac{r}{w(\delta)}\right]^2\right\}\right]_0^{r_f} \\
&= \frac{1}{2}\pi^2 N_f \sin^2 \theta_a w_f^2 \cdot \left(1 - \exp\left\{-2\left[\frac{r_f}{w(\delta)}\right]^2\right\}\right)
\end{aligned} \tag{7.22}$$

The power response P_{do} is given as

$$P_{do} = T_i P_{ao} \tag{7.23}$$

7.5.2. Response from an object surface located at a random position

If the vertical object surface is positioned at other than the location of the object plane, the power intercepted by the area dm on the aperture is con-

tributed by the radiation rays which originated from the object surface and passed through the path determined by the area ds on the object plane and the area dm on the aperture, as described in Figure 7.4.

The area of the object surface, the radiation from which can pass through this path and enter the area dm, can be determined by projecting the whole aperture of the imaging system through the area ds and onto the object surface.

The power $dP_{dm|ds}(z)$ intercepted by the aperture area dm can be derived as follows.

The radial distance r' to an infinitesimal area dn on the object surface from the system axis is given by

$$r' = r + (z - \delta)\tan\theta\cos\beta. \tag{7.24}$$

where z is the distance between the object surface and the waist of the illumination beam.

The distance z' from ds to dn is given as

$$z' = \frac{(z - \delta)}{\cos\theta}. \tag{7.25}$$

The area of dn is expressed as

$$\begin{aligned} dn &= (z - \delta)\tan\theta d[(z - \delta)\tan\theta]d\beta \\ &= (z - \delta)^2 \tan\theta \sec^2\theta d\theta d\beta \end{aligned} \tag{7.26}$$

The power $dP_{dm|ds}(z)$ intercepted by the aperture area dm can be derived, from the irradiance $dH_{ds|dn}(z)$ produced at ds by the radiation area within

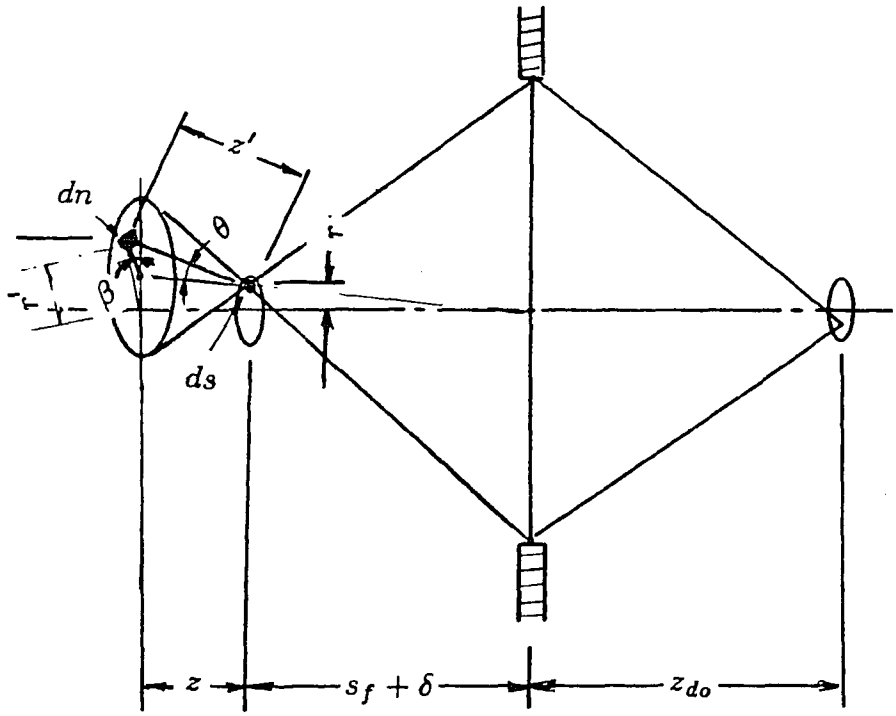

Figure 7.4. Imaging of a vertical surface - random location

the projected aperture on the object surface, as

$$
\begin{aligned}
dP_{dm|ds}(z) &= dH_{ds|dn}(z)ds \\
&= N(z,r')\cos^2\theta\frac{dn}{z'^2 ds} \\
&= N(z,r')\cos^2\theta\frac{(z-\delta)^2\tan\theta\sec^2\theta d\theta d\beta}{\left[\frac{(z-\delta)}{\cos\theta}\right]^2}ds \\
&= N_o\frac{w_f^2}{w^2(z)}\exp\left\{-2\left[\frac{r+(z-\delta)\tan\theta\cos\beta}{w(z)}\right]^2\right\} \\
&\qquad \times\cos^2\theta\tan\theta d\theta d\beta \qquad (7.27)
\end{aligned}
$$

Of the radiations which pass through the area ds on the object plane, the power $dP_{|ds}(z)$ intercepted by the whole aperture can be given by

$$
\begin{aligned}
dP_{|ds}(z) &= \int_0^{2\pi}\int_0^{\theta_a} dP_{ds|dm}(z) \\
&= \int_0^{2\pi}\int_0^{\theta_a} N_o\frac{w_f^2}{w^2(z)}\exp\left\{-2\left[\frac{r+(z-\delta)\tan\theta\cos\beta}{w(z)}\right]^2\right\} \\
&\qquad \times\cos^2\theta\tan\theta d\theta d\beta \qquad (7.28)
\end{aligned}
$$

The total power $P_a(z)$ intercepted by the aperture can be obtained by integrating dP_{ds} over the whole circular region of the projected detection window at the object plane. This can be expressed as

$$
\begin{aligned}
P_a(z) &= \int_0^{2\pi} \int_0^{r_f} dP_{|ds}(z) r dr d\phi \\
&= \int_0^{2\pi} \int_0^{r_f} \left(\int_0^{2\pi} \int_0^{\theta_a} dP_{dm|ds} \right) r dr d\phi \\
&= N_o \frac{w_f^2}{w^2(z)} \int_0^{2\pi} \int_0^{r_f} \int_0^{2\pi} \int_0^{\theta_a} \cos^2\theta \tan\theta \\
&\qquad \times \exp\left\{ -2 \left[\frac{r + (z-\delta)\tan\theta\cos\beta}{w(z)} \right]^2 \right\} r d\theta d\beta dr d\phi \\
&= 2\pi N_o \frac{w_f^2}{w^2(z)} \int_0^{r_f} \int_0^{2\pi} \int_0^{\theta_a} \cos^2\theta \tan\theta \\
&\qquad \times \exp\left\{ -2 \left[\frac{r + (z-\delta)\tan\theta\cos\beta}{w(z)} \right]^2 \right\} r d\theta d\beta dr \quad (7.29)
\end{aligned}
$$

where r_f is the radius of the projected detection window on the object plane.

The power response $P_d(z)$ is given as

$$
P_d(z) = T_i P_a(z) \tag{7.30}
$$

The normalized power response can be expressed as

$$\frac{P_d(z)}{P_{do}} = \frac{T_i P_a(z)}{T_i P_{ao}}$$

$$= \frac{\left(2\pi N_f \frac{w_f^2}{w^2(z)} \int_0^{r_f} \int_0^{2\pi} \int_0^{\theta_a} \cos^2\theta \tan\theta \times \exp\left\{ -2\left[\frac{r + (z-\delta)\tan\theta\cos\beta}{w(z)} \right]^2 \right\} r d\theta d\beta dr \right)}{\frac{1}{2}\pi^2 N_f \sin^2\theta_a w_f^2 \cdot \left(1 - \exp\left\{ -2\left[\frac{r}{w(\delta)} \right]^2 \right\} \right)}$$

$$= \frac{\left(4 \int_0^{r_f} \int_0^{2\pi} \int_0^{\theta_a} \cos^2\theta \tan\theta \times \exp\left\{ -2\left[\frac{r + (z-\delta)\tan\theta\cos\beta}{w(z)} \right]^2 \right\} r d\theta d\beta dr \right)}{\pi \sin^2\theta_a w^2(z) \left(1 - \exp\left\{ -2\left[\frac{r_f}{w(\delta)} \right]^2 \right\} \right)} \qquad (7.31)$$

7.6. Response from an inclined object surface

If the object surface is inclined with angle γ from the normal plane , the power response of the detector can be derived based on the same principle discussed in the previous sections.

The power $dP_{dm|ds}(z)$ intercepted by an infinitesimal area dm on the aperture can be derived as follows.

From Figure 7.5, the distance z_{o2} between the object plane and the normal plane which passes through the radiation area dn on the object surface can be derived from the following relationships.

$$(z - \delta - z_{o_1}) \tan(\frac{\pi}{2} - \gamma) = r\cos\phi \qquad (7.33)$$

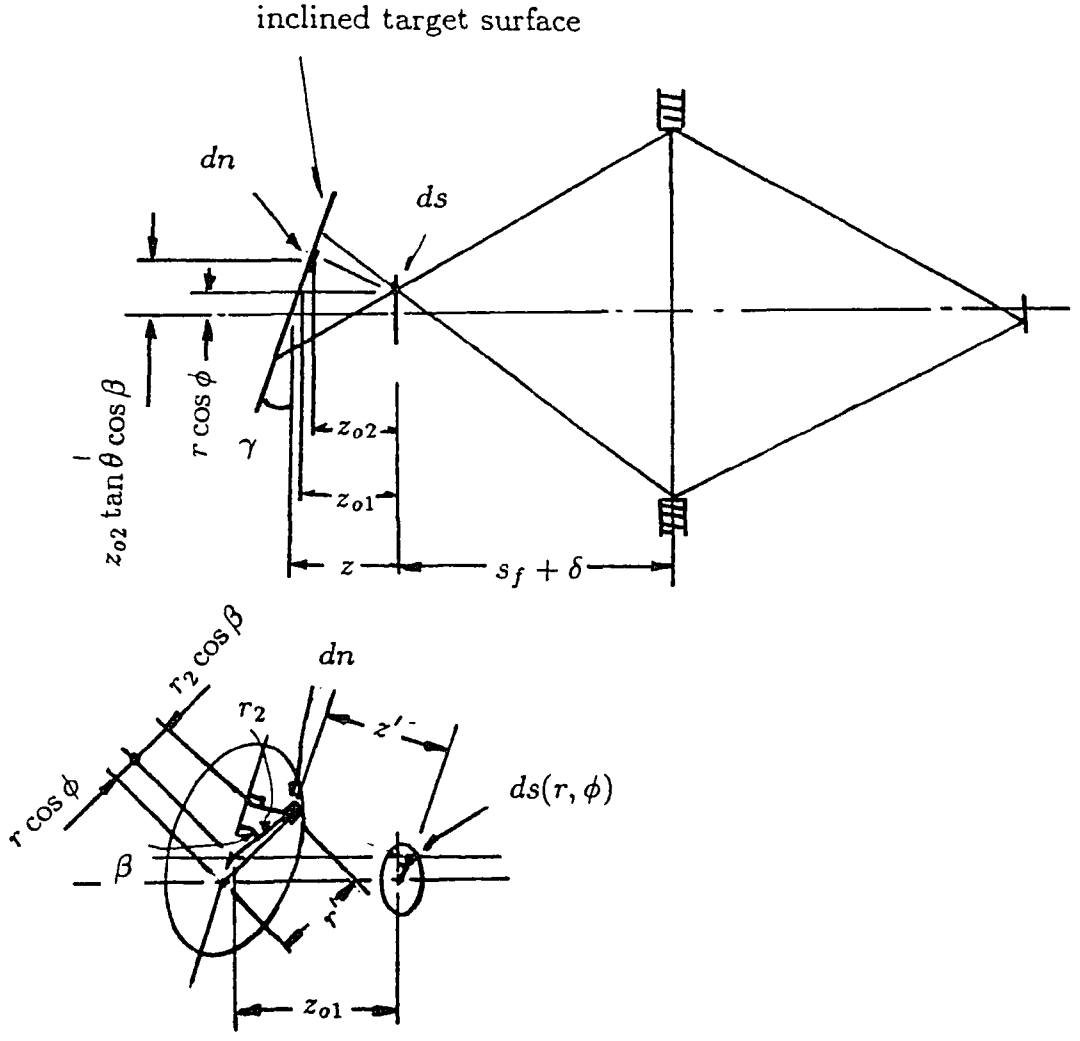

Figure 7.5. Imaging of an inclined surface

$$(z_{o_1} - z_{o_2}) \tan(\frac{\pi}{2} - \gamma) = z_{o_2} \tan\theta \cos\beta \tag{7.34}$$

From Eq. 7.33 and 7.34, z_{o2} can be given by

$$z_{o_2} = \frac{(z - \delta)\tan(\frac{\pi}{2} - \gamma) - r\cos\phi}{\tan\theta\cos\beta + \tan(\frac{\pi}{2} - \gamma)} \tag{7.35}$$

The distance r' between dn and the axis is given as

$$\begin{aligned} r' &= \sqrt{(r_2 \sin\beta)^2 + (r_2\cos\beta + r\cos\phi)^2} \\ &= \sqrt{r_2^2 + 2r_2 r\cos\phi + (r\cos\phi)^2} \\ &= \sqrt{(z_{o_2}\tan\theta)^2 + 2z_{o_2} r\cos\phi\tan\theta\cos\beta + (r\cos\phi)^2} \end{aligned} \tag{7.36}$$

The area dn can be expressed as

$$\begin{aligned} dn &= \frac{dn'}{\cos\gamma} \\ &= \frac{r_2 dr_2 d\beta}{\cos\gamma} \\ &= \frac{(z_{o_2}\tan\theta)(z_{o_2}\sec^2\theta)d\theta d\beta}{\cos\gamma} \\ &= \frac{z_{o_2}^2 \tan\theta\sec^2\theta d\theta d\beta}{\cos\gamma} \end{aligned} \tag{7.37}$$

The distance z' from dn to ds is given as

$$z' = \frac{z_{o_2}}{\cos\theta} \tag{7.38}$$

As illustrated in Figure 7.6, the area dn of the object surface faces the area ds with an angle θ' from the normal axis of the area dn. θ' can be given by

$$\theta' = \cos^{-1}\left(\frac{\left\{\begin{array}{l}(z_{o_2}/\cos\theta)^2 + (z_{o_2}/\cos\gamma)^2 \\ \quad -[(z_{o_2}\tan\gamma - z_{o_2}\tan\theta\cos\beta)^2 + (z_{o_2}\tan\theta\sin\beta)^2]\end{array}\right\}}{2\left(\frac{z_{o_2}}{\cos\theta}\right)\left(\frac{z_{o_2}}{\cos\gamma}\right)}\right)$$

$$= \cos^{-1}\left\{\frac{1}{2}\cos\theta\cos\gamma\left[\frac{1}{\cos^2\theta} + \frac{1}{\cos^2\gamma}\right.\right.$$

$$\left.\left. - (\tan^2\gamma - 2\tan\gamma\tan\theta\cos\beta + \tan^2\theta\cos^2\beta + \tan^2\theta\sin^2\beta)\right]\right\}$$

$$= \cos^{-1}\left\{\frac{1}{2}\left[\frac{\cos\gamma}{\cos\theta} + \frac{\cos\theta}{\cos\gamma}\right.\right.$$

$$\left.\left. - (\tan^2\gamma - 2\tan\gamma\tan\theta\cos\beta + \tan^2\theta)\cos\gamma\cos\theta\right]\right\} \qquad (7.39)$$

where

$$0 \le \gamma < \frac{\pi}{2},$$

$$0 \le \theta \le \theta' < \frac{\pi}{2}$$

The radiance at dn can be express as

$$N_1(z, \gamma, r, \phi, \theta, \beta) = N[z_{o2}(z, \gamma, r, \phi, \theta, \beta), r'(z, \gamma, r, \phi, \theta, \beta)] \qquad (7.40)$$

The power $dP_{dm|ds}(z)$ intercepted by dm can be expressed as

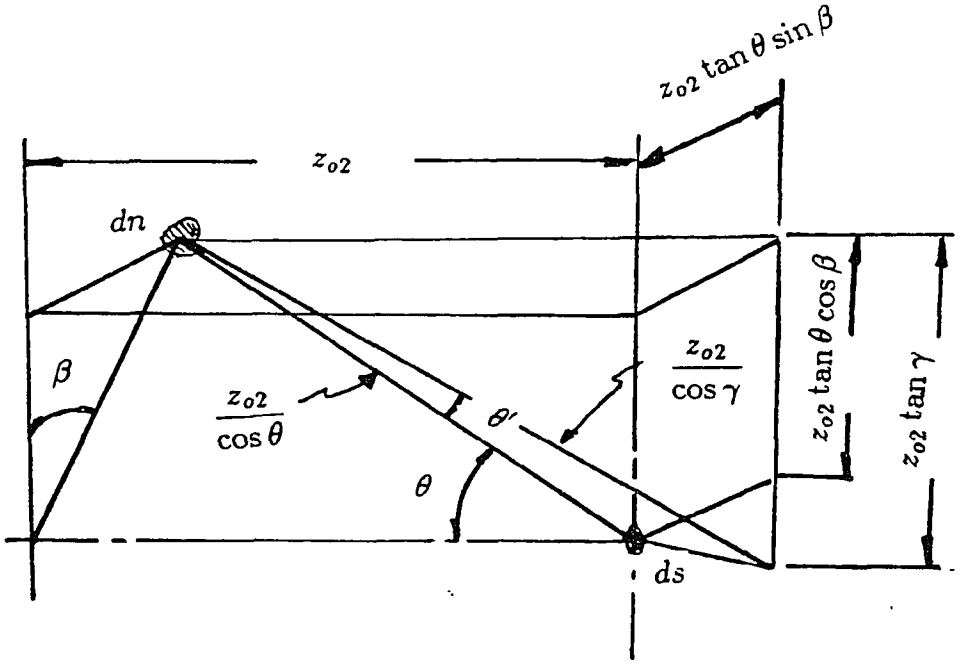

Figure 7.6. Radiation angle - θ'

$$dP_{dm|ds}(z) = N_1(z,\gamma,r,\phi,\theta,\beta)\cos^2[\theta'(\gamma,\theta,\beta)]ds\frac{dn}{z'^2}$$

$$= N_2(z,\gamma,r,\phi,\theta,\beta)\cos^2[\theta'(\gamma,\theta,\beta)]ds\frac{z_{o_2}^2\tan\theta\sec^2\theta d\theta d\beta}{\cos\gamma\cdot(z_{o2}/\cos\gamma)^2}$$

$$= N_2(z,\gamma,r,\phi,\theta,\beta)\cos^2[\theta'(\gamma,\theta,\beta)]\frac{\tan\theta}{\cos\gamma}dsd\theta d\beta \tag{7.41}$$

The power $dP_{|ds}(z)$ intercepted by the whole aperture is given by

$$dP_{|ds}(z) = \int_0^{2\pi}\int_0^{\theta_a} dP_{dm|ds}(z)$$

$$= \int_0^{2\pi}\int_0^{\theta_a} N_1(z,\gamma,r,\phi,\theta,\beta)\cos^2[\theta'(\gamma,\theta,\beta)]\frac{\tan\theta}{\cos\gamma}dsd\theta d\beta \tag{7.42}$$

The total power $P_a(z)$ intercepted by the aperture can be given as

$$P_a(z) = \int_0^{2\pi}\int_0^{r_f} dP_{|ds}$$

$$= \int_0^{2\pi}\int_0^{r_f}\int_0^{2\pi}\int_0^{\theta_a} N_1(z,\gamma,r,\phi,\theta,\beta)\cos^2[\theta'(\gamma,\theta,\beta)]$$

$$\times\frac{\tan\theta}{\cos\gamma}rd\theta d\beta dr d\phi \tag{7.43}$$

The power response $P_d(z)$ of the detector is expressed as

$$P_d(z) = T_i P_a(z) \tag{7.44}$$

The normalized power response is given as

$$\frac{P_d(z)}{P_d(\delta)} = \frac{\left\{ \int_0^{2\pi} \int_0^{r_f} \int_0^{2\pi} \int_0^{\theta_a} N_1(z,\gamma,r,\phi,\theta,\beta) \cos^2[\theta'(\gamma,\theta,\beta)] \times \frac{\tan\theta}{\cos\gamma} r d\theta d\beta dr d\phi \right\}}{\left\{ \int_0^{2\pi} \int_0^{r_f} \int_0^{2\pi} \int_0^{\theta_a} N_1(\delta,\gamma,r,\phi,\theta,\beta) \cos^2[\theta'(\gamma,\theta,\beta)] \times \frac{\tan\theta}{\cos\gamma} r d\theta d\beta dr d\phi \right\}} \tag{7.45}$$

where $P_d(\delta)$ is the power response when the inclined object surface is located at the object plane.

CHAPTER VIII

DISCUSSION OF EXPERIMENT

The topics related to the experiment are discussed in this chapter. The scope of the experiment includes the development of a functional optical system configuration, the analyses of the responses of the experiment system for different types of surfaces to test the validity of the theoretical predictions discussed in the previous chapters, the determination of the difficulties and limitations of the experiment system and the proposed method, and the investigation of the factors which influence the system performance.

8.1. Experimental system

The experimental system is based on the optical system discussed in Chapter IV, and its configuration is shown in Figure 8.1.

For a laser source, a low power HeNe laser operating in TEM*oo* mode is used. The wavelength of the laser output is 632.8nm. Functionally, the experimental system can be divided into two different sub-systems:the controlled illumination system and the imaging system. A beam splitter separates the optical path of the imaging system from that of the controlled illumination system. A single-axis positioning table provides a linear positional change of a target surface which is mounted on the top of the positioning table by a vertical mounting device. The movement of the translation stage is provided and controlled by a micrometer head which has 1" travel length with 0.0001" graduation.

The specifications of the system components are listed in Table 8.1.

8.1.1. Controlled illumination

Five lenses are involved in the laser beam shaping. The lenses L_1 and L_2

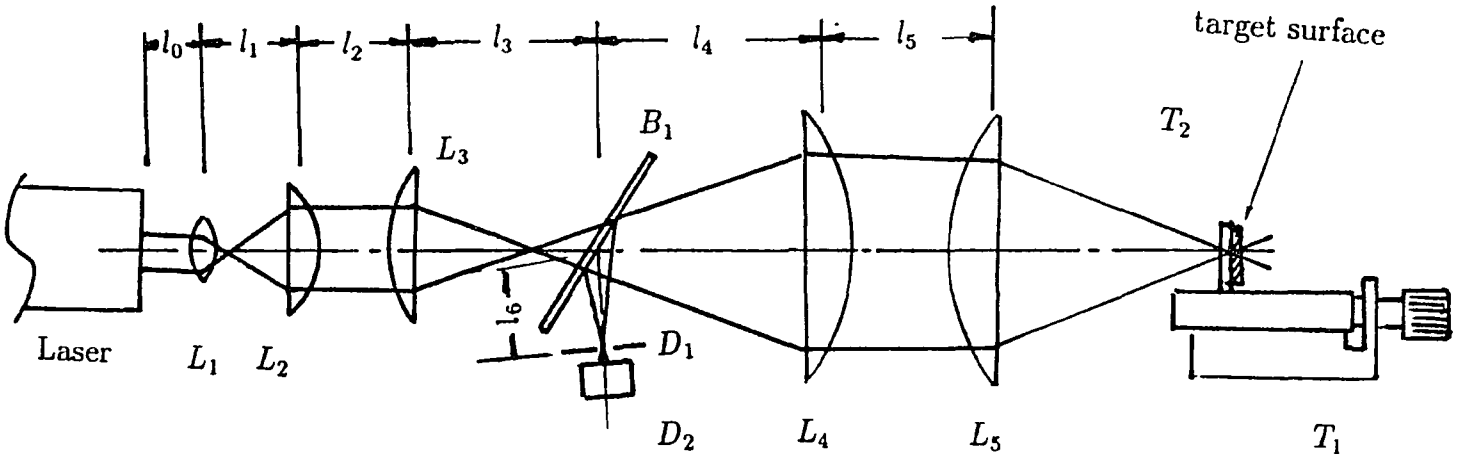

$l_1 = 10\text{mm}$
$l_2 = 88\text{mm}$
$l_3 = 58\text{mm}$
$l_4 = 79\text{mm}$
$l_5 = 126\text{mm}$
$l_6 = 78\text{mm}$

Figure 8.1. Experimental system

Components	Specification
Laser	He-Ne, output:0.8mW, beam dia.:0.53mm, random polarization manufacturer: Metrologic
L1	DCX, dia.:6mm, f1:6mm, uncoated
L2	PCX, dia:30mm, f1:50mm, uncoated
L3	PCX, dia:40mm, f1:76mm, uncoated
L4	PCX, dia:50mm, f1:81mm, uncoated
L5	PCX, dia:50mm, f1:81mm, uncoated
B1	beam splitter, mirror type, 35% transmission, 14% and 6% reflection, 25x38x3mm
D1	pinhole, copper plate, dia.:0.03mm approx. thickness:0.2mm, approx.
D2	silicon photodetector, range:0.02uW - 20mW, detection area: 1 sq.cm, display: 4 digit with range (0-1999) manufacturer: Metrologic
T1	single axis positioning table, travel length:1" micrometer head control with 0.0001" readout.
T2	optical bench
T3	components mounts, side sliding type
others	mounting plates, support columns, etc.

Table 8.1. System components specification

function as a beam expander to increase the size of the input beam considerably without increasing diverging or converging rate of the beam. This beam is focused by the lens L_3 to form a new beam waist in front of the beam splitter. This beam passes through the beam splitter B_1 and increases its size of the profile considerably before entering the lens L_4. The lenses L_4 and L_5 focus the beam to form a beam waist at the outside of the optical system. From the input, which is the laser output with diameter of 0.54mm, the experimental system produces an output which has its waist of radius 0.00172mm at a distance 39.7mm from the plane of the lens L_5. Table 8.2 shows the beam shaping data by the individual lenses, which are calculated using Eq. 5.1 - 5.5.

Also listed in the Table 8.2 are the truncation rates of the beam by the individual lenses due to their limited aperture size for determination of the effective beam radius and the sizes of the Airy disk patterns for comparison with the sizes of the beam waist.

During beam shaping, the laser beam is focused twice within the experimental system, and, as a result, considerable amount of spherical aberration is introduced and accumulated. The intensity distribution of the illumination beam is expected to deviate considerably from the ideal Gaussian pattern. The level of the deviation is aggravated by the imperfections of and dusts on the optical components, which cause scattering and interference in the beam propagation. No spatial filtering is used throughout the beam shaping process. The power loss during the beam shaping process is considerable due to reflection on the uncoated lens surfaces and the beam splitter.

8.2.2. Imaging system

The imaging system shares a portion of the optical path which is used in the

(All units are in mm)

lens element			beam-input		beam-output		airy	aperture
no	f	r	w1	d1	w2	d2	r	w1/r
L1	6.0	3.0	.270000	10.000000	.004442	6.001083	.001533	.090034
L2	50.0	15.0	.004442	81.998920	.006941	128.126900	.006544	.246012
L3	76.0	20.0	.006941	-70.126910	.003610	36.472820	.001397	.100986
L4	81.0	25.0	.003610	168.527200	.003341	155.959500	.004780	.373296
L5	81.0	25.0	.003341	-77.959550	.001702	39.725350	.001217	.186600

1. Notations
   - f: focal length
   - r: radius of lens
   - w1: input beam radius
   - d1: distance to the waist of the input beam
   - d2: " " output beam
   - w2: output beam waist
   - airy: radius of the expected Airy disk
   - w1/r: the ratio of the beam radius to lens radius on the lens plane

2. Specification of the input laser beam
   - beam radius: 0.27
   - location of the beam waist: 10mm is used (approximate value. from cavity mirror)

3. Specification of the final beam output
   - beam radius(wf) : .0017023
   - waist location from the last lens(sf): 39.7253500
   - size of the expected Airy disk pattern: .0012174
   - Maximum ratio of beam size to aperture size: .3732958 at element : L4

Table 8.2. Beam shaping data

beam shaping process. The optical path of the imaging system is determined by the reverse beam transformation path. The imaging system consists of the lenses L_4 and L_5, the detection window D_1, and the detector D_2 and its display unit. The imaging system can be represented as a single lens system using the combined focal length of the two lenses L_4 and L_5 as illustrated in Figure 8.2.

By assuming the lenses L_4 and L_5 are thin lenses, the combined focal length f_c is given as

$$\begin{aligned} f_c &= \frac{f_{L_5} f_{L_4}}{f_{L_5} + f_{L_4} - l_5} \\ &= \frac{81 \times 81}{81 + 81 - 78} \\ &= 78.1 \quad \text{mm} \end{aligned} \tag{8.1}$$

where f_{L_5} and f_{L_4} are the focal lengths of the lenses L_5 and L_4, respectively, and l_5 is the spacing between the two lenses.

The back focal length is

$$\begin{aligned} b.f.l. &= \frac{f_c(f_{L_4} - l_5)}{f_{L_4}} \\ &= 2.9 \quad \text{mm} \end{aligned} \tag{8.2}$$

The distance s_f between the the waist of the final beam and the principal plane of the single lens imaging system is

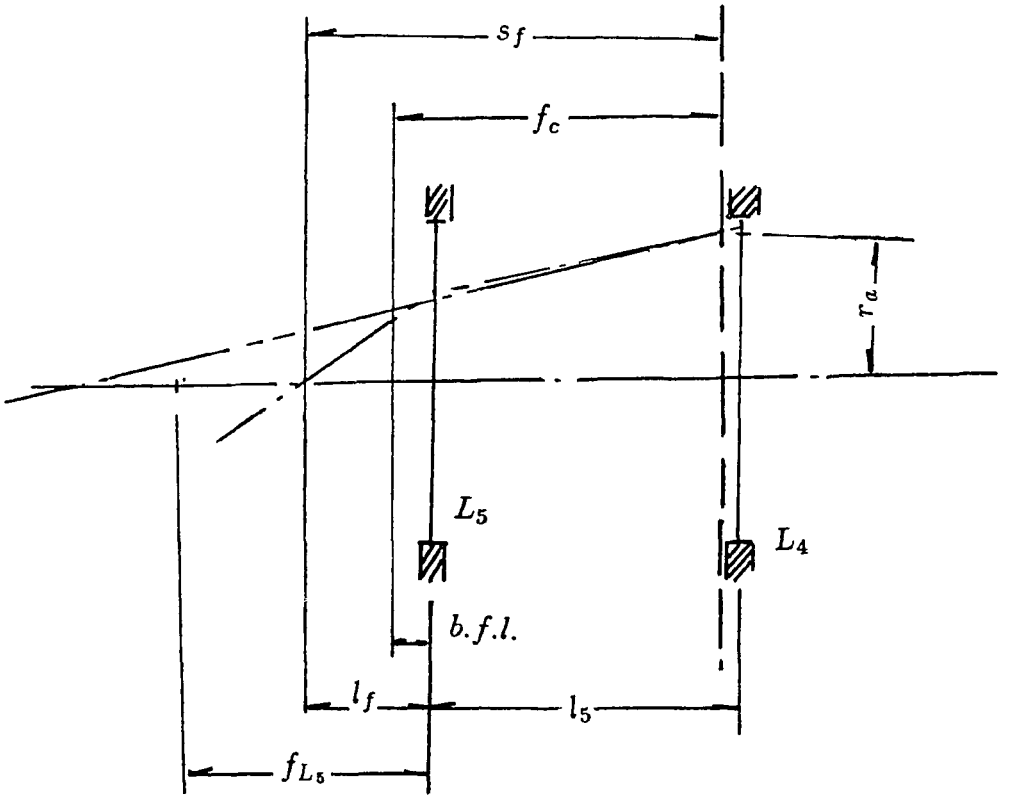

Figure 8.2. Single lens representation of the imaging system

$$
\begin{aligned}
s_f &= l_f + f_c - b.f.l. \\
&= 39.7 + 78.1 - 2.9 \\
&= 114.9 \qquad \text{mm}
\end{aligned}
$$

where l_f is the distance between the waist of the final beam and the principal plane of the lens L_5. The radius r_a of the clear aperture of the single lens imaging system is derived as

$$
\begin{aligned}
r_a &= r_{L_4} \frac{f_c - b.f.l. - (l_f l_5/(l_f - f_{L_5})}{l_5 - (l_f l_5/(l_f - f_{L_5})} \\
&= r_{L_4} \frac{78.1 - 2.9 + 75}{78.1 + 75} \\
&= 0.98 r_{L_4} \\
&\approx r_{L_4} \\
&= 20
\end{aligned}
$$

where r_{L_4} is the radius of the lens L_4 and is reduced to 20mm from 25mm considering the widths of the side portions which are blocked by the mounting clamps. The location of the detection window is determined by the reverse transformation of the illumination beam. Although the location of the beam waist obtained by the single-lens system with focal length given by Eq. 8.1 slightly differs with that obtained by the two-lens system, δ_1 and δ become zeros in the single-lens system.

The ideal size of the detection window can be determined by the size of the transformed beam waist formed by the reverse transformation. The ideal radius of the detection window of the experimental system is 0.0036mm from the data in Table 8.2. In the experimental system, the detection window is improvized by punching a small hole on the thin copper plate. The shape of the improvized pinhole is not exactly circular and some amount of burrs exist along the edge. The radius of the pinhole is about 20 - 50μm. The copper plate covers the face of the detector so that only the lights entering through the pinhole can reach the detector. The detection window is aligned approximately by positioning a mirror vertically at the waist of the illumination beam and finding the position of the detection window with maximum detection response.

8.1.3. Experiment procedure

A number of test surfaces are used for the response analysis. For each test, the surface is mounted vertically to the top surface of the positioning table. For each test, the location of the beam waist is determined by the position which gives the peak power response of the detector. From this position, the position of the surface is varied and the corresponding power response of the detector is obtained from the digital power meter.

All measurement and monitoring process is done manually without using any interfaces.

8.2. Reflective surface response

For the analysis of the reflective surface response, a first surface mirror is used in the experiment. Figure 8.3 shows the experiment results of the detector response curve of a mirror surface.

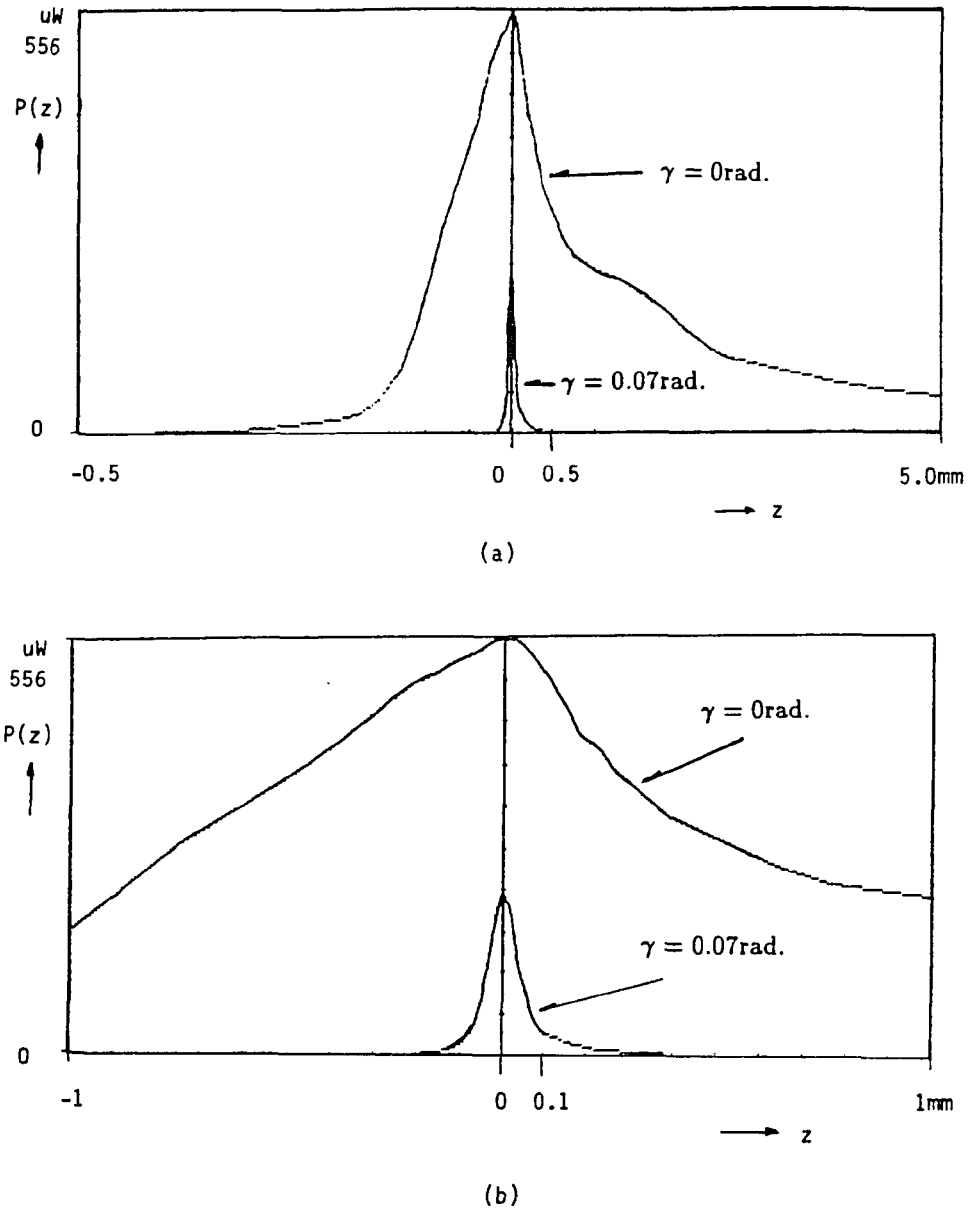

Figure 8.3(a,b). Reflective surface response - empirical

In Figure 8.3a shows the response curves of two different surface inclination angles - 0 radian and 0.07 radian- within the distance range $z = \pm 5$mm. In the both cases, the position change of minimum 0.02mm from the peak response position causes discernible change in the detection response. The response curves are not symmetrical about the center. These can be attributed to the differences of the aperture effects by the lenses L_5 and L_4 and the beam splitter B_1. A slight misalignment of the detection window also contributes these differences. In Figure 8.3b shows more detailed response curves within $z = \pm 1$mm.

Figure 8.3c shows the experimental results of the peak power response versus the surface inclination angle.

In the experiment, the response is measured by increasing the inclination angle to one direction, and the figure shown is the projected view of the one side measurement.

The theoretical detector responses are shown in Figure 8.4. The responses are calculated based on Eqs. 6.64-6.73. The composite Simpson method[24] is used for the numerical integration.

In detection response analysis, three different radii of the detection windows are considered: :0.03mm to approximate the pinhole radius of the experiment system, 0.0036mm radius for the ideal size as discussed in previous section, and 0.01mm for additional comparison.

The detection responses of the vertical surface are shown together with the experimental result of the mirror surface response. As the size of the detection window increases, the width of the plateau of the peak increases. The response curve of the experiment has less sharp curve shape because of the limited resolution of the detector and the larger sized detection window.

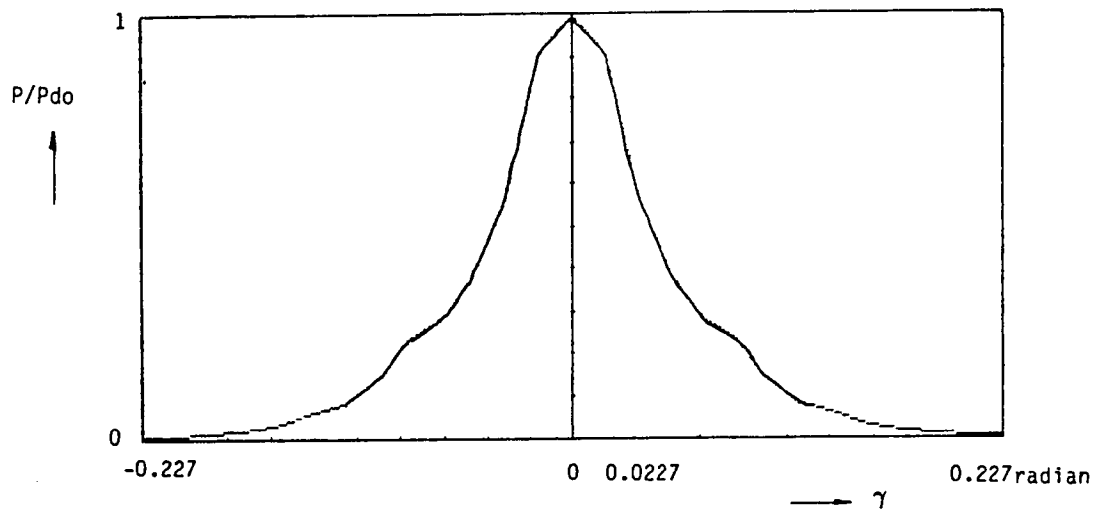

(c)

Figure 8.3(c). Reflective surface response - empirical

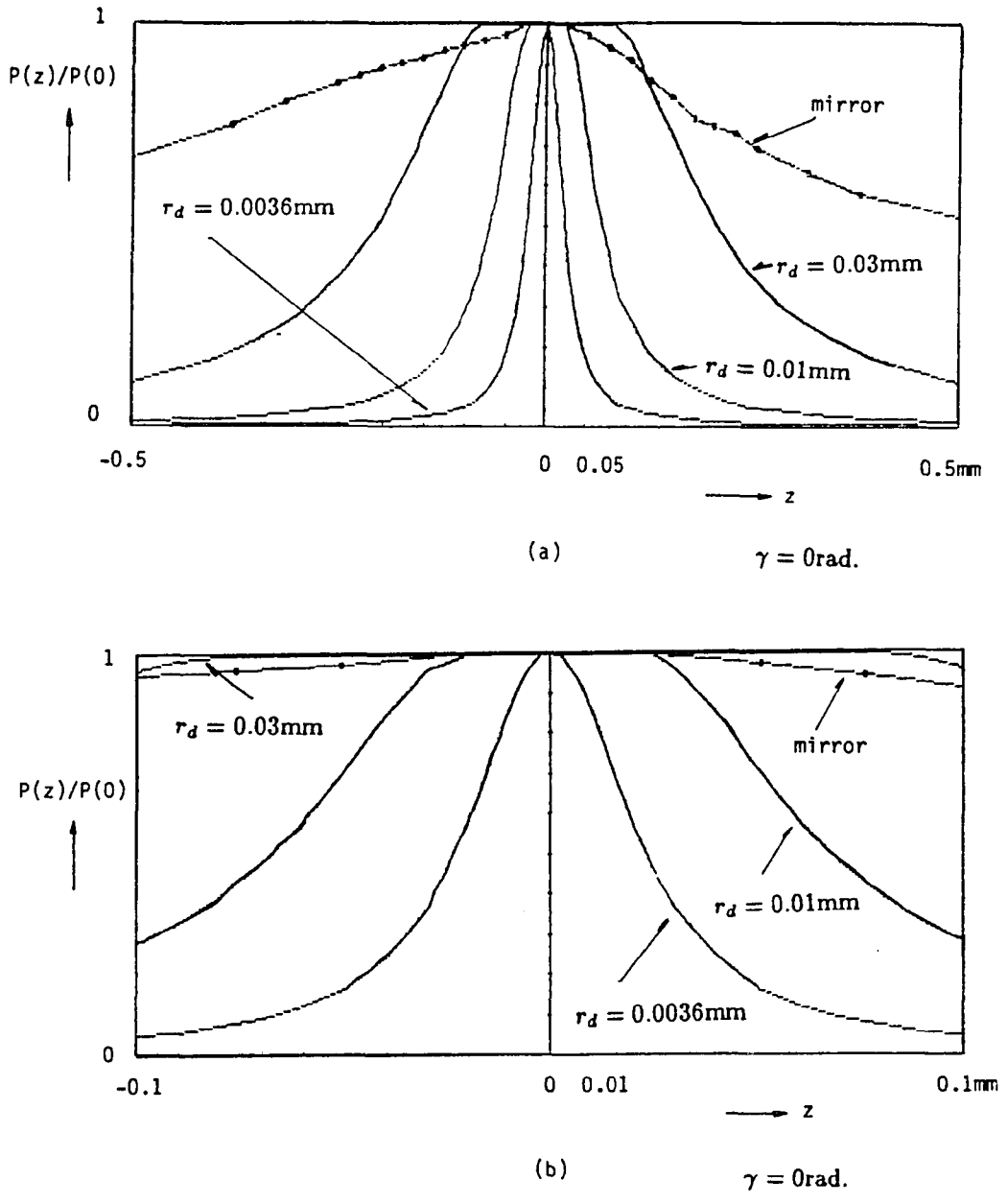

Figure 8.4(a,b). Reflective surface response - theoretical

Figure 8.4c and 8.4d show the responses of the surfaces with the inclination angle of 0.07 radian. The sharpness of the center portion of the curve increases with the increase of the inclination angle.

The lack of the center sharpness of the experiment cases may be attributed to the factors such as the accumulated aberration, the deviated Gaussian intensity profile, noises, the limited resolution of the detector, the imperfection and thickness of the pinhole, misalignment, etc.

The peak response versus the surface inclination angle is shown in Figure 8.5e together with the experiment result for comparison.

8.3. Diffusive surface response

The diffusive surface response could not be experimented because of the limited measuring range of the detector used.

The experiment was attempted using number of relatively diffusive surfaces such as a white chalk, matte surface paper, etc. The peak detection responses of theses surface are too weak for the measuring range of the detector for reasonable analyses.

The theoretical response of the experimental system is shown in Figure 8.5. These responses are calculated from Eq. 7.45 by numerical integration.

The normalized detection responses of vertical diffusive surfaces with different sizes of the detection windows are identical as shown in Figure 8.5a. The responses much sharper than those of the reflective surfaces. The widths of of the peaks of these response curves are less than 0.001mm as shown in Figure 8.5b.

The effect of the surface inclination is less clear as shown in Figure 8.5c and 8.5d. The normalized response curve of the inclined surface is identical with

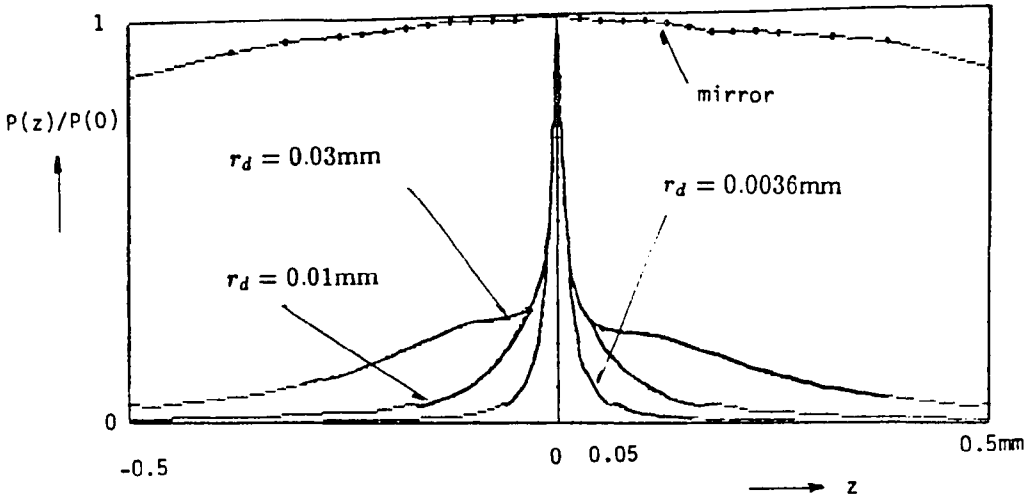

(c) $\gamma = 0.07$rad.

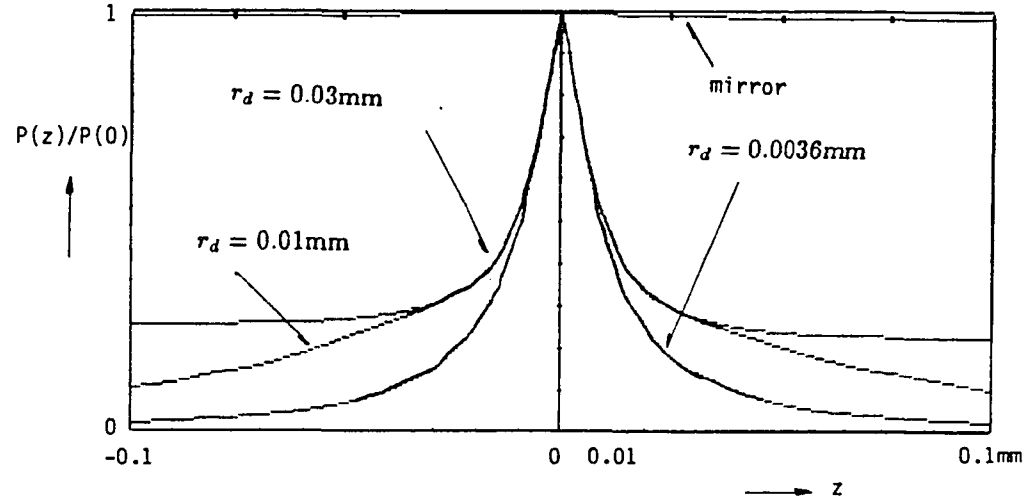

(d) $\gamma = 0.07$rad.

Figure 8.4(c,d). Reflective surface response - theoretical

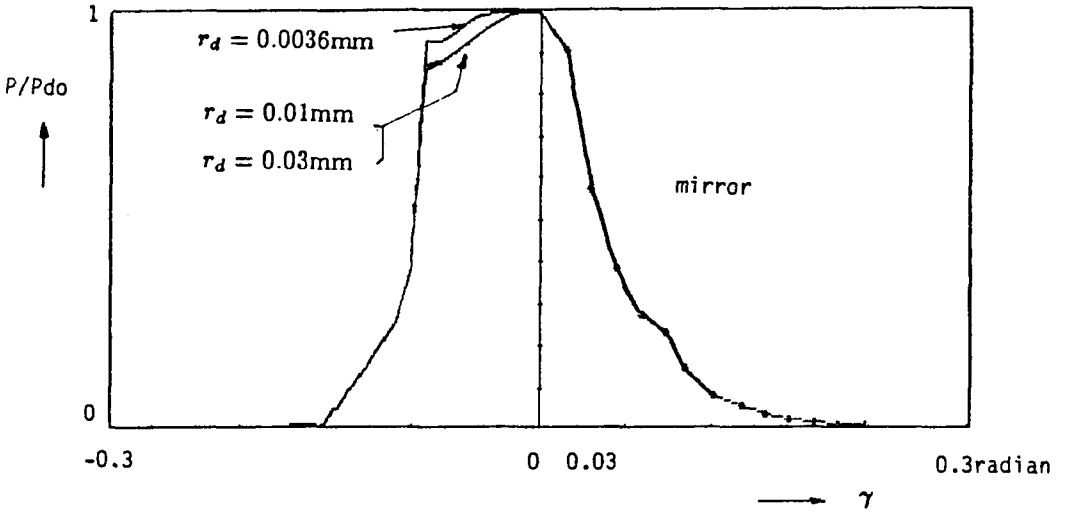

(e)

Figure 8.4(e). Reflective surface response - theoretical

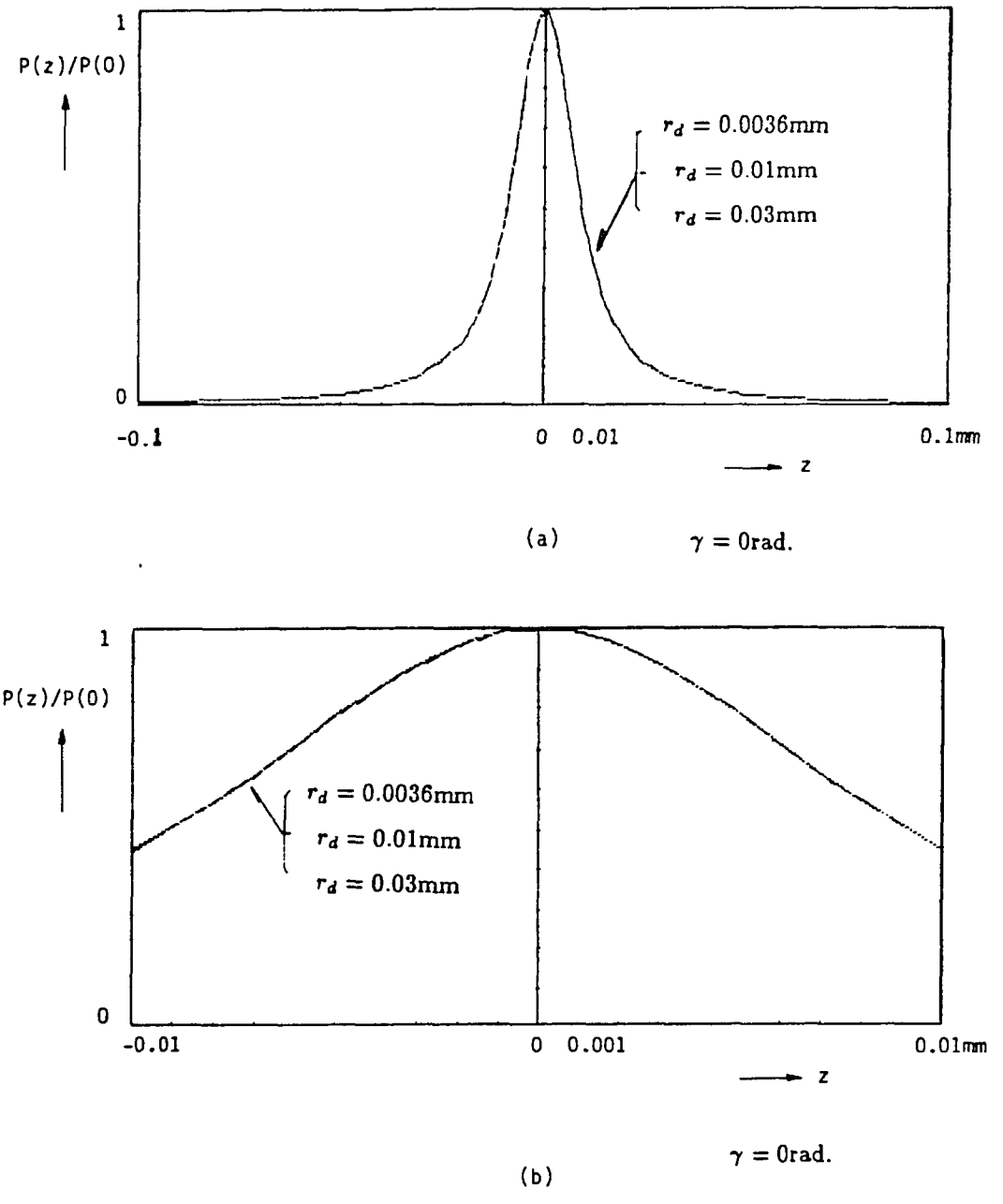

Figure 8.5(a,b). Diffusive surface response - theoretical

that of the vertical surface except the magnitude of the peak response which is shown in Figure 8.5e.

In Figure 8.5f, the diffusive surface responses are compared with the reflective surface responses, for the case of the detection window with radius of 0.0036mm.

8.4. Response from other target surfaces

Most of the typical surfaces in manufacturing environment are partly diffusive and partly reflective.

Four different surfaces are used in the experiment as listed in Table 8.3. The detection responses are measured for these surfaces with zero inclination angle. Because of the considerable amount of scattering on the surfaces, the range of the power responses are considerably low for the detector measuring capability. Only two decimal digit resolutions can be obtained for the detection responses.

The individual responses are shown in Figure 8.6a-8.6d. The normalize detection responses are compared in Figure 8.6e - 8.6h with different scales to show the detail.

The response of the aluminum bar which has face milled surface shows the effect of the surface roughness on the detection response as shown in Figure 8.6a. Even with the low detection resolution, the positional variation of about 0.003mm around the peak is detectable. Other surfaces shows the sensitivities of under 0.03mm. In Figure 8.6i, the responses are compared with the mirror surface responses. Even with the low detection resolution, the responses of these surfaces show more sensitive responses than the mirror responses, because of the partial diffusiveness of the surfaces.

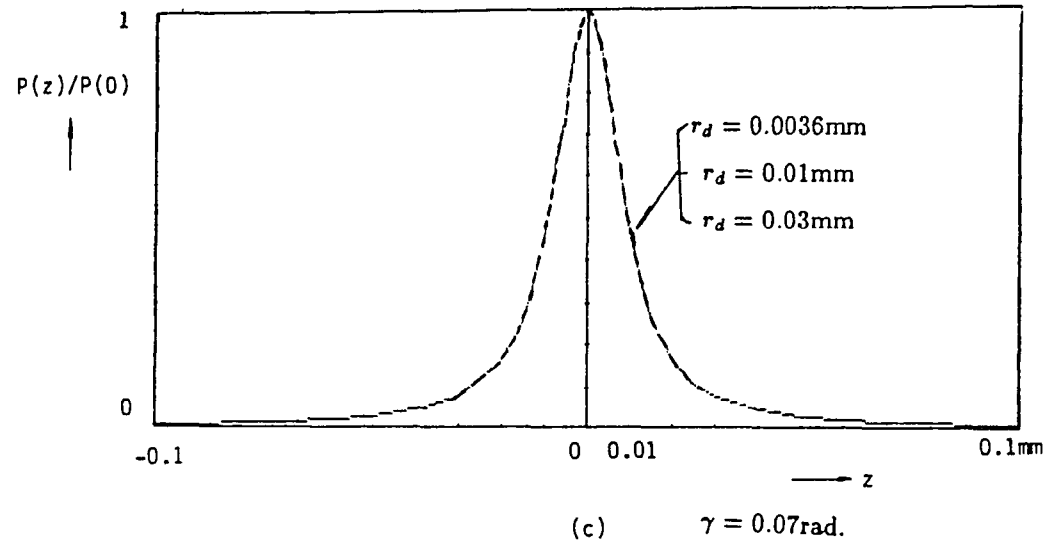

(c) $\gamma = 0.07$rad.

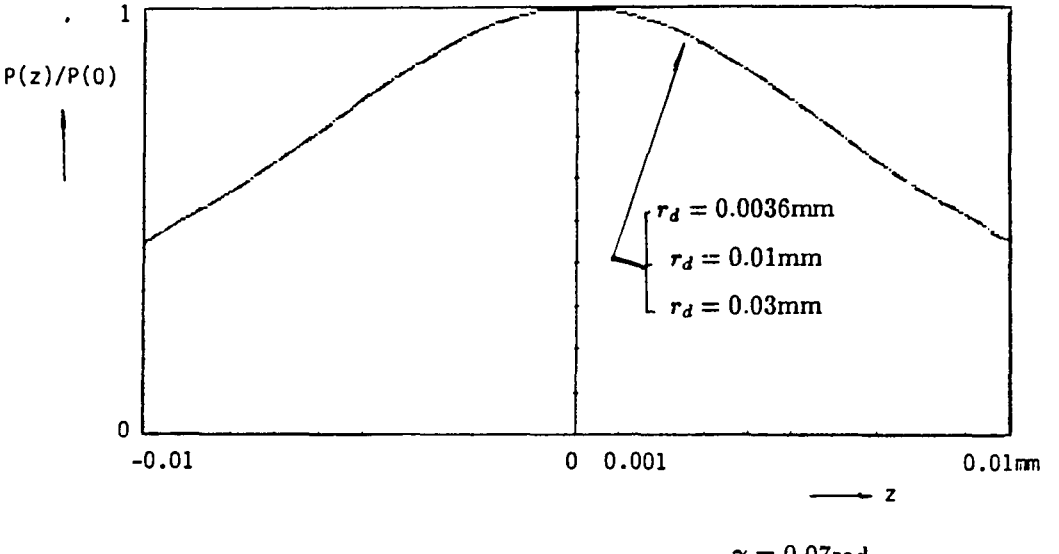

(d) $\gamma = 0.07$rad.

Figure 8.5(c,d). Diffusive surface response - theoretical

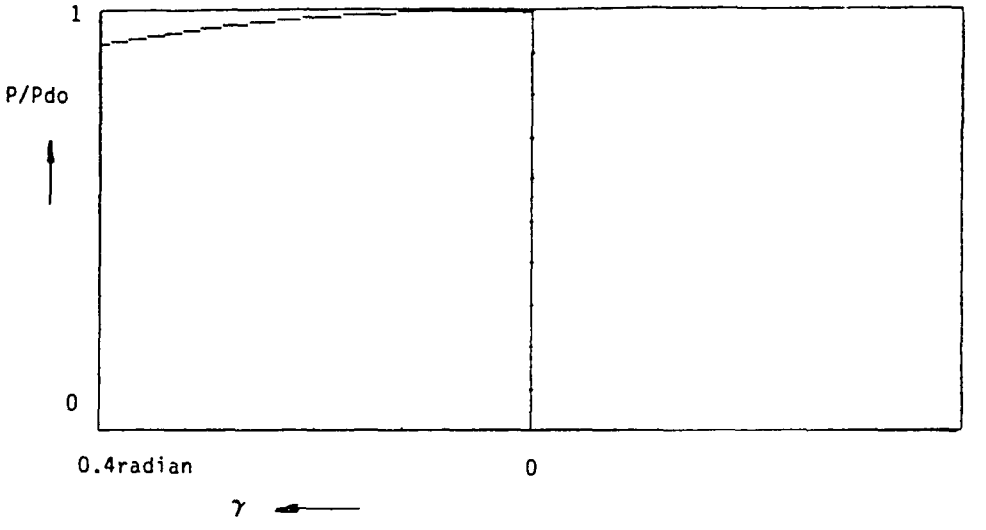

(e)

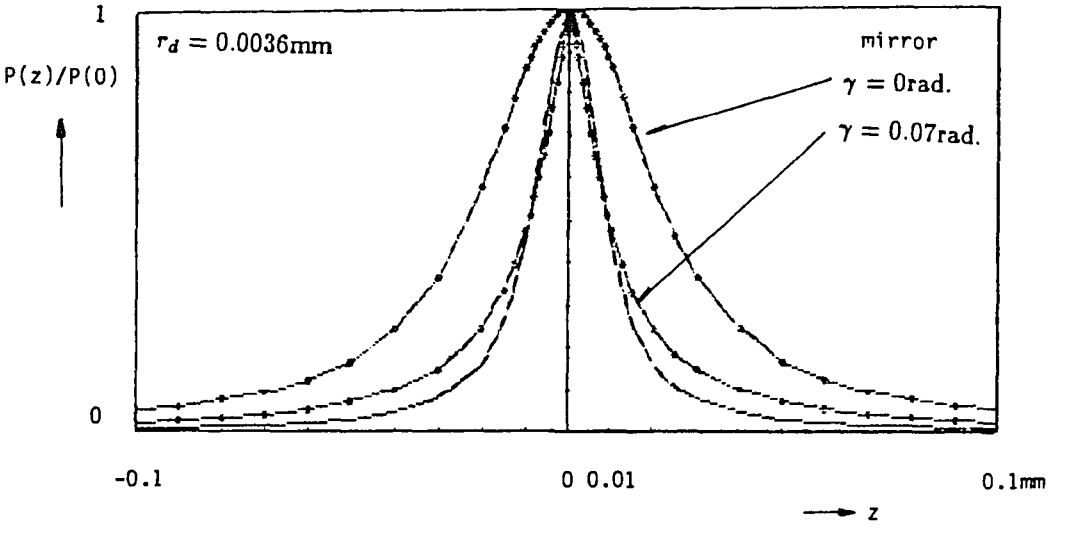

(f)

Figure 8.5(e,f). Diffusive surface response - theoretical

Test surface	Specification
S1	Aluminum plate, standard product, 1/16" thickness
S2	Aluminum bar, face-milled surface.
S3	Stainless steel, matte finish
S4	Molded polymer surface, white and smooth.

Table 8.3. List of test surfaces

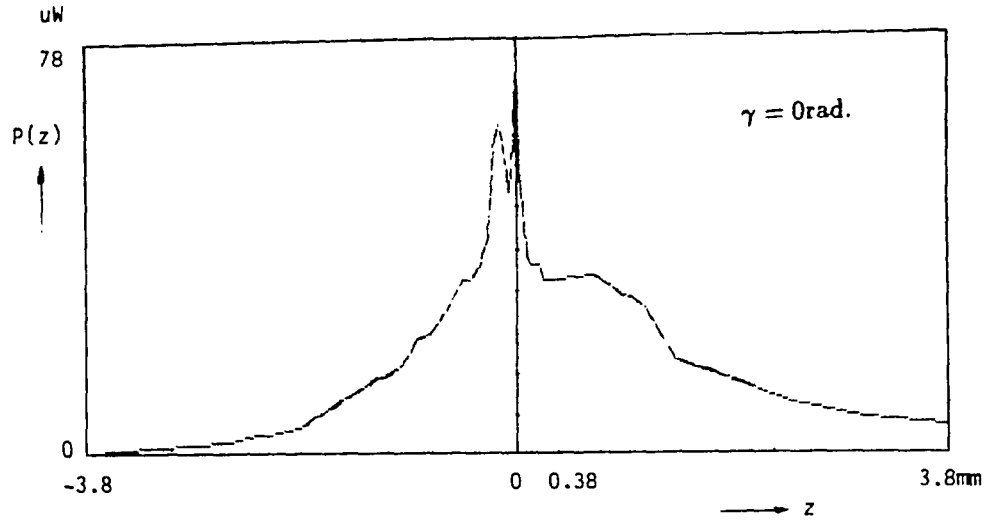

(a) Response from S_1

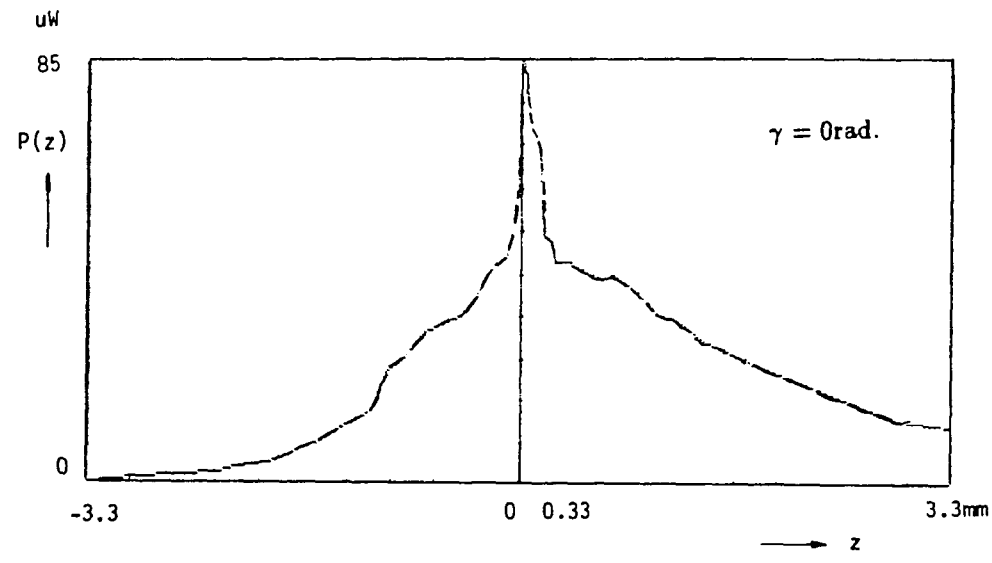

(b) Response from S_2

Figure 8.6(a,b). Responses from test surfaces

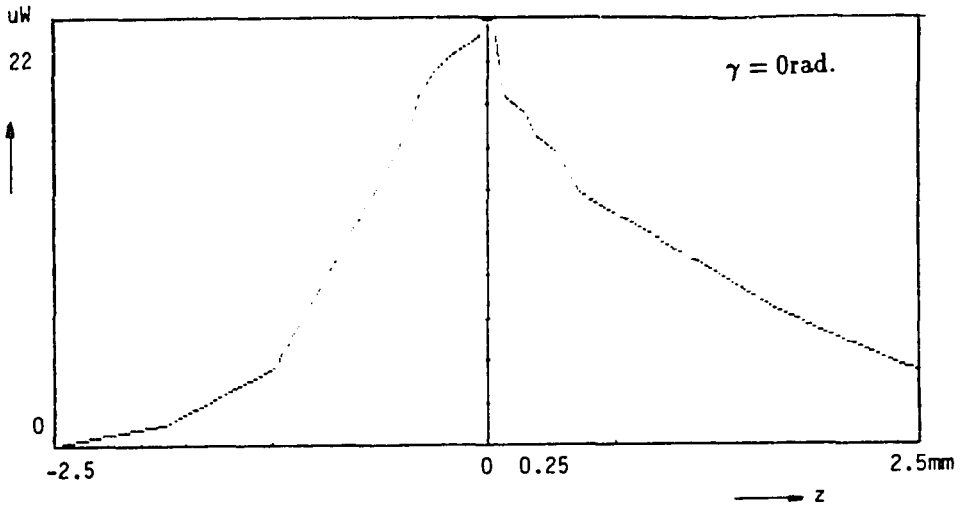

(c) Response from S_3

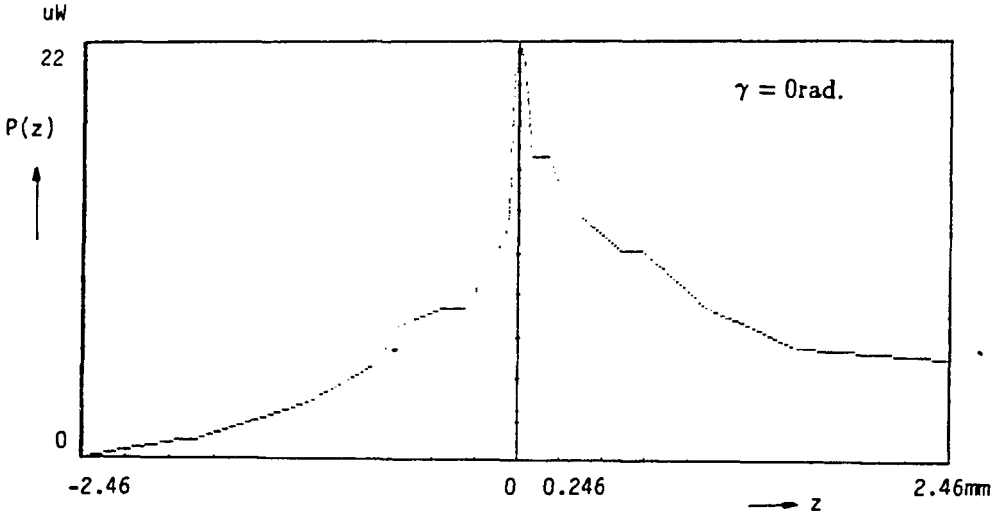

(d) Response from S_4

Figure 8.6(c,d). Responses from test surfaces

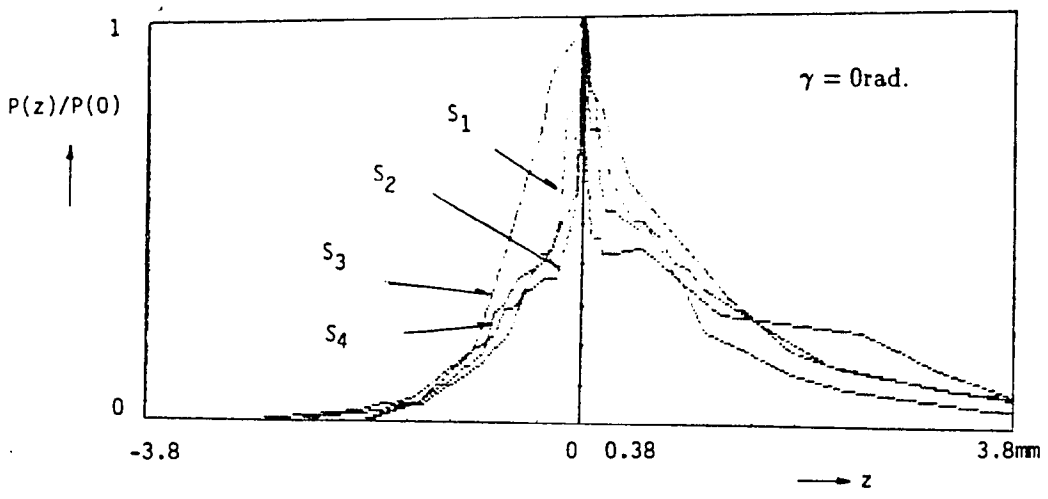

(e)

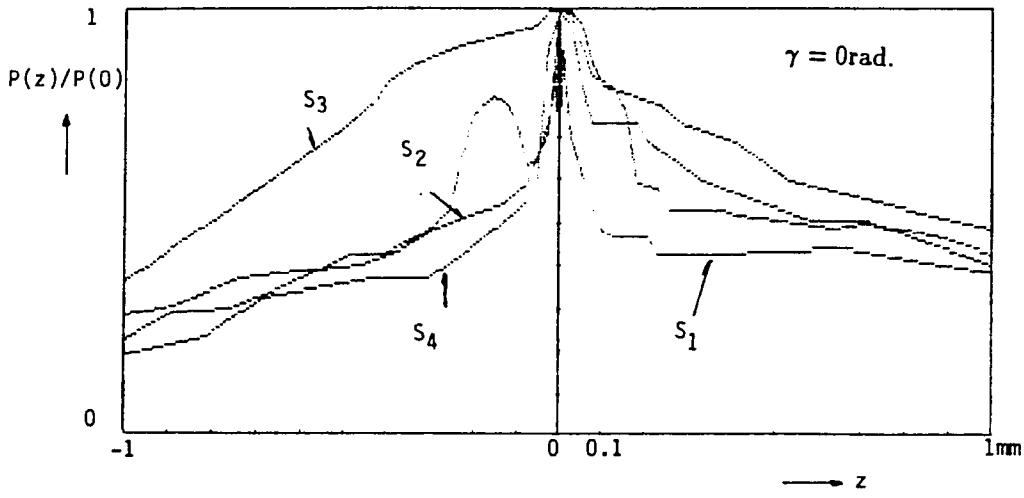

(f)

Figure 8.6(e,f). Responses from test surfaces

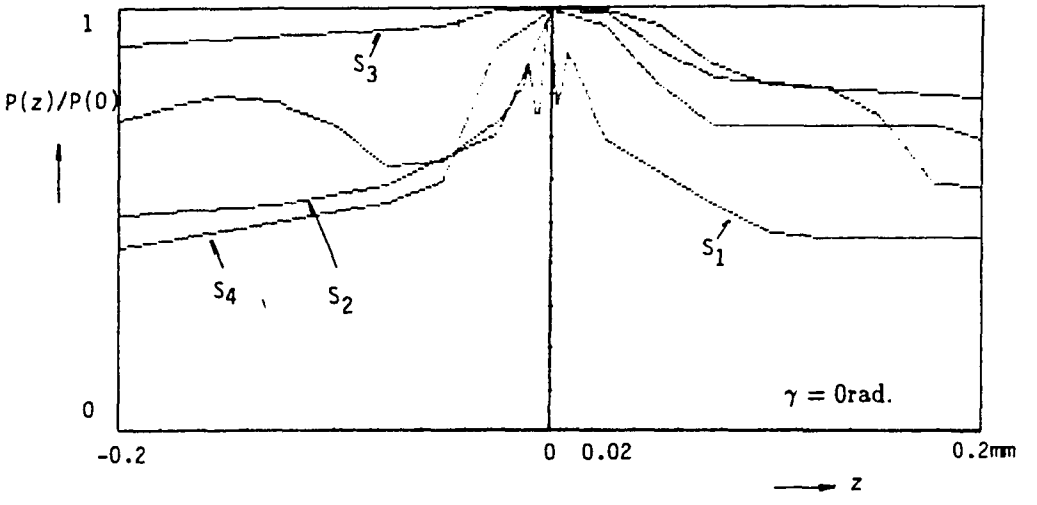

(g)

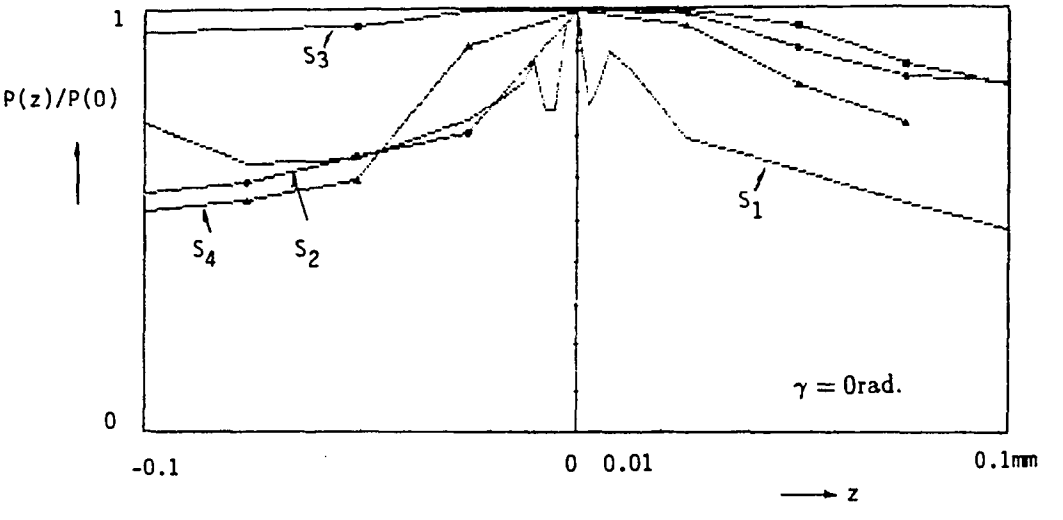

(h)

Figure 8.6(g,h). Responses from test surfaces

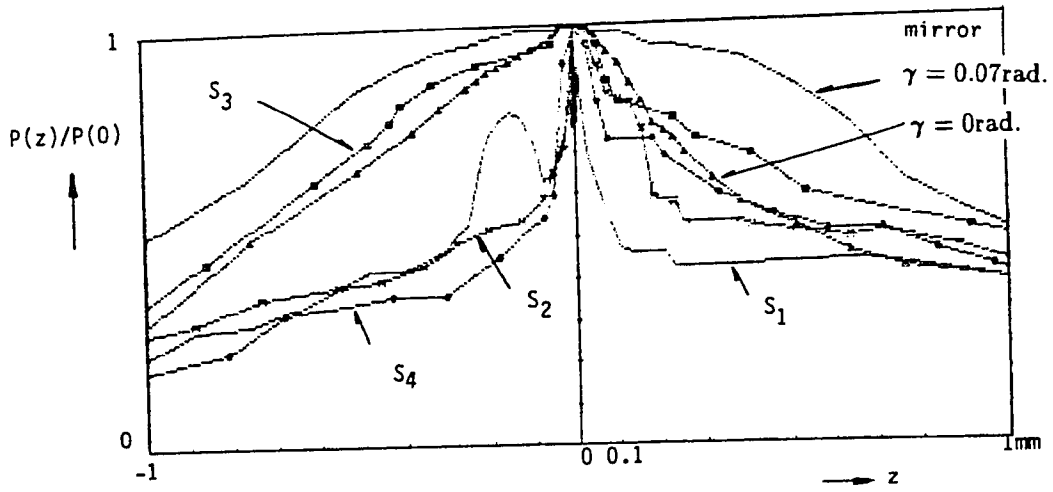

(i)

Figure 8.6(i). Responses from test surfaces

CHAPTER IX

ADDITIONAL DISCSSION

The experiment was limited in scope and quality mostly bacause of the lack of available resources. The difficulties and problems encountered in the experiment, the corrective measures for the problems, and the consideration for practical system are discussed in this chapter.

9.1. Difficulties and problems in the experiment

The difficulties and problems can be summarized as follows.

Laser source

The HeNe laser used in the experiment has noticeable noise and output variation as discussed in Chapter V. The stray beams in the original source is not removed. The fluctuation of the power output is considerable. Even after warm-up, the power of the beam varies in quasi periodic pattern with slowly varying period of from several minutes to more than 20 minutes and with amplitude variation of up to 16 percent. Along with this wave-like fluctuation, there is a small ripple with amplitude variation of 1 to 2 percent and with period of several seconds.

Optical components

In the experimental system, all the lenses used are of converging type. During beam process, the beam is focused twice within the system, and considerable amount of spherical aberration is introduced and accumulated.

The imperfections of and dusts on the lense surfaces cause scattering and interference in the beam propagation. This disturbs the coherent beam profile This disturbance together with the accumulated spherical aberration and

the inherent noise in the laser beam causes considerable departure from the perfectly coherent beam profile and propagation.

As all the lenses are not coated, the reflection on the lens surfaces are considerable. Although these reflections do not cause noticeable noise in the detector response but causes considerable amount of the power loss.

Detection system

The improvized pinhole used in the experiment is not The size and the shape of the improvized pinhole used in the experiment are far from the perfection. As the thickness of the pinhole is considerable(about 0.2mm), the effect of the scattering on the wall of the pinhole can not be ignored.

The limited measuring range and resolution of the detection system is the most

The limited measuring range and resolution of the detection system are the most critical limiting factors in the experiment. The responses in the experiment(0 - 6.56μW) are two weak for the measuring range of the detector, which is 0.00μW - 20mW, to provide proper resolution.

Misalignment

Considerable misalignment is present in the experimental system. The alignment of the detection window is considerably difficult. In the experimental system, the detection window is aligned rather roughly.

9.2. Suggested corrective methods

The instability of the laser output can be easily compensated by use of dual detector. One detector can be used to monitor the power variation of the laser beam output, and the response from the other detector can be compensated of this power variation. Spatial filtering can be used to remove the stray

lights which are present in the laser beam.

The focusing error will be reduced with use of the lenses which are corrected of spherical aberration to the Rayleigh degree. The anti-reflection coating on the lens surface will reduce the noise and energy loss caused by the reflection on the lens surfaces.

The performance of the system will be increased greatly if the detector can provide proper measuring range and high resolution.

9.3. Consideration for practical system

The performance of the system will be increased as the size of the detection window approaches the size of the waist of the imaged beam on the detection window.

Most of the surface The response will be affected more by the reflective components. If reflective effect is low or the a surface inclination is considerable so that the effect of direct reflection is insignificant, the response will follow that of diffusive surface.

Even the highly polished surface, there is always surface irregularities as discussed in Chapter V. For considerable surface inclination so that the refelctive response can not be expected, there is a very weak scattering occurs by these microirregularities. if the detector is sensitive enough, this can be detected and the response will follow that of the diffusive surface.

The response curve of the detector is well defined. The peak response can be easily detected during the distance variation. In this case, the distance with the peak response can be found by an open loop control if the response and the position of the system is recorded by a suitable memory device. If this peak is not well defined, the proper position can be found by finding the center of the plateau of the response curve.

If maintaining the correct distance between the system and a target surface is the objective, the positioning control can be done by searching for the peak by constantly varying the distance in a mall degree and checking the slope of the movement as the slope of the curve at both sides of the peak is almost identical.

CHAPTER X

CONCLUSION

The dimensional measurement and/or check of workpieces is a major part of the inspection and quality control in manufacturing In the majority of the applications, the contact methods are used. While a number of non-contact methods are available, most of them are inflexible, require special attention and configuration, and are limited in applications. Regardless of the methods used, the measurement process requires considerable time and skill. If higher level of accuracy is required, the time and skill involved increases accordingly. This process is a very difficult one to automate if the measurement of a single or multiple point coordinates on workpieces is required and if the use of the go-and-no-go type limit inspection gages is impractical, uneconomical, or impossible. This is especially true for such applications in which the production quantities are low, in which the workpieces are large and have complicate shapes, and in which the measurement requires high accuracy.

These difficulties are the backgrounds for the development of the proposed non-contact method. Based on a rather simple principle, a number of different approaches have been tried, and tested. The proposed method is the possible conclusion of these approaches considering several factors:the essential features of the close-range measurement, the automation possibility, the available technology, etc.

Of this development process, the background and motives, the required features for a measurement system, the configuration of the proposed system, and the theoretical analyses have been explained and described in this dissertation. The experimentation of the proposed method was too limited in

scope and quality due to the limited availability of resources, equipments, and components. It is expected that the empirical result will closely follow the theoretical predictions, if good quality components are used and the suggested corrective measures are taken in the experiment.

The performance of the proposed method can be affected by the surface condition of a target and any floating particles between the proposed system and the target surface. These are the drawbacks, but these drawbacks can be used for other applications:surface roughness measurement, the examination of floating particles in the air and fluid, etc.

As the level of automation and computer integration increases, the demand for flexible, versatile, non-contact measurement method will grow. This proposed method can be proved to be quite valuable or, at least, can provide an alternative in the conventional or automated measurement applications in inspection and quality control in manufacturing.

BIBLIOGRAPHY

[1]. H. W. Pollak, *Tool Design*, Reston Publishing Company, Reston, VA, 1976, pp255-293.

[2]. S.S. Charschan, editor., *Lasers in Industry*, Van Nostrand Reinhold Company, New York, 1972.

[3]. J. T. Luxon and D. E. Parker, *Industrial Lasers and Their Applications*, Prentice Hall, Englewood Cliffs, NJ, 1985, pp154 - 157.

[4]. W. J. Smith, *Modern Optical Engineering*, McGraw-Hill, New York, 1966.

[5]. J. W. Goodman, *Introduction to Fourier optics*, McGraw-Hill, New York, 1968, pp57-65, pp102-103.

[6]. H. Kogelnik, "Propagation of Laser Beams", *Applied Optics and Optical Engineering*, **vol vii**, Academic Press, New York, 1979.

[7]. H. Kogelnik and T. Li, "Laser Beams and Resonators", *Proc. IEEE* 54:1312, Oct., 1966.

[8]. L. J. Pinson, *Electro-Optics*, John Wiley & Sons, New York, 1985

[9]. J. Walsh, *Photometry*, Constable & Company Ltd, London, 1953.

[10]. A. E. Siegman, *Lasers*, University Science Books, 1986.

[11]. J. E. Eby and R. E. Levin, "Incoherent Light Sources", *Applied Optics and Optical Engineering*, **vol vii**, Academic Press, New York, 1979.

[12]. H. G. Heard, *Laser Parameter Measurement Handbook*, John Wiley & Sons, New York, 1968, pp413-431.

[13]. A.L. Bloom, *Gas Lasers*, John Wiley & Sons, New York, 1968, pp113-115, pp115-122.

[14]. A. L. Bloom and D. J. Innes, "Design of Optical Systems for Use with Laser Beams", *Spectra-Physics Laser Tech. Bull. No. 5*, Spectra-Physics Inc., Mountain View, CA.

[15]. R. G. Schell and G. Tyras, "Irradiance from an aperture with a Truncated-Gaussian Field Distribution", *J. Opt. Soc. Am*, **61**, 31, 1971.

[16]. Instruction Manual:*Metrologic Hard-Sealed Helium-Neon Lasers*, Metrologic Instruments, Inc., NJ.

[17]. J. M. Elson, H.E. Bennet, and J. M. Bennet, "Scattering from Optical Surfaces", *Applied Optics and Optical Engineering*, **vol vii**, Academic Press, New York, 1979.

[18]. H.E.Bennet and J.O.Porteus, *J. Opt. Soc. Am.*, **51**, 123, 1961.

[19]. P. Beckmann and A. Spizzichino, "The Scattering of Electromagnetic Waves from Rough Surfaces", Macmillian, New York, 1963.

[20]. P. Beckmann, "Scattering of Light by Rough Surfaces", *Progress in Optics*, **vol vi**, North-Holland, Amsterdam, 1967.

[21]. J. D. Gaskill, *Linear Systems, Fourier Transforms, and Optics*, John Wiley & Sons, New York, 1978, pp483-484.

[22]. R. Kingslake, "Illumination in Optical Images", *Applied Optics and Optical Engineering*, **vol ii**, Academic Press, New York, 1965.

[23]. P. D. Foote, *Bull. Bur. Std.*, **12**, 583, 1915.

[24]. R. L. Burden, J. D. Faires, and A. C. Reynolds, *Numerical Analysis*, 2nd edition, PWS Publishers, Boston, MA, 1981, pp147-151.

[25]. R. W. Ditchburn, *Light*, 2nd ed., Wiley, NY, 1964.

[26]. M. Kerker, *Scattering of Light and Other Electromagnetic Radiation*, Academic Press, NY.

[27]. G. Mie, *Ann. Phys*(Leipzig), **25**, 377.

[28]. J. A. Amstrong and A. W. Smith, "Experimental Studies of Intensity Fluctuations in Lasers", *Progress in Optics*, **vol vi**, North-Holland, Amsterdam, 1967.

[29]. F. A. Jenkins, *Fundamentals of Optics*, 4th ed., McGraw-Hill, NY, 1976.

[30]. L. E. Drain, *The Laser Doppler Technique*, John Wiley & Sons, NY, 1980.